Universidade Federal de Pernambuco
Centro de Ciências Exatas e da Natureza
Departamento de Física
Programa de Pós-Graduação

Florentino Gomes de Oliveira Silva

Forest Fire in Heterogeneous Environments: The Role of Enlarged Active Neighborhoods and Random Forbidden Sites

Recife
2016

Florentino Gomes de Oliveira Silva

Forest Fire in Heterogeneous Environments: The Role of Enlarged Active Neighborhoods and Random Forbidden Sites

Dissertation submitted to the Graduate Program in Physics at UFPE (Universidade Federal de Pernambuco) as partial fulfillment of the requirements for the Master of Science degree.

Supervisor: Prof. Dr. Sérgio Galvão Coutinho

Co-supervisor: Prof. Dr. Gustavo Camelo Neto

Recife

2016

Catalogação na fonte
Bibliotecário Jefferson Luiz Alves Nazareno CRB 4-1758

S586f Silva, Florentino Gomes de Oliveira.
Forest fire in heterogeneous environments: the role of enlarged active neighborhoods and random forbidden sites / Florentino Gomes de Oliveira Silva. – 2016.
101f.: fig.

Orientador: Sérgio Galvão Coutinho.
Dissertação (Mestrado) – Universidade Federal de Pernambuco. CCEN. Física. Recife, 2016.
Inclui referências.

1. Física estatística . 2. Sistemas complexos . 3. Modelos de propagação. I. Coutinho, Sérgio Galvão(Orientador). II. Titulo.

530.1595 CDD (22. ed.) UFPE-FQ 2016-61

FLORENTINO GOMES DE OLIVEIRA SILVA

FOREST FIRE IN HETEROGENEOUS ENVIRONMENTS: THE ROLE OF ENLARGED ACTIVE NEIGHBORHOODS AND RANDOM FORBIDDEN SITES

Dissertação apresentada ao Programa de Pós-Graduação em Física da Universidade Federal de Pernambuco, como requisito parcial para a obtenção do título de Mestre em Física.

Aprovada em: 15/08/2016.

BANCA EXAMINADORA

_____

Prof. Dr. Sérgio Galvão Coutinho
Orientador
Universidade Federal de Pernambuco

_____

Prof. Dr. Gustavo Camelo Neto
Co-orientador
Universidade Federal de Pernambuco

_____

Prof. Dr. Marcelo Andrade de Filgueiras Gomes
Examinador Interno
Universidade Federal de Pernambuco

_____

Prof. Dr. José Soares de Andrade Júnior
Examinador Externo
Universidade Federal do Ceará

"Cascos, cascos, cascos
Multicoloridos, cérebros, multicoloridos
Sintonizam, emitem longe
Cascos, cascos, cascos
Multicoloridos, homens, multicoloridos
Andam, sentem, amam
Acima, embaixo do mundo
Cascos, caos, cascos, caos
Imprevisibilidade de comportamento
O leito não-linear segue para dentro do universo
Música... quântica?"
Chico Science & Nação Zumbi.
Coco Dub (Afrociberdelia), 1994.

"On a le devoir de faire tout ce qu'on veut,
de penser tout ce qui vous semble bon, de n'être responsable que devant soi-même
et de remettre en question, constamment, tout ce qu'on pense et tout le monde."
Jean-Paul Sartre.
L'âge de raison, 1945.

Acknowledgements

I am deeply grateful to my parents Helena and Florentino (*in memoriam*), who brought me up in wholesome home and whose values passed to me, and to my grandfather José Rodrigues (*in memoriam*), who taught me to pursue knowledge and always stimulated my creativity and reasoning. Thank you for all your support and advice.

I would like to thank my colleagues and friends for the support throughout these years of research and learning: Kainã Terto, Guilherme de Aquino, Liêve Ferreira, Camila Stavola, Rebeca Cardim, Raul Montagne, Euzébio Simões Neto, Guilherme de Almeida, André De'Carli, Fábio Lopes, Mario Pereira, Victor Hugo de Holanda, Thiago Sobral, Plínio Ribeiro, Eglanio Pessoa, Clarissa Cozzi, Lucas de Queiroz, Paulo Cesar Pereira, Rafael Bibiano (*in memoriam*), Alejandro Fonseca, Wilmer Cordoba, Victor Manuel Martinez, Elizane Moraes, Leonardo Dornelles, Paulo Guerra, Tiago Araújo and to all those who were part of my life in recent years but I am not able to remember right now. Special thanks to my dear friends Cecília Veras Campos and Tiago Saraiva for being ever-present and for their help during the writing process.

I also would like to thank my supervisors professor Sérgio Coutinho and professor Gustavo Camelo Neto as well as the master's dissertation board members professor José Soares Jr. and professor Marcelo Gomes for the enlightening discussions and relevant comments on the manuscript. In addition I would like to thank professor Henrik Jensen (Imperial College) for the brief but encouraging conversation during the poster session at the XXXVI Brazilian Meeting on Condensed Matter Physics, 2013.

Finally, I would like to express my gratitude to Sérgio Coutinho and Raul Montagne for their guidance and confidence. They have believed in me even when I though that I wouldn't make it, and I am ever grateful.

This work only was possible due the financial support from FACEPE, CNPq and CAPES.

Abstract

In the present work, the spread of forest fires in heterogeneous environments is studied through cellular automata (CA) models, that are commonly used to simulate contact processes, and display a critical self-organized dynamics. The concept of self-organized criticality (SOC) is related to the ability of a dynamical system to evolve towards a critical phase spontaneously. The signature of these processes is the scale invariance (power-law behavior) of its observables. The forest fire model proposed by Drossel and Schawbl (DSFFM) in 1992, regards an homogeneous population of trees and its fire-size and fire duration distributions suggest typical SOC behaviors. In the other hand, the literature reports wildland fires whose frequency-area histograms are either power-law distributions or 'heavy-tailed' distributions. In 2011, Camelo-Neto and Coutinho proposed a CA model in which two distinct populations of trees are considered: one comprising trees with low flammability (with a parameter R of resistance to ignite) and the other composed by high flammability (susceptible trees). Aiming to generalize this model, some ingredients have been added in order to amplify or constrain the effective reach of the fire spreading. By increasing the reach of the interactions, the system performs fires that spread more like a 'field' of heat than like a contact process as in the DSFFM. Another novel aspect of the model – related to the heterogeneity of the population – is the addition of a fraction s of forbidden sites (randomly placed), at which trees are not allowed to sprout. Moreover, theses forbidden sites do not interact with fire. Results have showed that the fire-size distributions can display either a 'heavy-tailed' behavior or a power-law behavior, depending on the resistance parameter R and on the fraction s of forbidden site.

Keywords: Forest-fire model. Spreading model. Forest fires. Self-organized criticality.

Resumo

Nesta dissertação, a propagação de incêndios em florestas heterogêneas é estudada através de modelos de autômatos celulares (AC) que descrevem processos de propagação por contato e apresentam características de uma dinâmica crítica auto-organizada. O conceito de criticalidade auto-organizada (CAO) está relacionado com a capacidade de um sistema dinâmico evoluir espontaneamente para um estado crítico. A assinatura desses processos é a invariância de escala (comportamento tipo lei de potência) das distribuições de certas grandezas observáveis. O modelo de incêndio florestal proposto por Drossel e Schawbl (DS), em 1992, considera apenas florestas homogêneas e as distribuições de tamanhos e duração das queimadas encontradas sugerem a existência de um estado crítico auto-organizado. A literatura, no entanto, reporta incêndios reais cujos histogramas de frequência de tamanho apresentam tanto distribuições tipo lei de potência, quanto casos de distribuições com "caudas pesadas". Em 2011, Camelo-Neto e Coutinho propuseram um modelo de AC, onde são consideradas duas populações de árvores distintas, uma com baixa inflamabilidade, árvores com distintos graus R de resistência à ignição, e outra com alta inflamabilidade, ditas árvores susceptíveis. Com o intuito de generalizar o modelo, alguns ingredientes foram adicionados de modo a ampliar ou limitar o alcance efetivo da propagação do fogo na vizinhaça de uma árvore em chamas. O aumento do alcance das interações produz incêndios que se propagam como um "campo de calor", desta forma difere dos processos de contato característicos do modelo DS. Outro novo aspecto do modelo para explorar a heterogeniedade da floresta foi a inclusão de um fração s de sítios proibidos (distribuídos aleatoriamente) nos quais árvores não podem brotar, além disso eles também não interagem com o fogo. Os resultados alcançados mostram que as distribuições de tamanho dos incêndios podem exibir tanto um comportamento de "cauda pesada", como comportamento tipo lei de potência, dependendo do ajuste do parâmetro de resistência R e da concentração s de sítios proibidos.

Palavras-chave: Modelo de incêndio florestal. Modelo de propagação. Incêndios florestais. Criticalidade auto-organizada.

List of Figures

List of abbreviations and acronyms

CA	Cellular Automata
DSFFM	Drossel-Schawbl Forest-fire Model
FFMIT	Forest-fire Model with Immune Trees
FFMRT	Forest-fire Model with Resistant Trees
GoL	Game of Life
SOC	Self-Organized Criticality

Contents

Chapter 1

Introduction

"Systems in balance or equilibrium,
by definition, do not go anywhere."
Per Bak[†]

In recent years, wildfire risk has been increasing in many regions of the world due to warmer temperatures, more frequent droughts and changing precipitation patterns. Climate change has unleashed longer and more intense fire seasons[50]. On this background, a shed fire can lead to an awful destruction, which is precisely what happened in Lake County, California, in September 2015. Due to several causes, the blaze that started at Boggs Mountain State Forest rapidly became an inferno. A complete burn scar is showed in Figure 1.0.1. The red and grey shades image was composed by infra-red band data collected by OLI[*] on Landsat8 satellite[9] in September 20th, 2015; which was overlaid on a Google Earth image (from March 13th, 2016), in order to give a perception of the whole region. The charred landscape are orange-red, whereas unburned forests appear grey and buildings are white. The Valley Fire, as it was called, has become the third most damaging fire in California[10].

In the literature, it can be found several analyses of wildfires from all around the world: Brazil[26, 93], Canada[54], China[97], Italy[61, 102], Japan[96], Portugal[65], USA[68, 76]. Moreover, the analysis of frequency-area histograms shows either power-law distributions or heavy-tailed distributions[**] [64, 67, 69, 83, 84, 107, 126]. This has given rise to speculations on whether wildfire regimes could drive forests to self-organization.

The concept of self-organized criticality (SOC) is related to the ability of a dynamical system to spontaneously evolve to a critical phase; that is, instead of a temperature-like parameter, the tuning is consequence of the resultant interaction among its elements, which

[†] From "How Nature Works: the Science of Self-organized Criticality"[17].
[*] Operational Land Imager[12].
[**] Probability distributions that neither have exponentially bounded tails[8], nor they are purely power-law distributions.

drives the system towards a critical phase. The signature of critical self-organized processes is the scale invariance of the observables, i.e. distributions displaying power-law behavior. In other words, it is the absence of a characteristic length scale: not because it does not exist, but due to the fact that several length scales are coexisting. The Drossel-Schawbl forest-fire model (DSFFM)[34] is a paradigmatic SOC model, assembled on a cellular automata (CA) template, where the most studied observables are the avalanche size and its duration at the stationary state of a homogeneous forest.

In ecology, an important definition is the concept of flammability, which characterizes the ease of burning. As a system variable, flammability can summarize many aspects of the tree[103], such as moisture content, chemical make-up (lignin, cellulose), size (thickness) and shape (trunk bark). Camelo-Neto and Coutinho[25] have studied the DSFFM with two distinct populations, one comprising trees with low flammability (resistant trees) and the other composed by high flammable trees (susceptible trees). Furthermore, the interaction takes place within the Moore neighborhood, which comprises the eight nearest neighbors of a given site on a square lattice. In this CA model, the fire spreading rules are deterministic: susceptible trees need at least one burning neighbor to ignite and, in the other hand, resistant trees need a number R of burning neighbors to ignite.

In the present work, some ingredients have been added to the forest-fire model with resistant trees, in order to either amplify or constrain the reach of the fire. By generalizing the Moore neighborhood to higher ranges than its default 8 neighbors, the system performs fires that spread more like a field of heat than like a contact process. Hence the fire becomes capable of tunnelling barriers of resistant trees or even empty sites. Another novel ingredient of the model is that it includes a fraction of random forbidden sites, i.e. blocks. These blocks are inert sites that behave as an empty site, but at which a tree can not sprout. The model details will be depicted in chapter 4. Throughout chapters 2 and 3, it will be presented some of the model foundations, such as cellular automata models and complex system. The most relevant results will be presented and discussed in chapter 5. All figures and graphics on the text have been made by the author (using Gnuplot software[119]), except whenever indicated.

All increments on the forest-fire model have showed more clearly that the fire size and duration distributions can display either a heavy-tailed behavior or a power-law behavior, depending on the resistance parameter R and on the fraction of forbidden sites s. The results corroborates the possibility of developing cellular automata models by relying on underlying physical arguments that could simulate more realistic wildfire regimes. In a near future, these models may contribute to new perspectives in forest fire suppression and prevention.

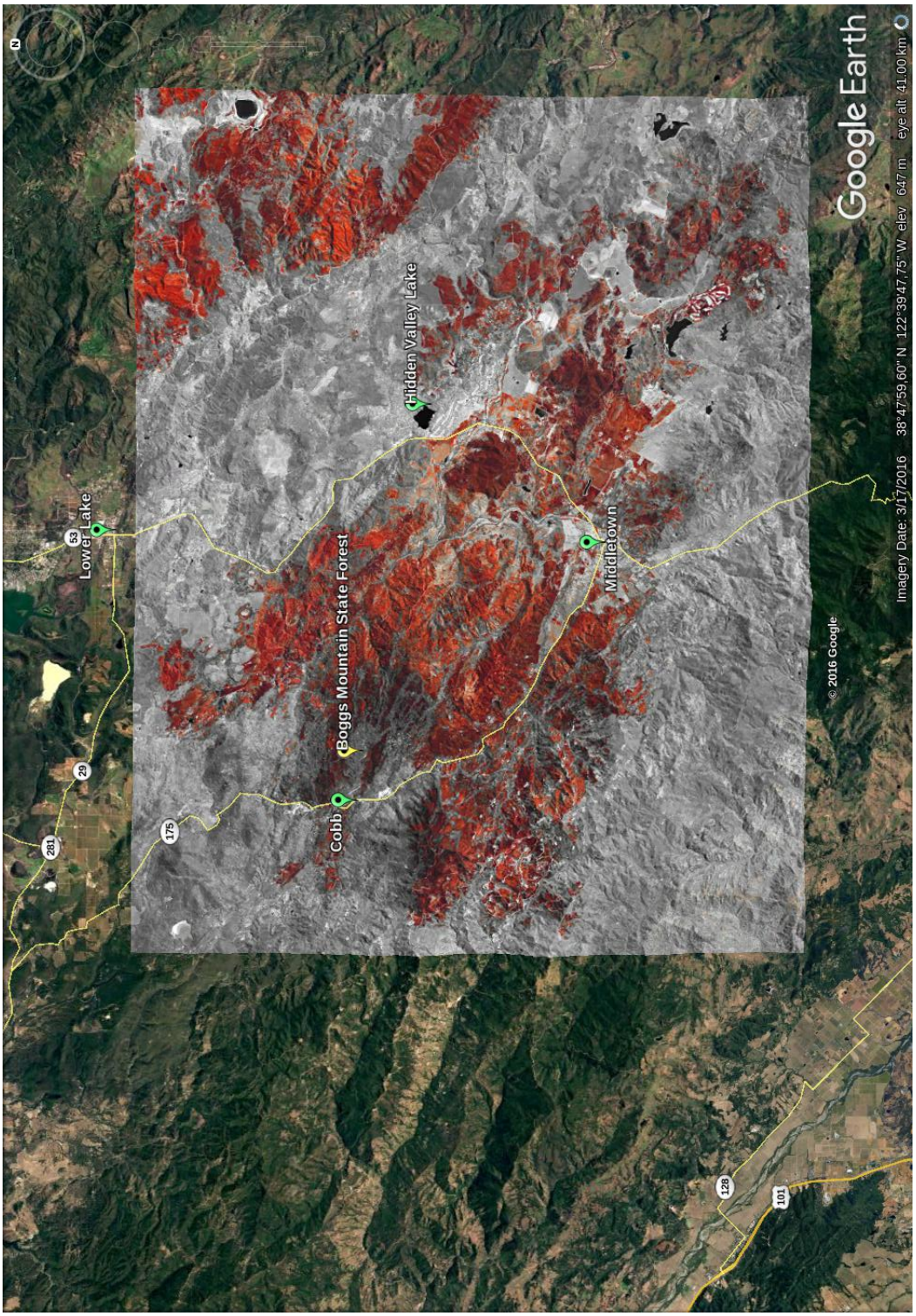

Figure 1.0.1 – Infra-red image of a burn scar from NASA's Earth Observatory[10] overlaid on a Google Earth landscape image. The grey-red shades rectangle has sides around 31 km and 24 km, an area of nearly 744 km^2. According to the California Department of Forestry, the fire had burned nearly 284 km^2 as of September 22, 2015. The burn scar in north-east region of the screen (*top left*) is due to a previous wildfire (Rocky Fire, August 4, 2015[11]). Infra-red image: the newly burned landscape are orange-red, unburned forests appear grey and buildings are white.

Chapter 2

Cellular automata

" ... began to suffer from the computer disease,
that anybody who works with computers now knows about.
The disease with computers is that you play with them."
Richard P. Feynman[†]

A cellular automata (CA) can be loosely described as a set of fixed cells, each one labeled with a state, spread over a lattice and a transition rule, which depends on its own current state and the current state of its neighbors. The system evolves with discrete rather than continuous time, thus at each step a cell may change its state – only if the transition rule has been satisfied. An automaton is a sort of abstract machine that can resolve an algorithm using logical propositions.

Throughout this work it will be presented definitions and models mostly related to bidimensional cellular automata models, when otherwise it shall be indicated. This chapter starts with a brief note on the background of the main ideas of CA models as well as its conceivers, section 2.1. In section 2.2, the CA will be properly defined and its frameworks described in section 2.3. A major example comes in section 2.4 and, at last, dynamical classification and applications are reported in section 2.5.

2.1 A brief historical note

The first CA model was idealized, during the 1940s, by the hungarian-american mathematician John von Neumann. Driven by the self-reproduction ability of a biological organism, he was interested in *what kind of logical organization is sufficient for an automaton (an artificial device) to be able to reproduce itself*[112]. As Christopher Langton stated[59],

[†] Adapted from "Surely You're Joking, Mr. Feynman!"[37].

> *"Von Neumann's approach to the problem of self-reproduction was a classically logico-mathematical one: If self-reproduction is being carried out by a (highly complex) biochemical machine, then that machine's behavior is describable as a logical sequence of steps, i.e. as an algorithm."*

Thus, inspired by Alan Turing's conception of a universal machine[108], von Neumann proposed the universal constructor, a machine that could build *any* machine described on its input and, moreover, it could make a copy of the input (the recipe) to be included on its output. In other words, the input information is treated as instructions that must be interpreted and executed in order to construct a machine, whereas that same input is dealt as uninterpreted information, which will be copied (unmodified) and attached to the output machine. von Neumann works were expanded and afterwards edited into a book by his colleague Arthur Burks.

It was Stanislaw Ulam, mathematician and von Neumann's collaborator, who suggested that the automata should be defined on a discrete space, that is, they should be sites in a regular lattice. Therefore, these sites would exchange information among themselves, while lying on a discrete space and evolving in discrete time. So each automaton was labelled with a state, i.e. a finite number or a color. Ulam is also known for the invention of the Monte Carlo Method[35].

The universal constructor invented by von Neumann has exhibited a high level of complexity, far beyond the capacity of any computer at that time, once it worked with a 29 states automaton and each cell had four neighbors – the nearest neighbors in a square lattice. This number of states has drastically decreased to 8 states in the CA model created by Edward Codd, in 1968[29]:

> *"A 8-state, 5-neighbor (the cell itself together with its four immediate, non-diagonal neighbors) space was discovered which is capable of supporting not only the computation and construction behavior sought by von Neumann, but also certain reading and copying behaviors which probably cannot be exhibited in his space."*

Codd's model was reviewed and modified by Christopher Langton, in one of his first papers on the subject[59]. Langton has implemented Codd's CA, but he had chosen to put aside Turing's universality criteria in order to reduce complexity, and by doing so he noticed the emergence of complex patterns like arrays of colonies of loops. So, by adapting the rules of Codd's CA, Langton's loops became the simplest self-reproducing CA ever discovered. As Langton wrote[59],

> *"These loops (...) are sufficiently complex so as to be quite clearly self-reproductive, yet, at the same time, they are sufficiently simple so as to constitute 'believable' extensions of simpler copying processes."*

In October 1970, the popular science writer and Scientific American columnist Martin Gardner published in his 'Mathematical Games' column, the description of a game created by the mathematician John Conway, *a fantastic solitaire pastime he calls 'Life'*[41], as Gardner stated. John Conway's game of life (GoL) would become, and perhaps remains, the best known CA model. Based in simple rules, the game can be played with *a fairly large checker-board and a plentiful supply of flat counters of two colors*[41]. Made of 2-state automaton, Conway's game mimics life and death, but although it's astonishing simplicity, complex patterns can arise from it (details on section 2.4). *Its proliferating cells resemble skittering microorganisms viewed under a microscope*, says Cownay's biographer Siobhan Roberts, in a recently released biography[86]. As she briefly wrote on the impact of the GoL[85],

> *"Practically speaking, the game nudged cellular automata and agent-based simulations into use in the complexity sciences, where they model the behavior of everything from ants to traffic to clouds to galaxies. Impractically speaking, it became a cult classic for those keen on wasting time. The spectacle of Life cells morphing on computer screens proved dangerously addictive for graduate students in math, physics and computer science,(...) Life went viral in the early-to-mid-1970s, one-quarter of all the world's computers were playing".*

This 8-neighbor template, that was used in the Conway's GoL, had been defined by Edward F. Moore back in 1962, in a paper entitled 'Machine Models of Self-Reproduction'[73]. Moore had a great interest in the study of finite automata, which is a more general concept that encompasses the cellular automata, as shall be seen in section 2.2. His 'Gedanken Experiments on Sequential Machines'[91], published in 1956, is considered one of the foundation stones of Automata Theory and early pioneer in what would be known as artificial intelligence.

In the early 1980s, as a computer revolution was underway, the whiz kid and physicist Stephen Wolfram, published an extensive work on the behavior of one dimensional CA[122]. Wolfram needs no introduction, his software Mathematica is widely used and already plays a fundamental role in scientific research, once it is a reliable source to proceed with complicated equations by solving them numerically, among other useful tools. Mathematica has guaranteed its creator *his way out of what he considers the bureaucratic tangles of modern science*[100]. On Wolfram's research with the elementary CA, he had proposed a bold aim[122]:

> *"The ultimate goal is to abstract from a study of cellular automata general features of 'self-organizing' behavior and perhaps to devise universal laws analogous to the laws of thermodynamics."*

His accomplishment was classifying the behavior of the elementary CA in four different classes, and furthermore three of these classes had a parallel with dynamical systems[121, 123]. The outlier was the so called class IV. In this meantime, Chris Langton had created his CA and had just achieved a position as Ph.D. student under the supervision of Arthur Burks. Upon being aware of Wolfram's work on classification of elementary CA, Langton decided to get to grips with problem and succeeded by discovering that class IV had resemblances to second-order phase transitions[58, 63, 113]. The connection between the CA classes and dynamical systems shall be detailed forth in section 2.5.

Back to 1953, the Nature magazine published three remarkable papers on deoxyribonucleic acid (DNA)[115, 118, 114], where one can read how the authors have *put forward a radical different structure*. Due to these papers, molecular biologists Francis Crick, James Watson and physicist Maurice Wilkins were awarded with the 1962's Nobel Prize in Physiology or Medicine *for their discoveries concerning the molecular structure of nucleic acids and its significance for information transfer in living material*[15]. Quoting Watson and Crick's articles,

> *"It has not escaped out notice that the specific pairing we have postulated immediately suggests a possible copying mechanism for the genetic material."*[115]
> *"(...) our proposed structure for desoxyribonucleic acid may help to solve one of the fundamental biological problems – the molecular basis of the template needed for genetic replication."*[114]

The interpreted and uninterpreted informations have a clear parallel with the molecular translation and transcription that takes place inside the cell. As author Mitchell Waldrop wrote[113],

> *"They* (Watson and Crick) *discovered that it* (DNA) *fulfilled von Neumann's two requirements precisely. As a genetic program, DNA encodes the instructions for making all the enzymes and structural proteins that the cell needs to function. And as a repository of genetic data, the DNA double helix unwinds and makes a copy of itself every time the cell divides in two."*

Today it comes as no surprise that a biological organism has within itself a code capable of replicate itself and, besides that, passes on some of its features to its offspring. These biological processes involve some algorithms, as von Neumann has conceived a decade earlier the discovery of the DNA structure.

2.2 Definition

Automata theory, a branch of theory of computation, is concerned with the mathematical models of computation, its definitions and its properties. A finite automaton, also known as finite state machine, is the simplest model of computation, being capable of perform tasks even when memory is extremely limited. This abstract machine is composed of a finite set of states Q, an alphabet Σ, a transition function, $\delta : Q \times \Sigma \to Q$, a start state, $q_0 \in Q$ and a set of final states, $F \subseteq Q$. Coarsely speaking, the transition function receives the start state along with the alphabet, these inputs are processed and, as result, it returns a final state. Consider this example adapted from Michael Sipser's book on theory of computation[94]:

The finite automaton M_1 is made of $Q = \{q_1, q_2, q_3\}$ states, the alphabet $\Sigma = \{0, 1\}$, transitions for input alphabet letter $\{0\}$ is $q_1 \to q_1$, $q_2 \to q_3$, $q_3 \to q_2$ and for alphabet letter $\{1\}$, $q_1 \to q_2$, $q_2 \to q_2$, $q_3 \to q_2$, the start state is $q_0 = q_1$ and the final state set, $F = \{q_2\}$. For the machine M_1 is used the simplest output, Yes/No, i.e. a binary output.

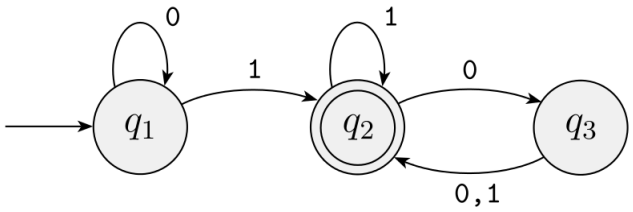

Figure 2.2.1 – Scheme of the finite automaton M_1 while it is processing the input string 1101. From Michael Sipser's *Introduction to the Theory of Computation*[94], section 1.1.

If the machine M_1 receives an input string 1101, it will processed like:

1. Start in state $q_0 = q_1$.
2. Read 1, proceed with transition $q_1 \to q_2$.
3. Read 1, proceed with transition $q_2 \to q_2$.
4. Read 0, proceed with transition $q_2 \to q_3$.
5. Read 1, proceed with transition $q_3 \to q_2$.
6. Output 'Yes', because M_1 is in a final state, q_2. ■

This kind of machine resembles a Markov chain, which in fact is the probabilistic counterpart of a finite automaton. For its simplicity and low memory cost, applications of finite automata are widely spread and they are specially useful in programming the logic port of electromechanical devices, for example, automatic doors.

A cellular automata can be described as a set of finite automata defined on the cells of a $\mathcal{D}$-dimensional lattice. Each automaton takes as input its own state and the states of its nearest automata within a previously defined neighborhood. A neighborhood template

Γ has dimension $\mathcal{D}_\Gamma \leq \mathcal{D}$ and its size $\mathcal{N}$ is given by the number of sites covered by Γ. The transition rule is a function of the automaton input, so its output is based on the neighbors' states. At each time step t, the transition rule puts together the state of the main site and the states of its neighbors, then it sets the new state of the automaton, which will be labelled in the next step, $t+1$. The transition rule is determined before the process begins and for each input configuration it releases a new state to the main site. As a matter of fact, the transition rule is a set of transition rules, once there is a rule for exchanging state on each local setup. After the transition rule has assessed all configurations, the automata shall evolve to their new states. The state changing is synchronous, that is, all automata have their states updated at the same time step. Consider the following example[58]:

Suppose that a cellular automata is defined on a square lattice, with four nearest neighbors, $\mathcal{N} = 4$, and each cell has eight possible states, $\Delta = 8$. The set of possible neighborhood states Σ is given by the number of states to the power of the number of neighbors plus one, that is $|\Sigma| = \Delta^{(\mathcal{N}+1)} = 8^{(4+1)} = 32,768$ states. For each of these, there is a choice of eight new states for each main cell, so there are $\Delta^{|\Sigma|} = 8^{8^5} = 8^{32,768} \approx 10^{30,000}$ possible transitions, an outstandingly large number to be taken into account. ■

After this example, it is relevant to observe that the set of possible states within a neighborhood plays a similar role that the alphabet does in the finite automaton model. Indeed, a transition rule can be written in the form of a transition function, i.e., the transition function $\delta : Q \times \Sigma \to Q$ turns to be a transition rule $\delta_\Gamma : \Delta^{(\mathcal{N}+1)} \to \Delta$. The transition rule, in addition to its local feature, is spatially homogeneous, which means that it does not depend explicitly on the cell position, although in particular cases the rule can be adapted to deal with, and even create, spatial inhomogeneities.

After the transition rule has received its input, it can return different outputs, giving the model another feature and so a CA model can be classified as deterministic or probabilistic. The deterministic CA has a new state settled for each possible local configuration. For example, assume that the cell states may be either 0, 1, 2 or 3. If the sum of the neighbors' states is even, the new state is 2, otherwise the new state is 1. On the other hand, in a probabilistic CA the transition to a new state takes place with a certain probability, that is, it is not completely determined by the input configuration. Taking the previous example to the probabilistic model, we have that if the sum of the neighbors' states is even, there is a probability ρ of having 2 as new state and a probability $(1-\rho)$ of getting state 3, otherwise, if it is an odd number, the new state is 1.

2.3 Geometry, neighborhood and boundaries

In CA models, geometry is an extremely relevant aspect as a different number of neighbors or changes in the boundaries can perform drastic responses in the dynamics, i.e.,

it can lead systems with equal initial settings and the same transition rules to completely unmatching configurations. As mentioned previously, cellular automata are defined on a regular lattice. In a 2-dimensional space, the only regular geometries that form a regular tessellation are triangular, rectangular (square) and hexagonal[16]. The triangular and hexagonal lattice exhibit a planar duality, i.e., the triangular (hexagonal) lattice is the planar dual of the hexagonal (triangular) lattice. The square lattice, on the other hand, is said to be self-dual[47]. The minimum number of neighbors that a site may have are the nearest neighbors (see Figure 2.3.1). A triangular lattice displays 3 nearest neighbors, whereas the square lattice has 4 and hexagonal lattice, 6.

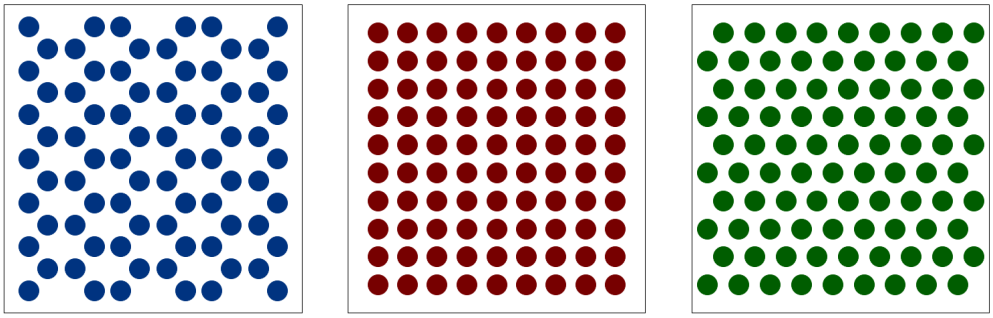

Figure 2.3.1 – Regular tessellation of the plane: triangular lattice (*dark blue*), square lattice (*dark red*) and hexagonal lattice (*dark green*).

Several types of neighborhoods can be defined in the square lattice[70], but the most popular are due to John von Neumann[112] and Edward F. Moore[73]. In both neighborhood schemes it is defined a range r ($\in \mathbb{Z} : r > 0$), which sets how far the interaction goes. The templates for $r = \{1, 2, 3\}$ are shown in Figure 2.3.2 and Figure 2.3.3. The main site in the von Neumann neighborhood, $\Gamma^{[vN]}$, has $2r(r+1)$ neighbors, while in the Moore neighborhood, $\Gamma^{[Mo]}$, has $(2r+1)^2 - 1$ neighbors. These neighborhoods are defined in Equation 2.1 and Equation 2.2, where x_0 and y_0 stand for the coordinates of the main site[117, 116]. Throughout this work, it will be referred to the Moore neighborhood of range $r = 1$ simply as Moore neighborhood, when otherwise it shall be indicated. It also applies for the von Neumann neighborhood of range $r = 1$, which will be simply called von Neumann neighborhood.

$$\Gamma^{[vN]}_{(x_0,y_0)} \equiv \{(x, y) : |x - x_0| + |y - y_0| \leq r\} \tag{2.1}$$

$$\Gamma^{[Mo]}_{(x_0,y_0)} \equiv \{(x, y) : |x - x_0| \leq r\,,\ |y - y_0| \leq r\} \tag{2.2}$$

At this point, a question that naturally arises is with whom the last column will interact to the right and who will be the neighbors of the top line from above? Otherwise, with whom the bottom line shall interact from below and who are the neighbors to the left

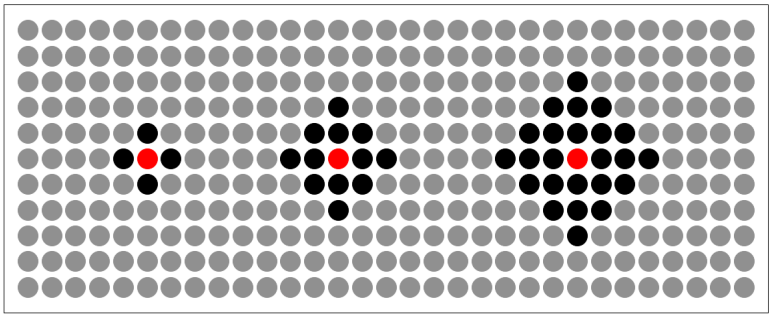

Figure 2.3.2 – von Neumann neighborhood for $r = \{1, 2, 3\}$. Range $r = 1$ spans 4 neighbors, while $r = 2$, 12 neighbors and $r = 3$, 24 neighbors. Main cell (*red*), neighbors (*black*) and cells that do not interact with the main cell (*grey*).

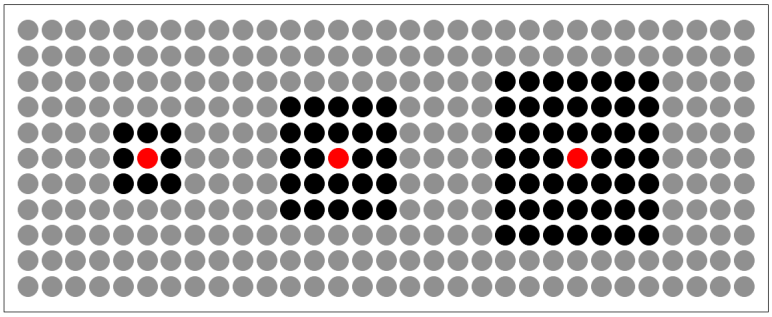

Figure 2.3.3 – Moore neighborhood for $r = \{1, 2, 3\}$. Range $r = 1$ spans 8 neighbors, while $r = 2$, 24 neighbors and $r = 3$, 48 neighbors. Main cell (*red*), neighbors (*black*) and cells that do not interact with the main cell (*grey*).

of the first column sites? These are the last, but not least, fundamental attribute when defining a grid. For a lattice of size L^2, with grid indexes L_x, L_y ($\forall \in \mathbb{Z} : 1 \leq L_i \leq L$), the trivial answer, is about building a boundary around the whole lattice, so that the lattice earns two more indexes, 0 and $L + 1$. Then cells with fixed state are placed on this new external layer, known as fixed boundary. Computationally, the problem is solved, but for most simulations of physical systems, that is a bad choice. Most simulations of many-particle systems require as many particles and space as possible, chasing the thermodynamic limit, where $N \to \infty$ and $V \to \infty$, such that $N/V = const$ [106]. When the cells of the boundary layer are labelled with fixed states, these walls become damping points for the whole dynamics, which makes them an undesirable constraint. Another solution for the boundaries sites, is to turn them into a mirror for their neighbors, the so called reflexive boundary. For confined particles or systems like billiards this may be friendly solution, but not for short-range interactions models like CA models, where it reduces the damping but does not help on reaching the thermodynamic limit.

In order to solve the 'damping walls' problem and get a better approach to the thermodynamic limit, the CA can be defined on a torus, i.e., the lattice is a grid embedded in a torus (see Figure 2.3.5). Which means that if a particle is released in this geometry

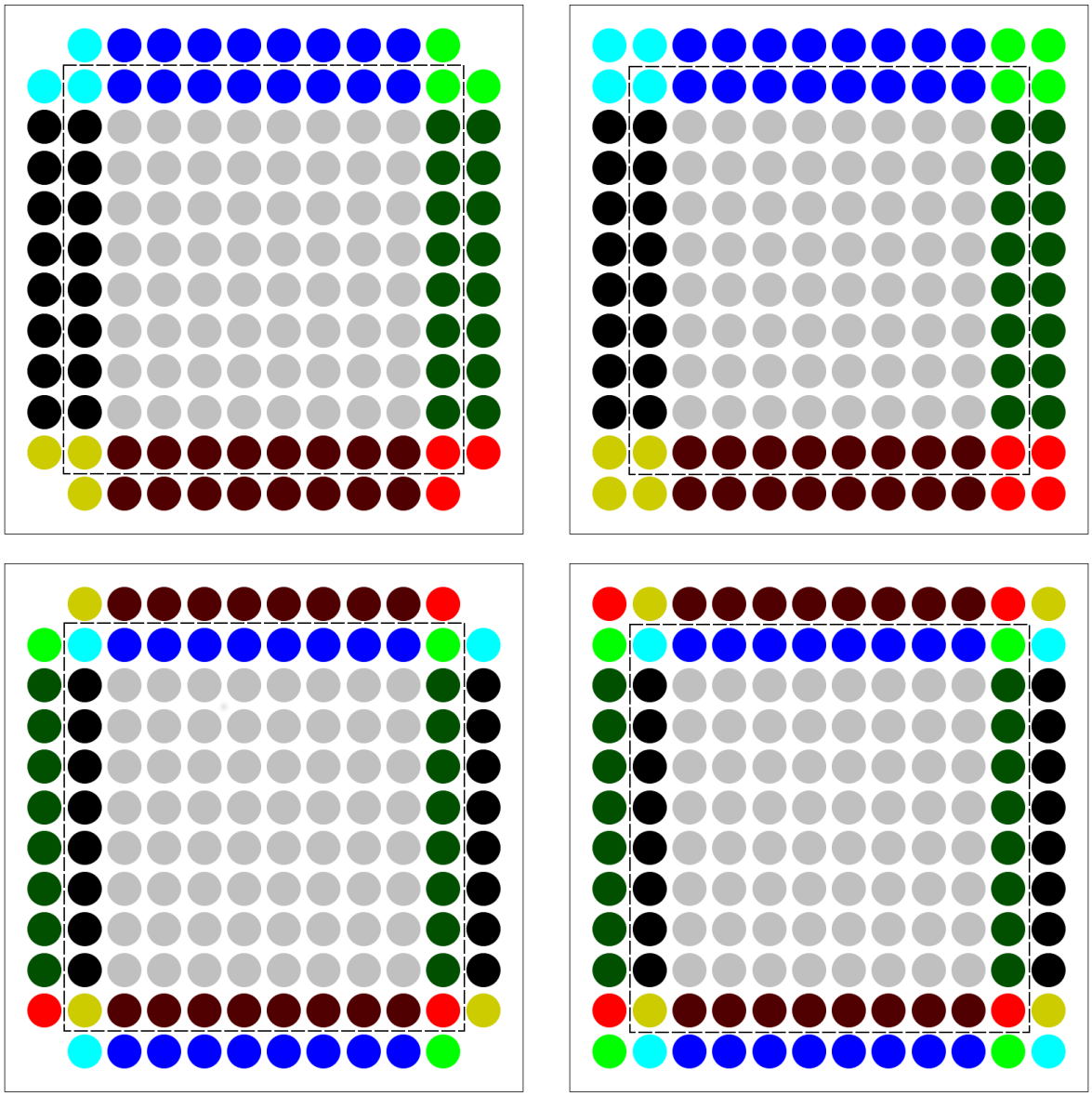

Figure 2.3.4 – Reflexive boundaries (*top*) and periodic (toroidal) boundaries (*bottom*) for von Neumann neighborhood (*left*) and Moore neighood (*right*), both with range $r = 1$. The *dashed line* surrounds the defined sites and *grey* dots represent the core cells – which neighbors are defined straightforward. Identical lines and columns have matching colors (*red, light green, light blue, black*), likewise for corner dots (*brown, yellow, pink, dark blue*).

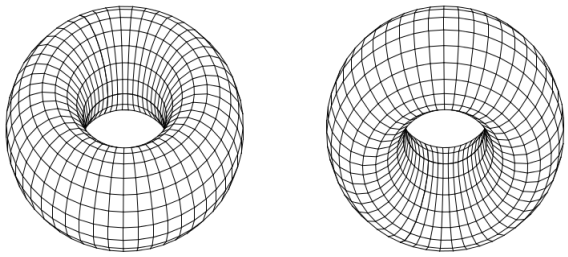

Figure 2.3.5 – Two tori, with the same size, covered with a rectangular grid.

(with finite momentum), it may hover around forever because of the absence of absorbing walls to get it moored. A grid defined over a torus is indeed a regular lattice with periodic boundaries, that is, both L_x and L_y are periodic coordinates. This procedure makes the dynamics more realistic, once the particles can drift freely over the torus surface, and besides that, it is a computational trick aiming to get closer to the thermodynamic limit. Figure 2.3.4 shows diagrammatic frames of both reflexive and periodic boundaries.

2.4 Conway's game of life

Enough have already been said about GoL since its publication in Gardner's column. All sorts of configuration have been tested, structures (animals) have been cataloged, applications have been proposed and theorems have been proved. There is a massive quantity of articles and textbooks, online videos and even online interactive software[111]. Still, the GoL continues to be a stunning example of how the simple rules of a CA can gear together in order to create such outstanding and unpredictable patterns. In this section, GoL rules will be built from approximations depicting elementary aspects ascribed to a population of living beings and afterwards try to have a glimpse of how this population behaves through time.

So, how to start building a model of life? As any scientific model, it shall begin as simple as possible, one should say the 'zeroth-order' approximation. Then enters death, which is the very antagonist of life, representing either 'non-born' or the 'after-live', that is all non-living entities, the void. A sort of binary model of life is already built. The second step could be related to the collective aspect of living, the first-order approximation. It is where the CA model plays his role, many living beings each one having a fixed address, thus it has became a binary life CA model. But nobody lives alone, hence couples (or groups) of beings may give birth to an offspring, thus the second-order approximation. So far, nothing was said about dying, only life has been regarded. As equilibrium is needed, neither a being can live a lonely life nor it can live on in a crowded environment, which is, at last, the third-order approximation of this life model. These simple approximations may be defied by a skeptic, but up until the moment that he puts an eye on the screen

and get dazzled by a swarm of blinking points.

The assumptions made for an 'approximated' model of life are similar to Conway's game rules. As already said, GoL is a CA defined on a square lattice, with Moore neighborhood and with periodic boundaries. The rules are the following:

- Birth rule: At time step t, if a dead cell has 3 live neighbors, then at time step $t+1$ the cell becomes alive.
- Survival rule: At time step t, if a live cell has 2 or 3 live neighbors, then at time step $t+1$ the cell remains alive.
- Death rules:
  - ▷ At time step t, if a live cell has at most 1 live neighbors, then at time step $t+1$ it dies due to isolation.
  - ▷ At time step t, if a live cell has at least 4 neighbors, the at time step $t+1$ it dies due to overcrowding.

In order to understand some of its features, the model will be assembled in a square lattice with linear size $L = 100$ and with a random initial configuration, that is, the live cells are spread randomly over the lattice, and then the game is ready to be tested. The initial density ρ_0 is the only parameter to be controlled, all others are due to intrinsic movements of the game. The live population density ρ varies in time, $\rho \equiv \rho(t)$. By the way, discrete time in the language of the GoL is not accounted in steps, but in generations, $t \equiv t_g$, to clearly remind the birth of a new offspring. The density $\rho(t_g)$ is the normalized number of live cells, i.e., the number of live cells N at generation t_g, $N(t_g)$, divided by the total number of cells, which is just the number of sites displayed on the lattice, L^2. So, $\rho(t_g) = N(t_g)/L^2$.

Figure 2.4.1 displays frames of a game that has started with $\rho_0 = 0.5$, which can give an idea of the evolution of the community through some generations. The zeroth generation, $t_g = 0$, is composed of randomly chosen live cells, as already said, and are represented by dark red dots. The red dots stand for 'newborn' cells, that is, live cells that were dead cells in the previous generation. The black dots are the 'mature' cells, which were alive in the previous generation. This color setting makes easier to segregate static clusters of cells from the oscillators, i.e. stationary, but dynamic. Just in the first iteration, the density quickly decreases. The generation $t_g = 100$ has an even lower density, around one percent, but it is possible to recognize many 'life-forms', like blinkers, blocks, (long) boats, beehives, two loaves and one pond. Generation $t_g = 500$ even shows one longbarge and one toad. In generation $t_g = 1,000$, although low, reactivity remains, but it ceases completely before generation $t_g = 2,000$. At the end, $t_g = 10,000$, the screen shows a very sparse configuration, with static clusters and simple oscillators (blinkers). Now, what would happen if the game had been started with a different ρ_0? Does any random initial configurations fade away or there is some that escalates? Some answers are given in

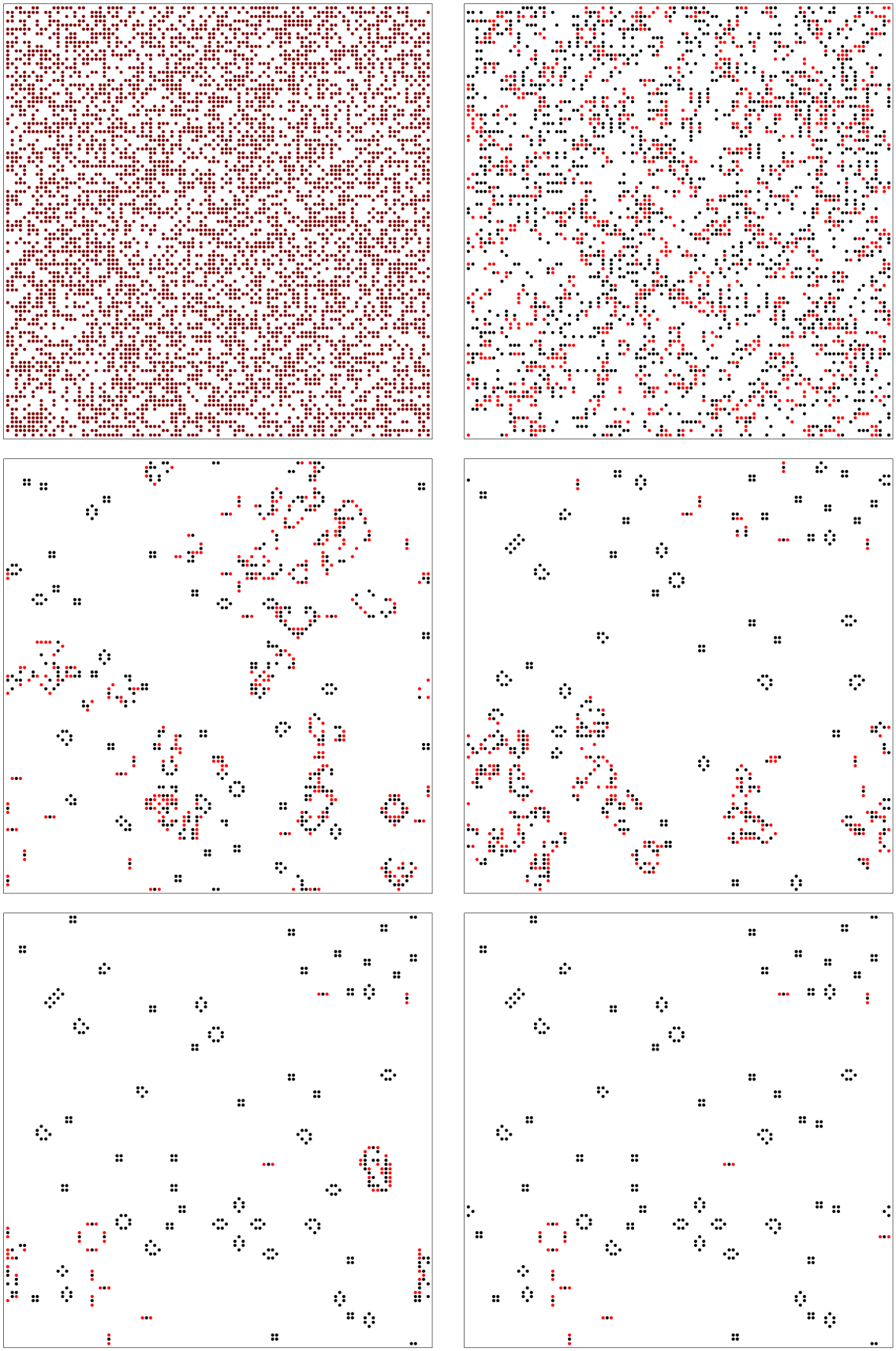

Figure 2.4.1 – Random configuration with $\rho_0 = 0.5$ (*top left*). First generation, $t_g = 1$ (*top right*). Generations $t_g = 100$ (*middle left*), $t_g = 500$ (*middle right*), $t_g = 1,000$ (*bottom left*). Last generation, $t_g = 10,000$ (*bottom right*). Random live cells (*dark red*), 'mature' live cells (*black*), 'newborn' live cells (*red*). Dead cells are left white colored.

Figure 2.4.2.

Several rounds of the game have been played for each $\rho_0 = \{\, 0.05, 0.1, 0.2, 0.3, 0.4, 0.5, 0.6, 0.7 \,\}$, but only one was picked to compose Figure 2.4.2. Clearly, for any initial population, the system never escalates, that it, none of the theses random configurations evolve to an unbounded growth. Indeed, it had been predicted in the very conception of the game that *there should be no initial pattern for which there is simple proof that the population can grow without limit*[41]. For the trials made here, all population fades away, becoming too sparse and with a remnant density near three percent, except for $\rho_0 = 0.05$ that goes lower.

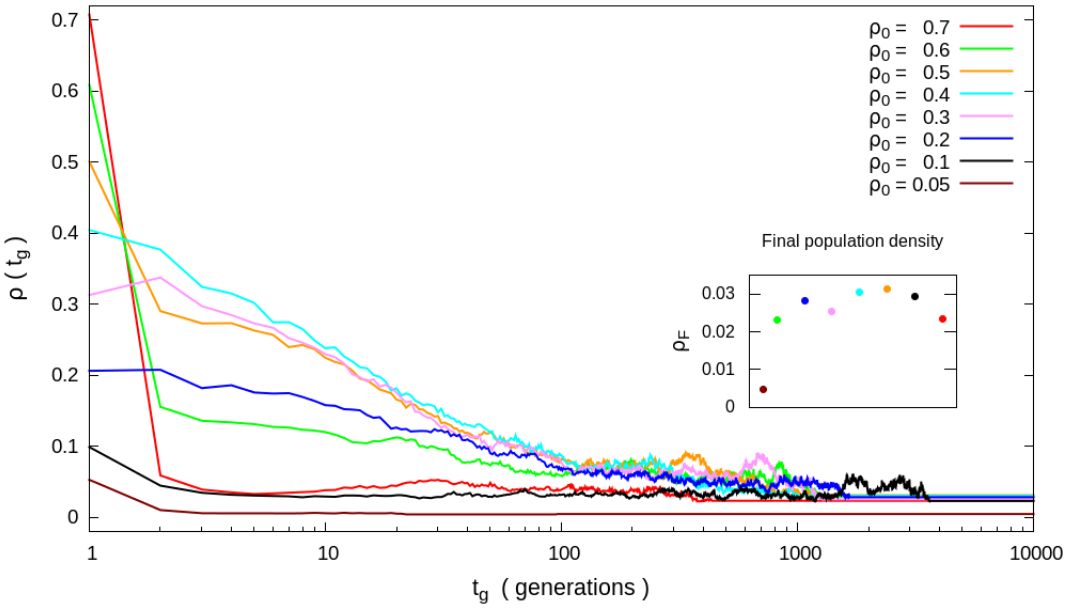

Figure 2.4.2 – Mono-log graph of the GoL population density $\rho(t_g)$ as function of time t_g, in generation units.

As it seems, the curves in Figure 2.4.2 have four different phases. In the very beginning, the density either slightly increases ($\rho_0 = \{0.2, 0.3\}$), slightly decreases ($\rho_0 = \{0.05, 0.1, 0.4\}$) both due to the randomness or dramatically decreases ($\rho_0 = \{0.5, 0.6, 0.7\}$), due to overcrowding – rounds with $\rho_0 = \{0.8, 0.9\}$ also were done, although not displayed in Figure 2.4.2 because their curves show an even steeper behavior than $\rho_0 = 0.7$. The second phase shows an exponential decaying, followed by a fluctuation around a stationary density, which characterizes the *self-sustained* third phase. At last, all ongoing activity ceases suddenly – but oscillators, e.g., blinkers – and the density curve becomes flat, reaching an *absorbing state* with final population density constant, $\rho_F = const$. These phases are consistent with the asymptotic behaviors $\rho_0 = 0$ and $\rho_0 = 1$, where no offspring is born and the whole colony collapses in the first generation, respectively.

As seen so far, the long-term behavior of the game is not so interesting, once it does not remain self-sustained but it fades into an absorbing state instead. It is true that

GoL has special patterns that keep the dynamics going on indefinitely, but not from a random population. Although the time scale in a CA model can be defined depending on its propose, the long-term behavior is relevant when modelling real life, since for humans a generation is defined around 20 years, instead for a colony of ants is 1 day and for some bacteria, even less. It is important to notice that the game has been played with $L^2 = 10^4$ cells, which may not be large enough whenever one is concerned with long-term behavior. So, if the lattice size is increased, it is possible to get longer times of self-sustained behavior than the ones found here. Indeed, in a trial made with $\rho_0 = 0.5$ and population $L^2 = 10^6$ cells, at generation $t_g = 10,000$ the game still self-sustained, but fades away few generations later*.

Despite the small lattice size ($L^2 = 10^4$ cells), this qualitative analysis reveals the emergence of an absorbing state when GoL is initialized from a random distribution of live cells. Other relevant dynamical aspects of GoL were investigated by Gomes *et al.*[44], among which is reported that before the self-sustained phase, the density of live cells evolves as $\rho \approx t_g^{-0.39\pm0.04}$. This power-law behavior was found for some ρ_0 values (10 experiments each) within the interval $0.15 \leq \rho_0 < 0.75$, on a lattice of linear size $L = 300$ – approximately tenfold larger than the lattice considered in the current example.

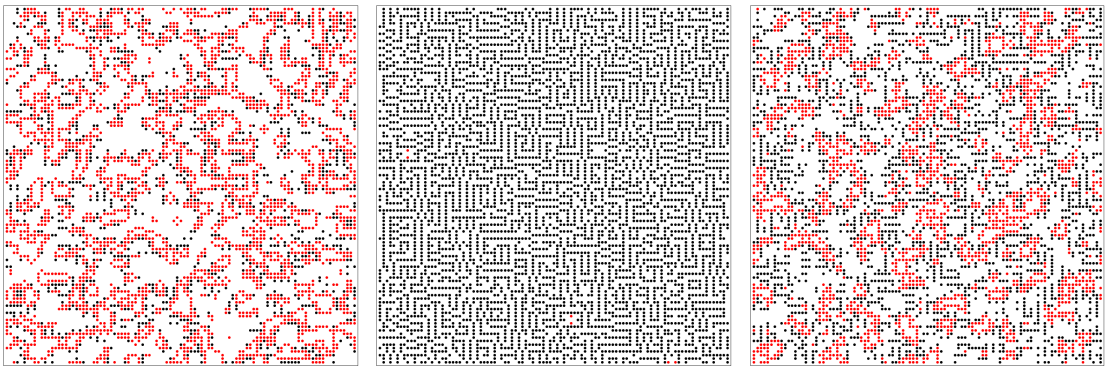

(a) (b) (c)

Figure 2.4.3 – Frames of modified GoL randomly initialized with $\rho_0 = 0.5$, at generation $t_g = 1,000$. 'Mature' live cells (*black*), 'newborn' live cells (*red*). Dead cell are left white colored.

Any minimal changing in the rules of a GoL leads to utterly distinct patterns (Figure 2.4.3). For example, if one changes the birth rules to include that dead cell with one or two live neighbors can be alive in the next generation, it arises a dense, quickly blinking, wave-like pattern (Figure 2.4.3a). Whether the survival rules are changed in order to include that a live cell with four live neighbors still alive in the next generation, it creates a static structure that resembles a maze (Figure 2.4.3b). At last, if one gets these

* "Monte Carlo simulation suggests that a disordered state of N^2 cells usually evolves to a steady state within about N^2 time steps (and typically an order of magnitude quicker); very few of the 2^{N^2} possible configurations are visited."[122]

two modified rules and gear them together, it results in *a maze where all of the walls all continually change*[71] (Figure 2.4.3c).

The road so far may lead to some questions like, does any physical system behave like a GoL? How does it manage a self-sustained phase? Why a slightly change in the game's rules can provide unpredictable responses? Could any GoL configuration evolve to chaotic phase? These inquiries might be answered in the following section.

2.5 Classification and applications

2.5.1 Wolfram's classification and Langton's parameter

During the 1980s, Stephen Wolfram was chasing the idea of figuring out general laws that could explain the self-organization capacity found in some systems. Self-organization is a property that enables the system to organize itself, that is, a disordered system can evolve to an ordered structure without external interference, there is no tuning parameter. As previously mentioned (section 2.1), Wolfram developed an extensive empirical investigation on a simple model of CA, that he called elementary cellular automaton[122] (see Figure 2.5.1). An elementary CA is made up of an one-dimensional array of cells with Q states and $n = (2r + 1)$ neighborhood (including the main cell), where r $(\in \mathbb{Z} : r > 0)$ is the number of neighbors at each side of the main cell.

Figure 2.5.1 – Example of an elementary cellular automaton. It is composed by empty cells $q_0 = 0$ (*white dots*) and occupied cells $q_1 = 1$ (*black dots*).

The simplest possible configuration has 2-state cells, $Q = \{0, 1\}$, and range $r = 1$, which leaves each main cell with 2 neighbors. Wolfram analysed several data containing variations of the transition rules, other array sizes, different neighborhoods and even with 3-state cells. Afterwards, he noticed that the outcome patterns had distinct qualitative types, either they disappear with time, evolve to a fixed finite size, expand indefinitely but at a fixed speed or expand and contract irregularly. Thus, Wolfram proposed that the patterns could be classified in four distinct classes, three of them having a dynamical system counterpart[121, 123]. The classes are:

- Class I. The CA evolves to a spatially homogeneous state. The dynamical system evolves to 'limit points', also called stable fixed points.
- Class II. The CA evolves to simple stable or periodic structures. The dynamical system evolves to 'limit cycles' .
- Class III. The CA yields aperiodic patterns. The dynamical system is chaotic.

• Class IV. The CA yields complicated localized structures, including propagating structures. There is no dynamical system counterpart.

In the Class I patterns, all sites evolve to the same state, like simple 'limit points'. The spatial and temporal dimensions for such attractors are zero. For Class II structures, changes in its initial configuration modifies them only locally. Theses CA are either stable or periodic, with short period cycles. The Class III structures are highly irregular, but some of them can exhibit self-similar patterns which are scale invariant.

Class IV contains stable and periodic structures, apparently self-sustained once they can persist for an arbitrary long time, and some propagating structures. But despite that the behavior of the systems in this class is essentially unpredictable. As the array of cells is enlarged, the transient fluctuations is decreased, in classes I and II, i.e., it reduces fluctuations that take place before the stationary structures are settled. This does not happen in class IV, that is, the enlargement of the array does not reduce the reactivity of the structures.

A self-sustained activity was not a novelty in dynamical systems, its classic prototype is the van der Pol oscillator, that has been studied since the decade of 1920[98]. Neither was a surprise the self-organizing collective behavior leading to a stable, time independent patterns. The great question mark laid on the fact that this self-organization process had this dynamical, seemingly self-sustained attributes. The GoL has some members on this class, which the most prominent are the glider and the glider gun. The glider is a self-propelling structure that hovers around the lattice until it crashes in some other structure – it is the simplest among all GoL 'spaceships' (see Figure 2.5.2). The glider gun, on the other hand, is a glider factory, i.e., it is a larger structure in which cells are placed in a very special way that enables it to assemble a glider and shoot it into the lattice.

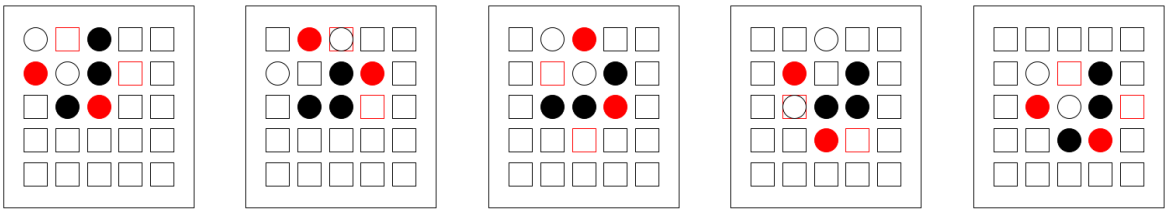

Figure 2.5.2 – The glider is the simplest self-propelling structure found in GoL. The snapshots show its complete periodic movement step by step – from left to right. 'Mature' live cells (*black filled circles*), 'newborn' live cells (*red filled circles*). Dead cells that were alive in the previous step (*white filled circles*); dead cells that become alive in the next step (*void red squares*); dead cells that remain dead in the next (or previous) step (*void black square*).

In the search for answers to the absence of physical analogy for class IV, Langton proposed a parameter λ to be used as tuning parameter[60]. Langton tested his parameter

in the framework he knew very well,a bi-dimensional CA with von Neumann neighborhood and 8-state cells, $Q = \{q_i \in \mathbb{Z} : 0 \leq q_i \leq 7\}$, where the only quiescent state is given by zero, $q_0 = 0$. The parameter can be smoothly tuned from zero to one, $0 \leq \lambda \leq 1$, and represents the probability for, in the next step, the main cell receives any non-zero state. Somehow, the λ parameter measures how much activity a transition will provide within its outputs, i.e., for lambda close to zero, there is only some sparse and rare reactivity structures in the lattice, otherwise if lambda is near one, the lattice is full of highly reactive cells.

Now Langton had a knob with which he could control the amount of activity that would be yielded at each trial. He then figured out that the class IV seemed to be misplaced, once it was an intermediate phase between ordered (class I,II) and disordered phases (class III). This complex behavior was not something beyond chaos, but in between order and chaos, at the edge of chaos[58, 63].

ORDER → COMPLEXITY → CHAOS

Later on, Langton has conceived a complexity scale as a transition from order to chaos. This transition behaved like a second order phase-transition with order parameter λ. With the λ parameter tuning the degree of complexity, low values of λ produce ordered low complexity, but as its values increase, complexity rises. At some point, the λ values keep increasing, but the complexity starts to decrease, indicating that λ has passed by its critical threshold and entered the disordered low complexity region. This threshold is given by $\lambda_c \approx 0.27$[124]. The ordered regime is so sparse that it forbids the existence of propagating structures, like gliders which are information carriers. In the other hand, during the disordered regime the information spreads so fast that its content gets lost in a noisy sea of blinking cells. Class IV became the perfect environment for research on artificial intelligence and related subjects, like the GoL class IV structures capacity of proceeding with universal computation. As an example, the glider is a information carrier and besides that it is a real life-form idealization, since it is self-propelled but conserves its structure. All these ideas converged to inquire on the complexity of life itself, giving birth to the expression 'life as a complex system', by the fact that life neither can emerge from a too static background, nor from a too noisy one.

Maybe at this point, it is clear that CA models have opened a gateway to a realm beyond differential equations. In fact, CA models can simulate models based in ordinary differential equations (non-linear or chaotic) and based in partial differential equations. The hidden realm of Wolfram's class IV has been explored since the early 80s and is the source of the whole new science of complex systems.

2.5.2 Some applications

One of the first connections between CA models and differential equations was presented by Toffoli[104], who argued that CA could become an alternative for modelling physical systems. Since then, CA model have been used in almost all sorts of systems, providing relevant results in physics, chemistry, biology, ecology and geology. Some examples in physics are the Ising model, random walkers simulations and the lattice gas cellular automata (LGCA), which was first proposed in 1986 by Frisch *et al.*[39] for modelling the Navier-Stokes equation. Despite the fact that CA cells are not allowed to move through the lattice, LGCA emulates the particle movements by interchanging their states (e.g., occupied $\leftrightarrow$ empty). Hence, each cell state is defined as an array of six elements, one for each degree of freedom in the phase space – three due to position vector, $\overrightarrow{x}$, and three others due to momentum vector, $\overrightarrow{p}$. In the LGCA framework, conservation laws and particle interactions are incorporated in the CA transition rules.

As for biological models, CA can be applied in problems usually formulated in the scope of differential equation, like epidemic models (SIS and SIRS models) and neuronal networks, as well as in systems that differential equations seem to be an inappropriate approach, like in the dynamics of HIV infection[128].As example of geological problems that have been investigated with CA models are shoreline erosion[89] and river delta formation[90].

The Belousov-Zhabotinsky reaction[120] is among many chemical reactions that can oscillate spontaneously and a good example of how non-linear equations can be modelled by a CA model. This reaction shows a self-organizing pattern through continuous formation of spiral waves. Moreover, it is easily found in dynamical systems textbooks, once it performs a Hopf bifurcation[98, 72]. As chapter closure, a simplified CA model of the Belousov-Zhabotinsky reaction[110] is presented below:

Suppose an autocatalyzed reaction, $A + B \rightarrow 2A$, where the reaction of the element A is catalyzed by B until the concentration of B vanishes. Adding an element C that catalyzes the reaction B, and furthermore, reaction C is catalyzed by A, it results in three coupled equations,

$$\begin{cases} A + B \rightarrow 2A \\ B + C \rightarrow 2B \\ C + A \rightarrow 2C \end{cases} \Rightarrow \begin{cases} \dfrac{d[A]}{dt} = \alpha[A][B] - \gamma[A][C] \\ \dfrac{d[B]}{dt} = \beta[B][C] - \alpha[A][B] \\ \dfrac{d[C]}{dt} = \gamma[A][C] - \beta[B][C] \end{cases} \Rightarrow \begin{cases} \dot{X} = X(\alpha Y - \gamma Z) \\ \dot{Y} = Y(\beta Z - \alpha X) \\ \dot{Z} = Z(\gamma X - \beta Y)\,, \end{cases} \tag{2.3}$$

where X, Y, Z stand for the concentration of element A, B, C, respectively, and α, β, γ are constants related to each reaction rate. Considering the approximation of the Euler's

method for solving ordinary differential equations:

$$\begin{cases} \dot{X} = f(X) \\ \dot{Y} = f(Y) \\ \dot{Z} = f(Z) \end{cases} \Rightarrow \begin{cases} X_{n+1} = X_n + f(X_n)\Delta t \\ Y_{n+1} = Y_n + f(Y_n)\Delta t \\ Z_{n+1} = Z_n + f(Z_n)\Delta t\,. \end{cases} \tag{2.4}$$

Then, applying the approximations in Equation 2.4 to Equation 2.3, it becomes

$$\begin{cases} \dot{X} = X(\alpha Y - \gamma Z) \\ \dot{Y} = Y(\beta Z - \alpha X) \\ \dot{Z} = Z(\gamma X - \beta Y) \end{cases} \Rightarrow \begin{cases} X_{n+1} = X_n + [X_n(\alpha Y_n - \gamma Z_n)]\Delta t \\ Y_{n+1} = Y_n + [Y_n(\beta Z_n - \alpha X_n)]\Delta t \\ Z_{n+1} = Z_n + [Z_n(\gamma X_n - \beta Y_n)]\Delta t\,. \end{cases} \tag{2.5}$$

It has been used the dynamical system approach so far, but now the equations shall be revised in order to fit on the CA approach. Consider a square lattice, with Moore neighborhood and periodic boundary conditions. The cell state will be given by a triple, where each coordinate stands for the concentration of one chemical element, $s = ([A], [B], [C]) = (a, b, c)$. The Euler's approach still useful, but the terms $X_n\Delta t$, $Y_n\Delta t$ and $Z_n\Delta t$ shall be replaced by $a_t\,(L_x, L_y)$, $b_t\,(L_x, L_y)$ and $c_t\,(L_x, L_y)$, respectively, which represent a kind of resultant concentration of each element at each cell (L_x, L_y). At time step t, the transition rule sums over the main cell and its 8 neighbors concentrations and then normalizes it, dividing by 9. The resulting number will be the mean concentration s_{t+1} of each element at the main cell at time step $t + 1$. Therefore,

$$\begin{cases} X_{n+1} = X_n + f(X_n)\Delta t \\ Y_{n+1} = Y_n + f(Y_n)\Delta t \\ Z_{n+1} = Z_n + f(Z_n)\Delta t \end{cases} \Rightarrow \begin{cases} a_{t+1} = a_t + a_t(\alpha b_t - \gamma c_t) \\ b_{t+1} = b_t + b_t(\beta c_t - \alpha a_t) \\ c_{t+1} = c_t + c_t(\gamma a_t - \beta b_t)\,. \end{cases} \tag{2.6}$$

As default, neither a chemical concentration can be negative, nor it can exceed 1, in these cases, the element concentration is set as zero or as one, respectively. The simulation is initialized in a random lattice (see *top left* frame at Figure 2.5.3), that is, random values (from 0 to 1) of concentration are placed for each element at each cell. The emergence of Belousov-Zhabotinsky spiral patterns can be seen after time step $t = 200$ (see Figure 2.5.3). ■

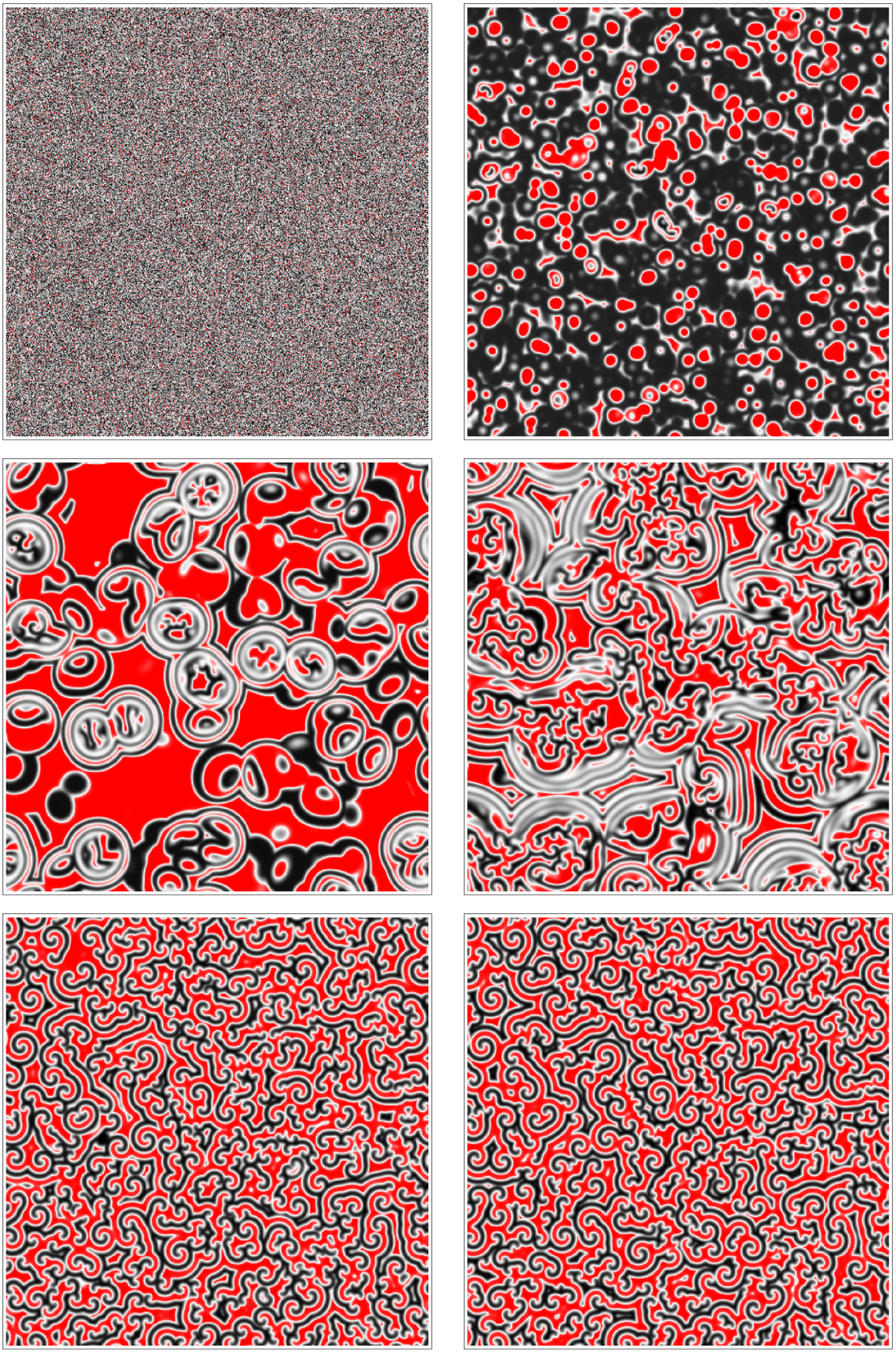

Figure 2.5.3 – Belousov-Zhabotinsky reaction simplified CA model, with linear lattice size $L = 500$. Frames of the chemical concentration of element A. Control parameters: $\alpha = 1.1$, $\beta = 0.9$ and $\gamma = 1$. Concentration reference colors: $a_t = 0$ (*red*), $a_t = 0.1$ (*white*), $a_t = 1$ (*black*). Step $t = 0$ (*top left*), step $t = 30$ (*top right*), step $t = 100$ (*middle left*), step $t = 200$ (*middle right*), step $t = 500$ (*bottom left*), step $t = 0$ (*bottom right*).

Chapter 3

Topics in physics of complex systems

"Living systems are never in equilibrium.
... Everything is moving and changing.
In a sense, everything is on the edge of collapse."
Michael Crichton[†]

In common language, 'complex' usually means something that is hard to explain or to understand, something that can not be precisely depicted or even something that displays a completely unpredictable behavior. As Murray Gell-Mann clarifies[42], one has *to distinguish between effective complexity and logical depth*. For example, to understand quantum mechanics one needs *a good deal of logical depth and very little effective complexity*. Although the understanding of quantum mechanics is quite a challenge, its basic laws are well defined. On the other hand, a neuronal network, for example, is a biological system whose behavior is based on the laws of electrochemical reactions, but also influenced by *the outcomes of an inconceivably long sequence of probabilistic events*. Through this perspective, the system is so called 'complex', *in the sense that a great many independent agents are interacting with each other in a great many ways*[113].

'Complexity' or 'complex systems' are found in the most assorted fields of knowledge, from astronomy to economics to linguistics, and also in natural systems like magnets, neurons or rainforests[28]. As many of these systems display (well-defined) macroscopic phases[95], the science of complexity has borrowed several tools from physics, specially from statistical mechanics – later incorporated to the framework of complex systems. Regardless of how miscellaneous these systems can be, they display many similarities: as a dynamical system, they evolve in time; they exchange information with the environment; they are also comprised of several units (many degrees of freedom), for whom interaction is locally defined among themselves. The system response to any changes is non-linear and some systems can be adaptive, meaning that they are capable of modulate their properties

[†] From "Jurassic Park: A Novel"[31].

in order to settle down in a new arrangement after a perturbative input. Others can also show an emergent order, that is, the system's elements has the ability to self-organize. Complex systems have regions of metastability, in which any tiny perturbation is capable of pushing the system to another macroscopic state. Another remarkable feature is that some of the system's observables does not exhibit any characteristic scale, i.e., the system observables can be measured at several different scales (known as scale invariants), which decreases (or even vanishes) the predictability of the system behavior in terms of these observables. This chapter aims to introduce some basic concepts and tools of physics of complex systems that shall be used henceforth.

3.1 Phase transitions in equilibrium thermodynamics

One of the features that characterizes a system at thermodynamic equilibrium is that the temperature is spatially uniform throughout the whole system. Irreversible processes, such as heat conduction and chemical reactions, drive the system towards a state of equilibrium. Due to heat exchange, substances (e.g., water) can change its microscopic structure, which gives rise to distinct macroscopic states such as gas, liquid or solid – called phases of a substance. At the threshold between vapor and liquid and between liquid and solid – called boiling point and melting point, respectively –, the heat supplied to the system (or withdrawn from it) does not increase (decrease) its temperature, instead it only has the effect of converting a fraction of the substance from one phase to another, which is called latent heat. At specific conditions, a substance may display two (or even more) phases coexisting in a state of thermal equilibrium, furthermore at the point where the transition happens, some thermodynamics quantities change discontinuously.

Consider an heterogeneous system of a pure substance in which liquid and gas phases of this substance coexist, that means that liquid converts into vapor and vapor is converted into liquid (both irreversibly) and thus changing the volume of each phase. This occurs until the equilibrium between the two phases is achieved, then

$$liquid \rightleftharpoons vapor\ . \tag{3.1}$$

At equilibrium, every irreversible process must vanish, implying that any entropy S production shall cease. As the process becomes reversible, the chemical potentials of both phases turn to be equal. Using Gibbs-Duhem relation, Clapeyron equation (Equation 3.4) can be derived[56] as shown below,

$$\begin{cases} \mu_{liquid}(P,T) = \mu_{gas}(P,T) \\ SdT - VdP + Nd\mu = 0 \end{cases} \tag{3.2}$$

$$\begin{aligned} -(S/N)_l\, dT + (V/N)_l\, dP &= -(S/N)_g\, dT + (V/N)_g\, dP \\ -s_l\, dT + v_l\, dP = -s_g\, dT + v_g\, dP &\Rightarrow \frac{dP}{dT} = \frac{s_l - s_g}{v_l - v_g} \end{aligned} \tag{3.3}$$

$$\frac{dP_{vap}}{dT} = \frac{\Delta h_{lg}}{T \Delta v_{lg}} \tag{3.4}$$

where $h_{lg} = T(s_l - s_g)$ is the enthalpy of the liquid-gas transition, T is the temperature at which the transition takes place and P_{vap} stands for the pressure of vaporization. The right hand side of Equation 3.4 gives the slope of the liquid-gas coexistence curve in a P-T phase diagram[21]. The Clapeyron equation also holds true for solid-liquid and gas-solid phase transitions.

When a solid-liquid, solid-gas or liquid-gas transitions occurs, it is due to a discontinuous change in the entropy $S(T)$ and, whereas the chemical potentials change continuously, its derivatives are discontinuous though. At the transition temperature, the heat absorbed by the system ΔQ does not change its temperature, i.e. $\Delta T = 0$, it is transferred as latent heat instead. Since the heat capacity depends on the variation of the temperature, $C_V(T) = \Delta Q/\Delta T$, as $\Delta T \to 0$, the heat capacity diverges, which is a typical signature of a phase transition. Systems that display a discontinuity at certain first order derivatives of the thermodynamic potentials are classified as going through a first order phase transition. On the other hand, some transitions exhibit changes on the thermodynamic quantities, such as variations in entropy and volume, that are not so drastic and are actually continuous, but their derivatives are discontinuous, the so called second order phases transitions. In other words, for second order phase transitions the first derivative of a thermodynamic potential varies continuously, but its second derivative does not. In such transitions, it is observed the existence of large fluctuations around the first derivative of a potential and these fluctuations have no characteristic size.

In 1873, Johannes van der Waals presented a model of a real gas in his doctoral thesis[56]. The van der Waals gas predictions about the liquid-gas transition are qualitatively correct, although quantitatively it does not yield an agreement with experiments. As he realized, there are two relevant factors that are not comprised by the ideal gas equation of state, which are the effect of the molecular volume and an effect due to intermolecular forces. A gas cannot be compressed to an arbitrary small volume, since its molecules have a finite volume, then the term of volume in the ideal gas should be replaced by $V - bN$, $V \to V - bN$. He has also noted that pressure decreased as result of certain attractive intermolecular forces. Because of such attraction between molecules, less molecules hit the container's wall and, moreover, the momentum of a molecule before the collision to the wall is reduced by the attraction due to other molecules behind it. Hence, van der Waals proposed that the pressure should also be corrected by summing a factor of $a(N/V)^2$, then

$P \to P + a(N/V)^2$. The Equation 3.5 shows the ideal gas equation of state corrected by van der Waals model, where a and b are constants. The terms of van der Waals equation of state can be rearranged as in Equation 3.6.

$$PV = Nk_BT \to \left(P + a\frac{N^2}{V^2}\right)(V - bN) = Nk_BT \tag{3.5}$$

$$P = \frac{Nk_BT}{V - bN} - \frac{aN^2}{V^2} \tag{3.6}$$

The isotherms of the van der Waals gas can be seen in Figure 3.1.1. The curve at $T = T_c$ is known as critical isotherm. Isotherms that resemble those of an ideal gas are above the critical isotherm, their temperatures are above the critical temperature. Curves of temperatures below T_c possess a region where P and V increase simultaneously, which is an unphysical behavior. These isotherms ($T < T_c$) exhibit a discontinuous change in the volume for slight variations in pressure, characterizing the occurence of a liquid-gas phase transition. The black dot in Figure 3.1.1 is called critical point, at which

$$\frac{\partial P}{\partial V} = 0\,, \qquad \frac{\partial^2 P}{\partial V^2} = 0\,. \tag{3.7}$$

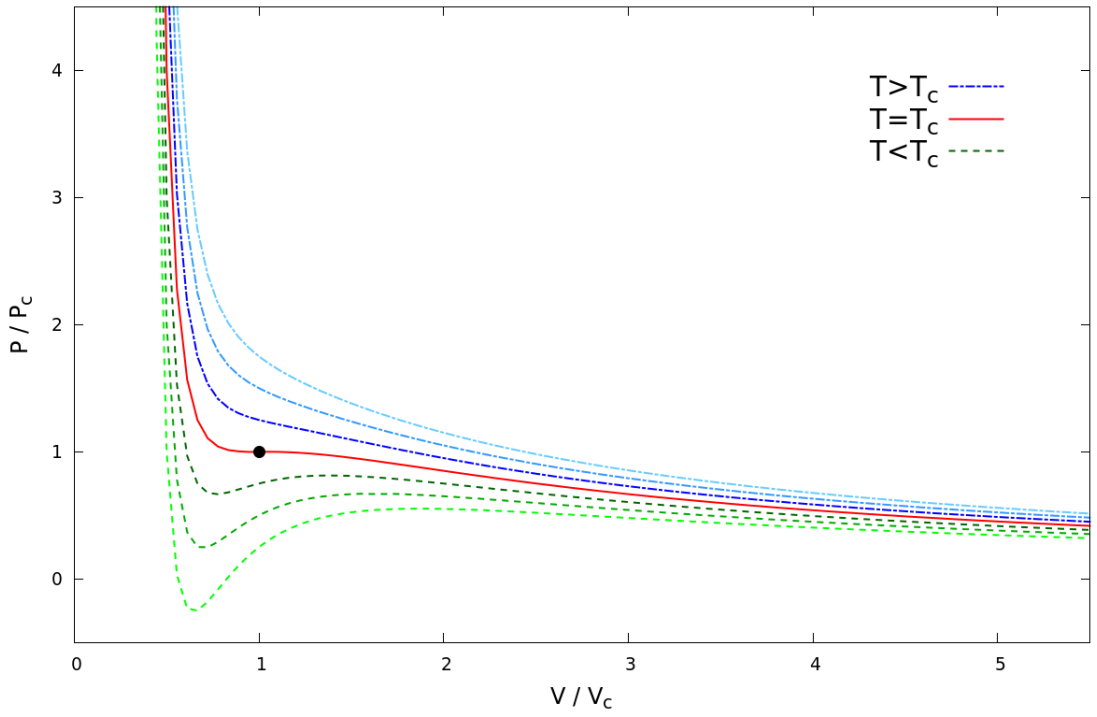

Figure 3.1.1 – Isotherms of the van der Waals gas. Curves in shades of blue are above T_c. Curves in shades of green are below T_c. The black dot in the red curve (critical isotherm) is the critical point.

Applying the conditions in Equation 3.7 to the equation of state Equation 3.6,

$$\frac{\partial P}{\partial V} = \frac{-Nk_BT}{(V-Nb)^2} + \frac{2aN^2}{V^3} = 0\,, \tag{3.8}$$

$$\frac{\partial^2 P}{\partial V^2} = \frac{2Nk_BT}{(V-Nb)^3} - \frac{6aN^2}{V^4} = 0\,, \tag{3.9}$$

the critical volume V_c and critical temperature T_c are found by solving these equations. Substituting V_c and T_c at the equation of state, one finds the critical pressure, P_c. So,

$$V_c = 3Nb, \qquad k_BT_c = \frac{8a}{27b}\,, \qquad P_c = \frac{a}{27b^2}\,.$$

Now, if each parameters in Equation 3.6 is replace by X/X_c, e.g., $P \to P/P_c$, and making $V/N = v$, the equation of state turns to is reduced form (Equation 3.10), which is precisely the equation that gives the curves in Figure 3.1.1, as T is slightly shifted near T_c.

$$\frac{P}{P_c} = \frac{8(T/T_c)}{3(V/V_c)-1} - \frac{3}{(V/V_c)^2} \tag{3.10}$$

As mentioned before, some thermodynamic quantities diverge near the critical point, this is what happens, for example, with the isothermal compressibility, defined as

$$\kappa_T = -\frac{1}{V}\left(\frac{\partial V}{\partial P}\right)_T = -\frac{1}{V(\partial P/\partial V)_T}\,. \tag{3.11}$$

At $V = V_c$,

$$\left.\frac{\partial P}{\partial V}\right|_{V=V_c} = -\frac{Nk_BT}{2N^2b} + \frac{2aN^2}{27N^3b^3} = \frac{1}{4Nb^2}\left(\frac{8a}{27b} - k_BT\right) = \frac{k_B}{4Nb^2}(T_c - T) \tag{3.12}$$

and then substituting Equation 3.12 in Equation 3.11,

$$\kappa_T \propto (T - T_c)^{-1}\,. \tag{3.13}$$

As the system approaches to its critical point, from $T > T_c$, the isothermal compressibility diverges as a power law (Equation 3.13) and its exponent is said to be a critical exponent. Experimentally, this divergence in κ_T has exponent γ, which is $\gamma = -1$ in the van der Waals theory. So, generally

$$\kappa_T \propto |T - T_c|^{-\gamma}\,. \tag{3.14}$$

The van der Waals liquid-gas transition is continuous only at the critical point, i.e., it is a second order phase transition, whereas the others ($T < T_c$) are first order phase transitions, as happens to any substance that crosses the coexistence curve in a P-T phase diagram[125]. In general, when a substance is in the vicinity of the critical point, the heat capacity C_V diverges as a power law with exponent α (Equation 3.15), but for the van

der Waals gas this exponent is $\alpha = 0$. Actually, for any gas that has an equation of state in which P is a linear function of T the heat capacity is equal to the heat capacity of an ideal gas, then it holds that $\alpha = 0$[56].

$$C_V \propto |T - T_c|^{-\alpha} \tag{3.15}$$

Although the phase transition is continuous at the critical point, the behavior of the system is far from what can be considered a smoothy change. As seen before, the second order phase transition is related to fluctuations of large amplitudes around the mean value of a specific parameter, resulting in the divergence of the characteristic size of these fluctuations. In the van der Waals gas, these fluctuations take place at the densities of gas and liquid during the transition through the critical point. So, the density fluctuations display values at nearly all scales of length, that is, there is no characteristic length scale. This is an example of scale invariance[62], which in equilibrium thermodynamics is the signature of systems going through a phase transition and it is identified by a power-law behavior of some thermodynamic variable at the critical point. As in Equation 3.14, the isothermal compressibility κ_T behaves like a scale invariant and this is deeply related to the large fluctuations in the densities. At the critical point, one may observe bubbles of liquid at low density, as well as bubbles of gas at high density; these bubbles can exhibit sizes at any scale, the scale is limited only by the volume of the container. The fluctuations make the fluid become turbid (with a cloudy aspect), this phenomenon is known as critical opalescence[62, 45, 129]. For the van der Waals gas, the exponent of the density fluctuation is $\beta = 1/2$, and generally,

$$\rho_l - \rho_g \propto (T_c - T)^{\beta}\,. \tag{3.16}$$

Critical exponents describe how the system responds at the vicinity of critical points. These exponents are the same for systems which underlying details are physically distinct from each other and are known as universal exponent. A set of systems with the same universal exponent is called a class of universality. The existence of universal exponents indicates that long-range cooperative effects (unleashed throughout the system at the critical point) do not depend on the nature of the local interactions among the particles.

3.2 Site percolation

The word 'percolation' comes from the latim *percolare*, which means 'to filter' or 'to strain through'[13]. Coffee beans must go through several processes before finally becoming this nice smelling and mostly beloved beverage, the last process is called percolation. Indeed, whenever a cup of coffee is prepared through infusion or drip filtering, it cannot be called an *espresso*[51]. A coffee that is brewed in a percolator (Figure 3.2.1) has much more

flavor than when prepared by other methods, because the fluid can recirculate through the ground coffee and at higher temperatures.

In a coffee percolator, the hot water trickles through the coarse-ground coffee chamber by gravity, instead of moving straight through it. In other words, boiling water collides with the ground coffee, changing its streamlines to a fluctuating path that resembles a self-avoided random walk.

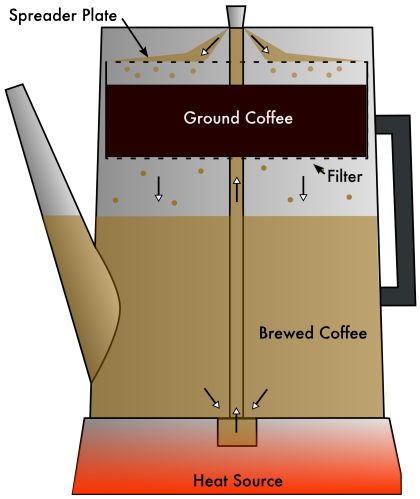

Figure 3.2.1 – Scheme of a coffee percolator. From Wikipedia's article, *Coffee Percolator*[2].

Random diffusion processes can be distinguished in two types: one which the randomness is related to unpredictable movement of a particle over a smoothly geometrical medium – its prototype is a random walk; the other type, the particle displays a 'deterministic' displacement, whereas the randomness is defined on the geometry over which the particle is roaming – the particle percolates through this random medium.

The percolation model[23] describes the simplest possible phase transition and it also displays long-range correlations as the controlling parameter gets near its critical value. Its nature is purely geometrical and *as there is relevant number of transport problems in disordered media exhibiting critical behavior*[52], its applications reach a great sort of biological, chemical and physical problems such as fluid flow in porous media[55], ground water flow[88], epidemic modelling[27], metal-insulator transition[87].

The modelling of a particle that is roaming on some random geometry can be focused on the sites themselves, is known as *site percolation*. Otherwise, models concerned with the bridges that are bonding neighbor sites, are known as *bond percolation* models. There is also site-bond percolation models, which are of great use in polymer science[30]. Problems of bond percolation can be mapped in the site percolation framework, but the opposite does not hold true, making site percolation a more general model.

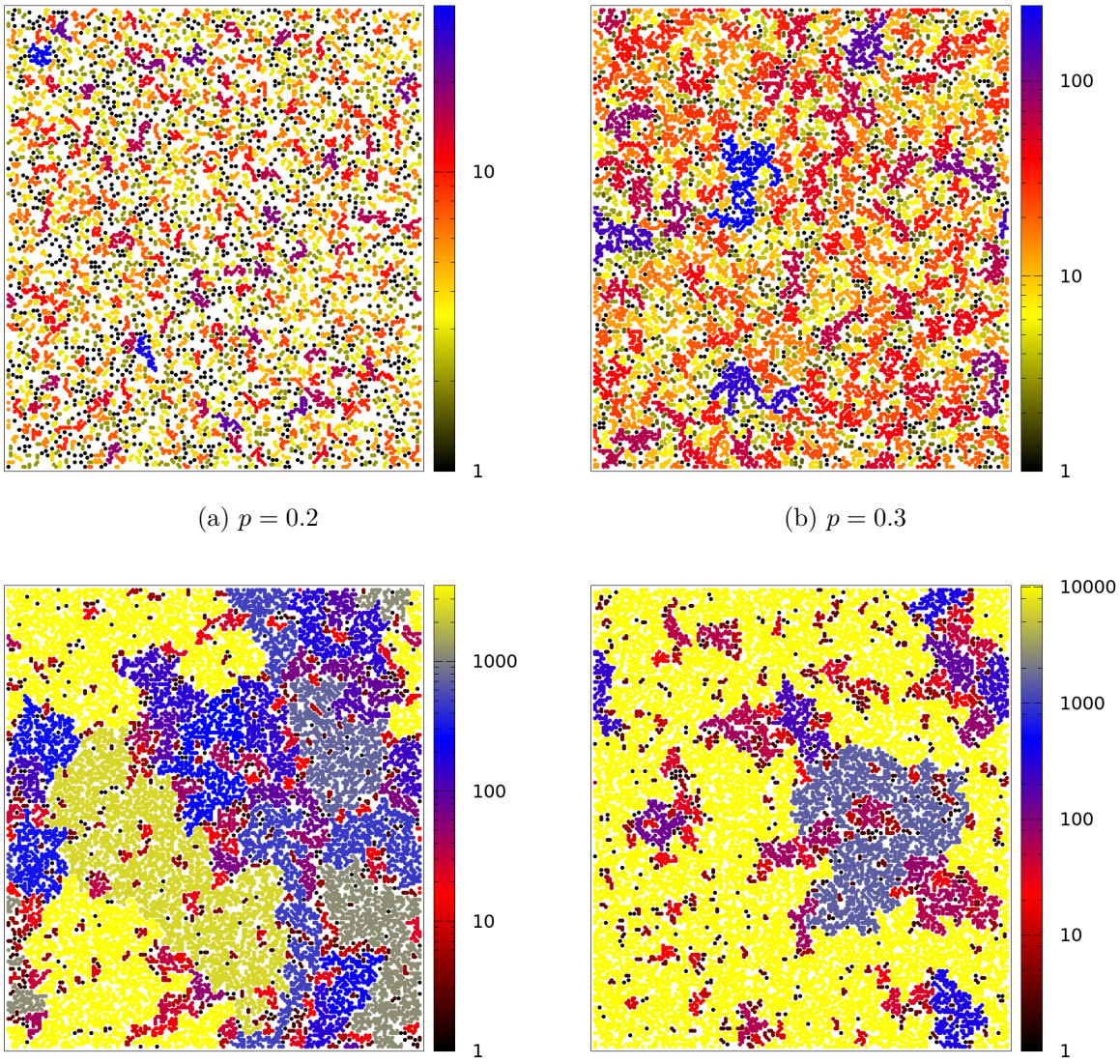

(a) $p = 0.2$ (b) $p = 0.3$

(c) $p = 0.39$ (d) $p = 0.40$

Figure 3.2.2 – Snapshots of two-dimensional lattices with linear size $L = 200$, Moore neighborhood ($p_c \approx 0.40$) and density p. The cluster size is indicated by the logarithmic color bar. For a better visualization of the small clusters, the empty sites were left *white* colored and occupied sites are larger than empty ones.

Consider a square lattice with linear size L and where a site is occupied with probability p, which also stands for the lattice mean occupation, i.e. the mean fraction of occupied sites. For low values of p, it is possible to identify small clusters only (Figure 3.2.2). Clusters are defined as a group of occupied sites that are connected to one occupied nearest neighbor at least. The cluster size s is just the number of occupied sites that comprise a certain cluster and different neighborhoods can be considered (as seen in section 2.3). In lattices displaying a low fraction of occupied sites (i.e. low density), a particle will not be capable of walking through the whole lattice (from one side to the other). For example, if

a marble is released from one side, it will not be able to percolate through the medium and reach the opposite side, because of the low connectivity among the sites – the medium acts as maze in which the marble is trapped. For large densities though, the particle shall easily percolate – the marble finds at least one way out of the maze.

Precisely speaking, a percolation happens when the occupied sites density is such that enables the existence of an infinite cluster (also called percolation cluster), which is basically a cluster that spans through the whole lattice. The concept of infinite cluster is well-defined only for infinite lattices, therefore for finite lattices the largest but finite clusters are called incipient infinite cluster instead[28]. Hence, at a certain threshold of density the lattice exhibits a percolation cluster, that is, if a bead is initially placed at one of its sites, it can percolates through the lattice.

The minimum probability at which a percolation cluster is found is called critical percolation probability p_c, which is also the critical mean density. As will be seen, the critical probability can be determined exactly in one-dimensional percolation model and also for percolation on the Bethe lattice. It had been conjectured and has been shown that there is no percolating infinite cluster in two-dimensional lattices[47].

The present work is intrinsically related to site percolation in a two-dimensional square lattice, since it is one of the foundations of the forest-fire model – although 'pure' percolation models have also been used in modelling wildfires critical behavior[66]. Percolation models introduce quantities that are also relevant in forest-fire models, such as cluster number distribution $n(s, p)$ and characteristic cluster size s_ξ, as well as the concept of finite-size scaling which is essential in the analysis of cluster distributions.

3.2.1 One-dimensional lattice

Consider the dot stripes of linear size $L = 30$ in Figure 3.2.3. The black dots stand for occupied sites, whereas grey dots are empty sites. These are typical configurations of one-dimensional clusters, in which each site had been chosen randomly with probability $p = \{0.3, 0.5, 0.7\}$.

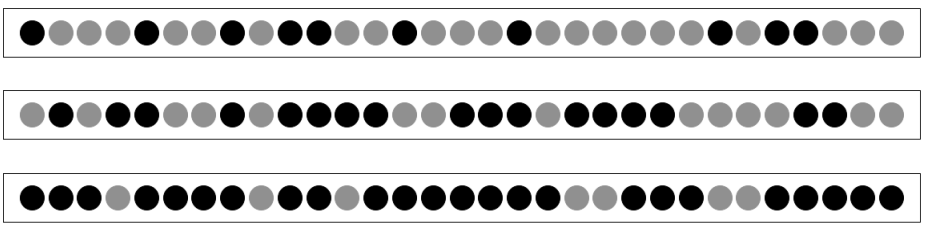

Figure 3.2.3 – One-dimensional lattices of size $L = 30$ with densities $p = 0.3$, $p = 0.5$, $p = 0.7$ – from top to bottom. Occupied sites (*black*), empty sites (*grey*).

After a first look at Figure 3.2.3 and it seems clear that the only possible way to move from one side to the other is when $p = 1$, considering only (two) nearest neighbors (one at the left side and one at the right side) and no 'site-jumping' is allowed. Ignoring the effect of the boundaries, the probability of having a cluster of size s is the probability of having s occupied sites surrounded by empty sites, that is the probability p^s times the probability $(1-p)$ for each empty site that limits the cluster, thus

$$\left.\begin{aligned} &s=1:(1-p)p(1-p)\\ &s=2:(1-p)p^2(1-p)\\ &s=3:(1-p)p^3(1-p)\\ &s=4:(1-p)p^4(1-p)\\ &\vdots \end{aligned}\right\} \Rightarrow n(s,p) \equiv (1-p)^2 p^s\,, \tag{3.17}$$

where $n(s,p)$ is the cluster number density, which is the probability of having cluster of size s. Moreover, for $p < 1$, the probability that a site belongs to a cluster of size s is $s\,n(s,p)$ and summing over all cluster sizes,

$$\begin{aligned} \sum_{s=1}^{\infty} s\,n(s,p) &= \sum_{s=1}^{\infty} s(1-p)^2 p^s = (1-p)^2 \sum_{s=1}^{\infty} s p^s \\ &= (1-p)^2 \sum_{s=1}^{\infty} p \frac{d(p^s)}{dp} = (1-p)^2 p \frac{d}{dp}\Big(\sum_{s=1}^{\infty} p^s\Big) \\ &= (1-p)^2 p \frac{d}{dp}\Big(\frac{p}{1-p}\Big) = (1-p)^2 p\Big[\frac{1}{1-p} + \frac{p(-1)^2}{(1-p)^2}\Big] \\ &= (p-p^2) + (p^2) = p\,. \end{aligned} \tag{3.18}$$

As s increases, $n(s,p)$ rapidly decays, this can be captured by the characteristic cluster size s_ξ, at which the curve has decreased by e^{-1}. So,

$$\begin{aligned} n(s,p) &= (1-p)^2 p^s = (1-p)^2 \exp[\ln(p^s)] \\ &= (1-p)^2 \exp[s(\ln p)] = (1-p)^2 \exp(-s/s_\xi)\,, \end{aligned} \tag{3.19}$$

thereof (see Figure 3.2.4),

$$s_\xi \propto -1/\ln p\,. \tag{3.20}$$

Expanding $\ln p$ around $p_0 = 1$, replacing it in Equation 3.20 and afterwards applying the limit $p \to 1^-$,

$$\begin{aligned} \ln(p)\Big|_{p_0=1} &\approx \ln(1) + \frac{d(\ln p)}{dp}\Big|_{p_0=1}(p-1) + \frac{d^2(\ln p)}{dp^2}\Big|_{p_0=1}(p-1)^2 + \mathcal{O}(p^3) \\ &\approx (p-1) - (p-1)^2 + \mathcal{O}(p^3) \approx (p-1) + \mathcal{O}(p^2)\,, \end{aligned} \tag{3.21}$$

$$\lim_{p\to 1^-}\{s_\xi\} = \lim_{p\to 1^-}\left\{\frac{-1}{\ln p}\right\} \to \frac{-1}{p-1}\,, \tag{3.22}$$

thus the characteristic cluster size $s_\xi(p)$ diverges as p approaches 1,

$$s_\xi(p \to 1^-) \propto (1-p)^{-1}\,. \tag{3.23}$$

The average cluster size χ is evaluated with weight p_k (Equation 3.24), which is the probability that an occupied site belongs to the cluster k, $p_k = s_k/N_{occ}$. The number of occupied sites is just $N_{occ} = pL$ and the total number of clusters, N_{clu}.

$$\chi(p) = \sum_{k=1}^{N_{clu}} p_k s_k = \frac{1}{N_{occ}} \sum_{k=1}^{N_{clu}} s_k^2 \tag{3.24}$$

Changing the summation over each cluster and now summing over the cluster size,

$$\begin{aligned}
\chi(p) &= \frac{1}{N_{occ}} \sum_{k=1}^{N_{clu}} s_k^2 = \frac{1}{N_{occ}} \sum_{s=1}^{\infty} s^2 N(s,p;L) \\
&= \frac{\sum_{s=1}^{\infty} s^2 N(s,p;L)}{pL} = \frac{\sum_{s=1}^{\infty} s^2 n(s,p)}{p} \\
&= \frac{\sum_{s=1}^{\infty} s^2 n(s,p)}{\sum_{s=1}^{\infty} s\, n(s,p)}\,,
\end{aligned} \tag{3.25}$$

where $N(s,p;L)$ is simply the cluster number, $N(s,p;L) = Ln(s,p)$. Evaluating Equation 3.25,

$$\begin{aligned}
\chi(p) &= \frac{\sum_{s=1}^{\infty} s^2 n(s,p)}{\sum_{s=1}^{\infty} s n(s,p)} = \frac{\sum_{s=1}^{\infty} s^2 n(s,p)}{p} = \frac{\sum_{s=1}^{\infty} s^2 (1-p)^2 p^s}{p} \\
&= \frac{(1-p)^2}{p} \sum_{s=1}^{\infty} p \frac{d}{dp}\Big(s p^s\Big) = \frac{(1-p)^2}{p} \sum_{s=1}^{\infty} p \frac{d}{dp}\Big(p \frac{d}{dp}\Big(p^s\Big)\Big) \\
&= \frac{(1-p)^2}{p} p \frac{d}{dp}\Big(p \frac{d}{dp}\Big(\sum_{s=1}^{\infty} p^s\Big)\Big) = \frac{(1-p)^2}{p} p \frac{d}{dp}\Big(p \frac{d}{dp}\Big(\frac{p}{1-p}\Big)\Big) \\
&= (1-p)^2 \frac{d}{dp}\Big(\frac{p}{(1-p)^2}\Big) = (1-p)^2 \Big[\frac{(1-p)^2 + p(-2p+2)}{(1-p)^4}\Big] \\
&= (1-p)^2 \Big[\frac{(1-p)^2 + 2p(1-p)}{(1-p)^4}\Big] = (1-p)^2 \Big[\frac{1}{(1-p)^2} + \frac{2p}{(1-p)^3}\Big] \\
&= 1 + \frac{2p}{(1-p)} = \frac{1+p}{1-p}\,.
\end{aligned} \tag{3.26}$$

The procedure above indicates that $\chi(p)$ also diverges (see Figure 3.2.4) as p is approaching to 1 with exponent -1,

$$\chi(p \to 1^-) \propto (1-p)^{-1}\,. \tag{3.27}$$

As already noticed, the cluster that will spans through the lattice only appears at $p = 1$, but the cluster number density $n(s,p)$ vanishes as $p \to 1^-$. Hence, the probability P_∞ that a site belongs to the percolating cluster must be

$$P_\infty(p) \equiv \begin{cases} 0 & \text{for } p < 1 \\ 1 & \text{for } p = 1\,. \end{cases} \tag{3.28}$$

Therefore,

$$P_\infty(p) + \sum_{s=1}^{\infty} sn(s,p) = p \tag{3.29}$$

is valid for all p. This relation (Equation 3.29) holds true for higher dimensions as well[28].

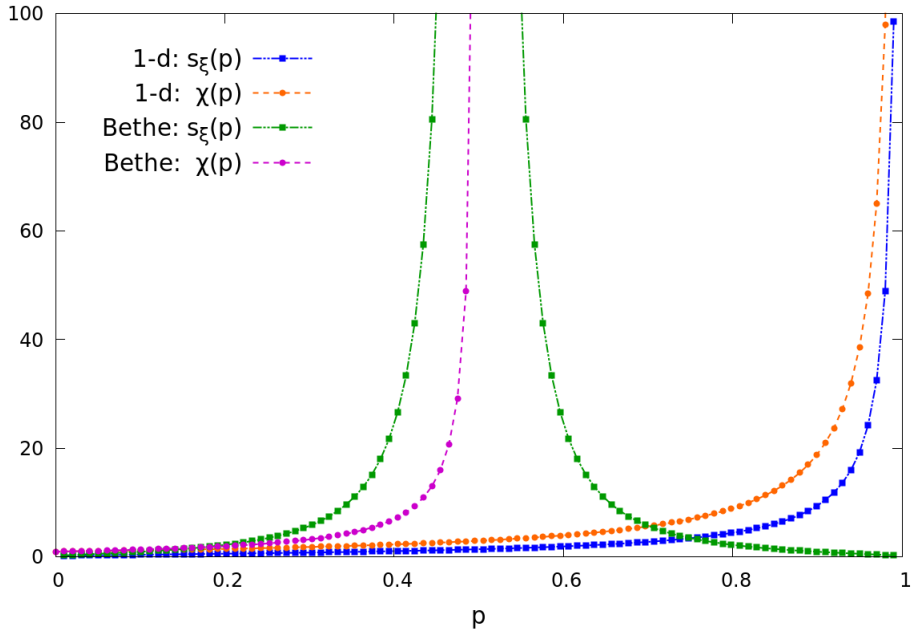

Figure 3.2.4 – Plots of s_ξ and χ for one-dimensional lattice (Equation 3.20 and Equation 3.26, respectively) and for the Bethe lattice with $z = 3$ (Equation 3.38 and Equation 3.32, respectively).

3.2.2 Bethe lattice

The Bethe lattice, introduced by Hans Bethe in 1935[20], shares an important property with the one-dimensional lattice: both structures display no loops. It implies that each pair of sites are connected by a unique path. This feature makes possible to obtain $n(s,p)$, $s_\xi(p)$ and $\chi(p)$ analytically.

Each site of a Bethe lattice has z neighbors and z is called the coordination number. At Figure 3.2.5, the coordination number is $z = 3$, with the parent site labelled with $\{1\}$ and the next four generations are indicated with dashed circles and labels $\{2,3,4,5\}$. In fact, for $z = 2$ the Bethe lattice turns into a one-dimensional lattice. For a walk starting from the parent site, from the second generation forth there are $z-1$ possible branches to walk along at each step, since retracing steps is not allowed. Thus, on average $p(z-1)$ branches are accessible. This walk only goes on if at each step there is at least one accessible branch, then

$$p(z-1) \geq 1\,. \tag{3.30}$$

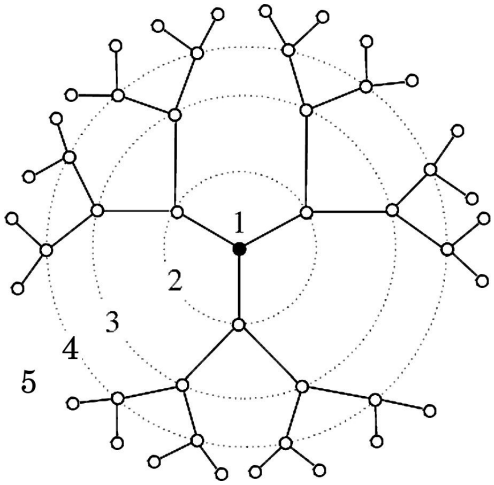

Figure 3.2.5 – Bethe lattice with coordination number $z = 3$, extracted from an article by Gleiser *et al.*[43].

The equality in Equation 3.30 gives the critical percolation density p_c as function of the coordination number z (Equation 3.31); and for the one-dimensional lattice ($z = 2$), the value $p_c = 1$ is restored.

$$p_c(z-1) = 1 \quad \Rightarrow \quad p_c = \frac{1}{z-1} \tag{3.31}$$

Considering the intrinsic relation between the Bethe lattice with coordination number $z > 2$ and the one-dimensional lattice, the average cluster size in Equation 3.25 can be generalized, as follows

$$\chi(p) = \frac{1+p}{1-(z-1)p} = \frac{p_c(1+p)}{p_c - p} \qquad \text{for} \quad 0 < p < p_c\,. \tag{3.32}$$

For $z = 3$, the lattice has $p_c = 1/2$ and its $\chi(p)$ is plotted in Figure 3.2.4. As $\chi(p)$ approaches the critical probability p_c, it diverges as

$$\chi(p \to p_c) \propto (p_c - p)^{-1}\,. \tag{3.33}$$

Now consider a cluster of size s, the set of its unoccupied nearest neighbors is its perimeter t, because it traces the limits of the cluster. The equation below generalizes the cluster number density $n(s,p)$ for any geometry[28],

$$n(s,p) = \sum_{t=1}^{\infty} g(s,t)(1-p)^t p^s\,. \tag{3.34}$$

As many clusters may have the same size s and even the same perimeter t, it is introduced a degeneracy factor, $g(s,t)$. For the Bethe lattice, all clusters of size s have the same quantity of perimeter sites, $t = [2 + s(z-2)]$[38]. Therefore,

$$n(s,p) = g(s,t)(1-p)^t p^s = g(s, 2+s[z-2])(1-p)^{2+s(z-2)} p^s\,, \tag{3.35}$$

and for $z = 3$,

$$n(s,p) = g(s, 2+s)(1-p)^{2+s}p^s\,. \tag{3.36}$$

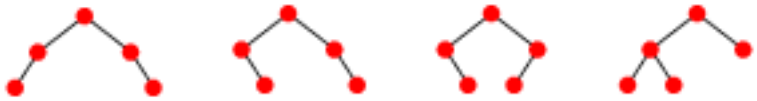

Figure 3.2.6 – Example of degenerate clusters of a Bethe lattice with coordination number $z = 3$. Each cluster has size $s = 5$ and perimeter $t = 7$. Edited from Wolfram Mathworld's article on binary trees[1].

The characteristic cluster size s_ξ can be determined by manipulating the ratio of $n(s,p)$ divided by $n(s,p_c)$,

$$\begin{aligned}\frac{n(s,p)}{n(s,p_c)} &= \frac{\cancel{g(s,2+s)}}{\cancel{g(s,2+s)}}\left[\frac{1-p}{1-p_c}\right]^2\left[\frac{(1-p)p}{(1-p_c)p_c}\right]^s \\ &= \left[\frac{1-p}{1-p_c}\right]^2 \exp\left(s\ln\left[\frac{(1-p)p}{(1-p_c)p_c}\right]\right) \\ &= \left[\frac{1-p}{1-p_c}\right]^2 \exp(-s/s_\xi)\,,\end{aligned} \tag{3.37}$$

and, finally,

$$s_\xi(p) = \frac{-1}{\ln\left[\dfrac{(1-p)p}{(1-p_c)p_c}\right]}\,. \tag{3.38}$$

For $p > p_c$, s_ξ decreases as p increases (Figure 3.2.4), which is expected since s_ξ is the measure of the typical size of the largest finite cluster; hence, it means that as the percolation cluster increases, it leaves even less space for finite clusters. As s_ξ approaches p_c, it diverges with exponent -2,

$$s_\xi(p \to p_c) \propto \frac{1}{4}(p-p_c)^{-2}\,. \tag{3.39}$$

The behavior of s_ξ and χ near the critical probability p_c suggests that cluster number density also has a power-law decay at $p = p_c$, that is $n(s,p_c) \propto s^{-\tau}$ for $s \gg 1$, and it can be shown that $\tau = 5/2$[28]. So, $n(s,p)$ can be approximated to the form

$$\begin{aligned} n(s,p) &\propto s^{-\tau}\exp(-s/s_\xi) \qquad &&\text{for} \quad s \gg 1, p \to p_c\,, \\ s_\xi &\propto (p-p_c)^{-2} \qquad &&\text{for} \quad p \to p_c\,. \end{aligned} \tag{3.40}$$

The validity of the scaling form in Equation 3.40 can be tested by calculating the average cluster size $\chi(p)$ directly from its definition (Equation 3.25) – at this point it is important to recall that $\sum_{s=1}^{\infty} s\,n(s,p)$ is finite. This procedure is detailed in the following (Equation 3.41):

$$\begin{aligned}
\chi(p) &= \frac{\sum_{s=1}^{\infty} s^2 n(s,p)}{\sum_{s=1}^{\infty} s\, n(s,p)} \\
&\propto \sum_{s=1}^{\infty} s^{2-\tau} \exp(-s/s_\xi) \\
&\approx \int_1^{\infty} s^{2-\tau} \exp(-s/s_\xi)\, ds\,, \qquad \text{using } u = s/s_\xi\,, \\
&= \int_{1/s_\xi}^{\infty} (u\, s_\xi)^{2-\tau} \exp(-u) s_\xi\, du \\
&= s_\xi^{3-\tau} \int_{1/s_\xi}^{\infty} u^{2-\tau} \exp(-u)\, du.
\end{aligned} \tag{3.41}$$

Now if $p \to p_c$, then $1/s_\xi \to 0$, and the integral becomes a gamma function*,

$$\begin{aligned}
\chi(p \to p_c) &\propto s_\xi^{3-\tau} \int_{(1/s_\xi)\to 0}^{\infty} u^{2-\tau} \exp(-u)\, du \\
&\propto s_\xi^{3-\tau}\, \Gamma(3-\tau)\,.
\end{aligned} \tag{3.42}$$

Comparing with Equation 3.33 and including Equation 3.39,

$$\begin{aligned}
\chi(p \to p_c) &\propto (p_c - p)^{-1} \\
&\propto s_\xi^{3-\tau} \\
&\propto (p_c - p)^{2\tau - 6}\,.
\end{aligned} \tag{3.43}$$

Therefore, the scaling form (Equation 3.40) is consistent and the exponent τ for the Bethe lattice is really $\tau = 5/2$, as expected.

The probability that a site belongs to the percolating cluster is given by Equation 3.44. Although $P_\infty(p)$ is continuous, it is not differentiable at $p = p_c$, and as the critical value p_c is signalling for a transition between a percolating phase and a 'finite clusters' phase, it is characterized a continuous (second order) phase transition.

$$P_\infty(p) = \begin{cases} 0 & \text{for} \quad p \le p_c \\ p\left[1 - \left(\dfrac{1-p}{p}\right)^3\right] & \text{for} \quad p > p_c \end{cases} \tag{3.44}$$

3.2.3 Two-dimensional lattice

The exact results obtained for the one-dimensional lattice and the Bethe lattice are possible because of the absence of loops. Though two-dimensional lattice lacks of analytical results, some numerical approaches have showed that for a von Neumann neighborhood the phase transition occurs at $p_c \approx 0.59$, whereas for the Moore neighborhood $p_c \approx 0.407$[74, 70].

* The gamma function $\Gamma(z)$ can be represented by the convergent integral $\Gamma(z) = \int_0^{\infty} x^{z-1} \exp(-t) dt$, where $z = \{z \in \mathbb{C} \,|\, \Re(z) > 0\}$[22].

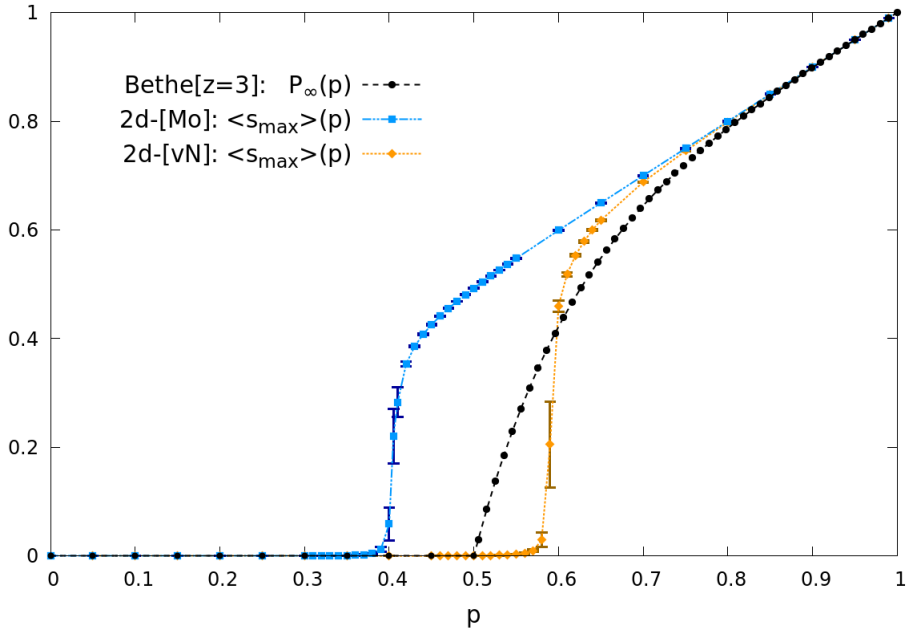

Figure 3.2.7 – Plot of $P_\infty(p)$ for the Bethe lattice with $z = 3$ (*black*) and normalized mean of the maximum cluster size $\langle s_{max} \rangle$, for von Neumann (*orange*) and Moore (*blue*) neighborhoods. Statistics based on 100 samples with linear size $L = 1,000$ and periodic boundary conditions.

Although some quantities behave as a power law with exponents that do not depend on the lattice details – geometry, neighborhood or boundaries (section 2.3)–, the critical density p_c depends[28]. For example, the probability that a site belongs to the percolating cluster is $P_\infty = 0$ for $p \leq p_c$ and, for $p > p_c$, it diverges with exponent β,

$$P_\infty \propto (p - p_c)^\beta \qquad \text{for} \quad (p \to p_c^+)\,, \tag{3.45}$$

with $\beta = 1$ for Bethe lattices with $z > 2$ and $\beta = 5/36$ for the two-dimensional lattice[28, 47], regarless of the lattice details.

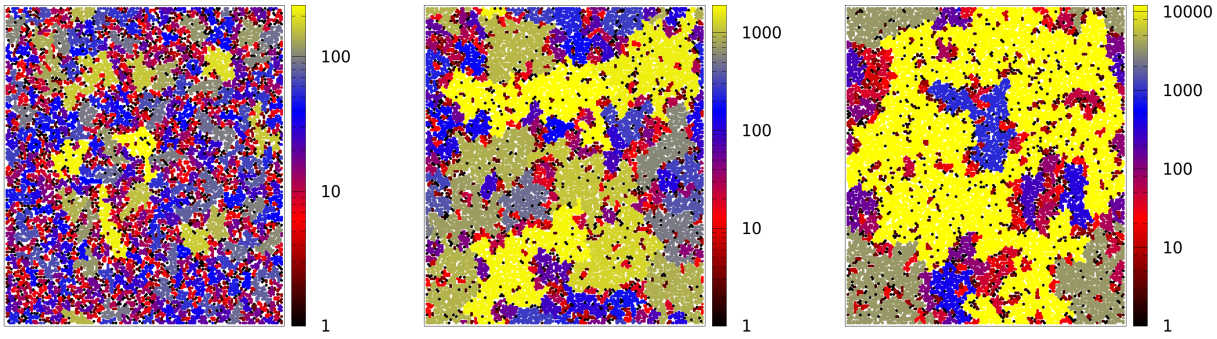

(a) $p = 0.5$ (b) $p = 0.58$ (c) $p = 0.59$

Figure 3.2.8 – Snapshots of two-dimensional lattices with linear size L = 200, von Neumann neighborhood ($p_c \approx 0.59$). The cluster size is indicated by the logarithmic color bar. The occupied sites are larger than empty ones (*white* colored).

The average cluster size $\chi(p)$ diverges for $p \to p_c$ as a power law with exponent γ,

$$\chi(p \to p_c) \propto |p_c - p|^{-\gamma}\,, \quad \text{for } p \to p_c\,. \tag{3.46}$$

For the Bethe lattice $\gamma = 1$ and for two-dimensinal lattice $\gamma = 43/18$. At $p = p_c$, the characteristic cluster size s_ξ diverges with exponent $1/\sigma$, which value is $\sigma = 36/91$ for two-dimensional lattice and $\sigma = 1/2$ for the Bethe lattice (see Equation 3.39). Thus, the scaling form (Equation 3.40) becomes,

$$\begin{aligned} n(s,p) &\propto s^{-\tau}\exp(-s/s_\xi) \qquad \text{for } s \gg 1, p \to p_c\,, \\ s_\xi &\propto (p - p_c)^{-1/\sigma} \qquad \text{for } p \to p_c\,. \end{aligned} \tag{3.47}$$

Applying the same procedure of (Equation 3.43),

$$\begin{aligned} \chi(p \to p_c) &\propto s_\xi^{3-\tau} \\ &\propto |p - p_c|^{-(3-\tau)/\sigma} \\ &\propto |p_c - p|^{-\gamma}\,, \end{aligned} \tag{3.48}$$

implies in the scaling relation

$$\gamma = \frac{3-\tau}{\sigma}\,. \tag{3.49}$$

The most remarkable geometrical aspect of a two-dimensional cluster at the critical density p_c is self-similarity. The fractal dimension of the incipient cluster is $D = 91/48 \approx 1.9$, that relates its mass to the area in which it is immersed. That is,

$$M_\infty(p_c; l) \propto l^D\,, \tag{3.50}$$

where $M_\infty(p_c; l)$ is the number of site composing the percolation cluster in window of size $l \times l$. From this relation (Equation 3.50), the probability that a site within the window of size $l \times l$ belongs to the percolation cluster is given by

$$P_\infty(p_c; l) = \frac{M_\infty}{l^2} \propto l^{D-d}\,, \tag{3.51}$$

where d is the euclidean dimension in which the percolation cluster is immersed, for instance $d = 2$.

When the correlation length ξ is much smaller than the lattice linear size, i.e. $L \gg \xi$, all quantities (such as the average cluster size) are determined by the clusters up to size $s_\xi (\propto \xi^D)$. On the other hand, in the regime with $L \ll \xi$, it is imposed a cut-off diameter L to s_ξ, which is the finite-size effect. All quantities now will depend on clusters up to size L^D, instead of s_ξ. For example, the cluster number density (Equation 3.47) becomes

$$n(s,p;L) \propto \begin{cases} s^{-\tau}\mathcal{G}(s/\xi^D) & \text{for } p \to p_c, s \gg 1, L \gg \xi \\ s^{-\tau}\mathcal{G}(s/L^D) & \text{for } p \to p_c, s \gg 1, 1 \ll L \ll \xi\,. \end{cases} \tag{3.52}$$

3.3 Self-organized criticality

In 1987, Per Bak, Chao Tang and Kurt Wiesenfeld proposed an explanation for some scale invariance behavior related to $1/f$ noise*, which has become known as Self-Organized Criticality (SOC)[19, 17, 53, 28]. Scale invariance is also found in phase transitions, where the critical phase is trigged by a temperature-like control parameter[62]. In SOC models, scale-free phenomena emerge in the system due to cooperative processes with effective long-range interactions that results in a macroscopic state that is different from the mere sum of its microscopic parts. The scale invariance signature in some measurable quantities (observables) suggests that the system is able to self-organize towards an underlying critical point, regardless of a control parameter[80].

3.3.1 Basic definitions

A SOC model possesses three basic elements: many interacting degrees of freedom, an external drive and separation of time scales. The degrees of freedom are mostly finite, discrete and are well-defined in space (sites on a lattice) and their interaction takes place within a finite region, i.e. a local, short-range interaction. These degrees of freedom are local variables that can act as dynamical variables, that is, they can represent an amount of a physical quantity, such as energy. This quantity is distributed among the interacting neighbors, once a certain threshold is reached. The degree of freedom is called stable whenever it stands below the threshold, whereas above the threshold it is called active.

The external driving is responsible for changing or charging the local variables. It can be either uniform driving (the whole set of variables is affected) or a local driving (which affects a particular variable or a small set of variables). The driving is usually a small amount of charge, that can be fixed or random. Stochastic and deterministic driving are terminologies that stand for the choice of the variable position, as well as for the amount of charge it receives. The external driving can behave as a supplier, that is, by loading a stable variable until it reaches the threshold. But it can also act as a perturbation, triggering the variable to its active state.

Once a variable reaches the threshold, it turns active and the interaction starts. The interaction happens as a toppling, the amount of charge is reduced (or even drained out completely), since it is redistributed among the bulk neighbors, by either charging or activating them. The amount of charge each neighbor will receive from the toppling can also be defined as stochastic or deterministic. The toppling is a relaxation process and the set of theses relaxation events is known as an avalanche. The avalanching mechanism is one of the fundamental concepts in SOC models, it shows how small perturbations can trigger a strong response that may spread throughout the whole system. Due to this metastability,

* Generally, any time series with algebraic power spectrum $S(f) \propto 1/f^{\alpha}$ is called '$1/f$ noise'.

it can be argued that the system moves toward in a critical state spontaneously. This is corroborated by the power-law behavior in the histograms (probability density function) of the avalanche observables (such as size and duration), signalling the existence of scale invariance.

During an avalanching event, no external driving is released into the system. This defines another SOC fundamental features, the separation of the time scales. The time scale in which the relaxation processes occur is the microscopic time scale, i.e. the time scale of the microscopic mechanisms within an avalanche. In the microscopic time scale, an external driving might be perceived as a fairly distant event. Otherwise, in the macroscopic time scale external drivings are described by a finite frequency, while avalanches last a tiny amounts of time. An avalanche is characterized by its size, duration, area covered and radius of gyration. These observables are measured within the interval between the external driving and the moment when the relaxation processes ceases, hence the size of an avalanche S is given by the number of topplings that occurred and the duration T is the time elapsed. Each measured quantity is described by a probability density function $\hat{\mathcal{P}}_k(K;L)$,

$$\begin{cases} \hat{\mathcal{P}}_s(S;L) = a_s\, S^{-\tau_s}\, \mathcal{G}_s(S/S_c(L)) & \text{with} \quad S_c = b_s\, L^{D_s} \\ \hat{\mathcal{P}}_t(T;L) = a_t\, T^{-\tau_t}\, \mathcal{G}_t(T/T_c(L)) & \text{with} \quad T_c = b_t\, L^{D_t}\,, \end{cases} \tag{3.53}$$

and its cumulative distribution function $\mathcal{P}_k(K;L)$,

$$\begin{cases} \mathcal{P}_s(S) = \displaystyle\int_0^S \hat{\mathcal{P}}_s(S';L)\, dS' \\ \mathcal{P}_t(T) = \displaystyle\int_0^T \hat{\mathcal{P}}_t(T';L)\, dT'\,. \end{cases} \tag{3.54}$$

Where τ_s and D_s are respectively the avalanche size exponent and the avalanche dimension; whereas τ_t and D_t, the avalanche duration exponent the dynamical exponent, respectively[79, 80]. These exponents can be found using the moment analysis method[32, 101], which also gives the following relation,

$$\tau_k = 2 - (1/D_k) \quad \text{with } k = \{\, s,\, t \,\}\,. \tag{3.55}$$

3.3.2 Drossel-Schawbl forest-fire model

In 1992, Barbara Drossel and Franz Schwabl proposed a forest-fire model(DSFFM)[34], which was an enhanced version of a previous model due to Bak *et al.*[18]. In DSFFM, a fire spreads over an homogeneous population of trees, randomly placed on a square lattice. The criticality of its observables have been disputed for a long time[79, 46, 81, 82], and it is known now[80] that despite the fact that *avalanche size distribution violates simple scaling approach*[46], *its moments follows power law robustly*[82]. This model differs

from other SOC models not only for being a dissipative model – which requires a particle influx, implying the existence of a control parameter –, but also for displaying three distinct time scales, instead of two. In DSFFM, the avalanche is the fire (i.e. active sites) spreading through the lattice trees (i.e. stable sites), whereas the lightning strike is the (local) external driving.

The DSFFM is a two-dimensional CA model – it can also be defined on higher dimensions ($d \geq 2$). Though originally designed with von Neumann neighborhood, in the present work the model is set at the framework of Moore neighborhood instead. The simulation is initialized in a two-dimensional lattice of linear size L with a random configuration: each site of the lattice is occupied either by a tree, by a burning tree, or is empty. For each time step t, the CA evolves according to the following set of rules:

- Each burning tree becomes an empty site, in the next step $t + 1$.
- Every tree with at least one burning nearest neighbor becomes a burning tree, in the next step $t + 1$.
- A tree becomes a burning tree with probability f, regardless of its nearest neighbors.
- An empty site becomes a tree with probability p.

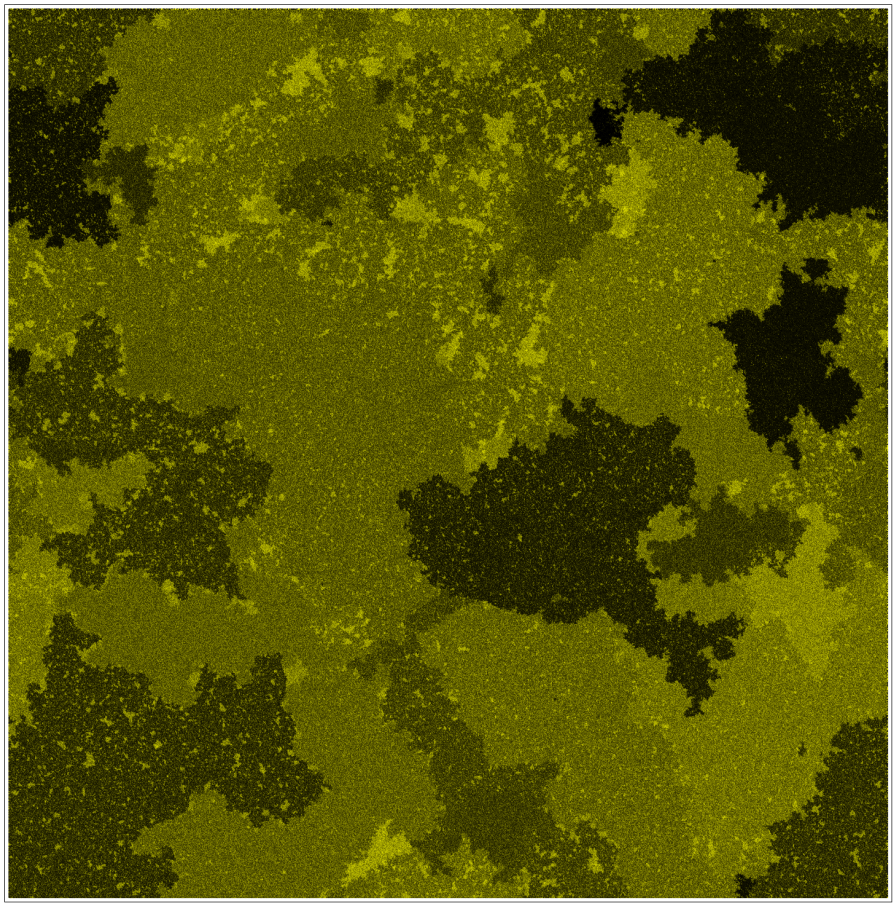

Figure 3.3.1 – DSFFM simulation at the stationary state, after a fire is extinguished. This snapshot shows a whole lattice with 10^8 sites. Linear lattice size $L = 10^4$ and states: tree (*yellow*), empty site (*black*).

The observables, such as fire size and duration, are measured at the stationary state, right after a fire is extinguished. In the present work, the number of trees is also measured at the end of each fire, which provides an auxiliary time scale in units of fire-steps, t_f. Figure 3.3.1 shows a snapshot of the system at the stationary state, after a fire is extinguished; at this point, the distribution of trees has clearly become non-uniform and, moreover, there are dense clumps of trees, i.e. patches of occupied sites.

The tree density evolves in time as showed in Figure 3.3.2. The DSFFM with Moore neighborhood displays a stationary density $\rho_s \approx 0.27 \pm 0.02$[25], whereas with von Neumann neighborhood it is $\rho_s \approx 0.4084 \pm 0.0001$[49]; both values are lower than the critical density $p_c \approx 0.40$ and $p_c \approx 0.59$, respectively, due to (static) percolation model. This divergence is caused by the influx of particles ('sprouted trees'), which creates clumps of trees (clusters of occupied sites). So, even at a lower density than the critical static percolation density ($\rho_s < p_c$), it is likely to happen a fire that can percolate through the lattice – due to highly non-uniform distribution of trees in the system.

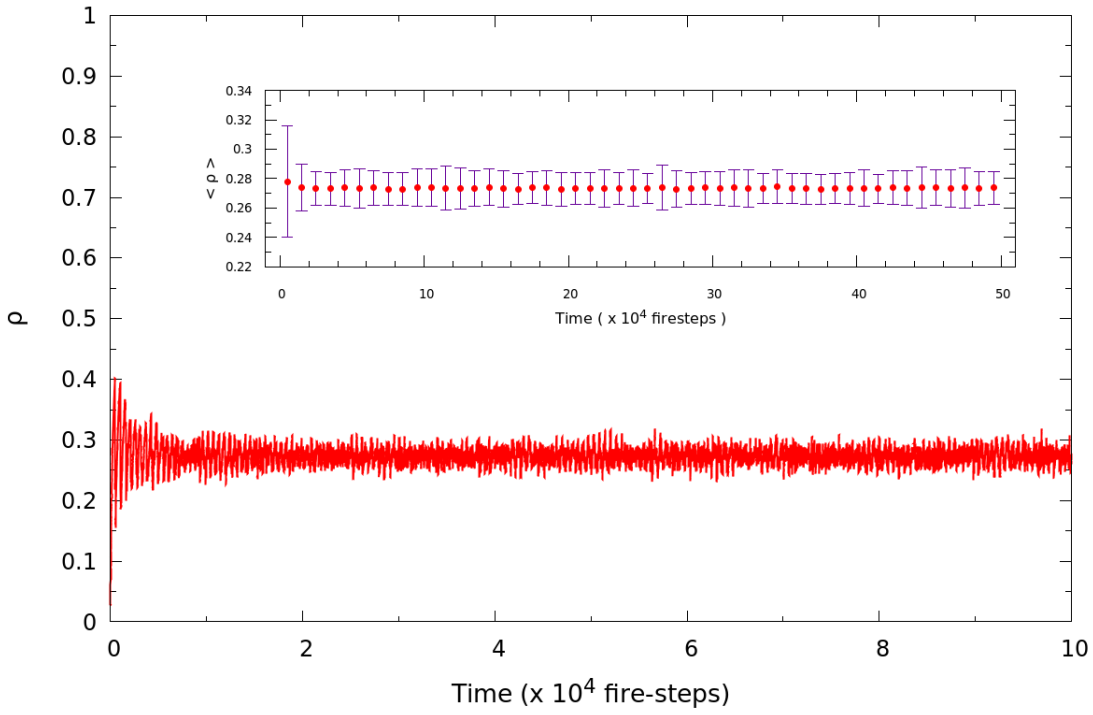

Figure 3.3.2 – Population density $\rho \equiv \rho(t_f)$ and mean population density $\langle\rho\rangle$, in the detail. Linear lattice size $L = 10^4$ and parameter $\Theta = 10^5$.

Besides the avalanche duration, the DSFFM possesses other two characteristic time scales: the average time for a tree to grow $1/p$ and the average time between fires $1/f$. At the limit of the time scale separation $f/p \to 0$, that is $1 \gg p \gg f$, the system reaches a (supposed) self-organized critical state. The parameter $\Theta\,(\equiv p/f)$ controls the number of trees that grows in the system between two lightning strikes. Although $\Theta = p/f \to \infty$ for infinite systems, in finite lattices the Θ parameter must be bounded by the lattice size,

that is $\Theta \ll L^2$ – the role of Θ will be detailed in the next chapter (section 4.1, section 4.2). In DSFFM, the finite-size scaling is given by Equation 3.56, where the cut-off functions $\mathcal{G}_k$ depend on Θ, instead of L. The cumulative distributions (Equation 3.57) are displayed in Figure 3.3.3, with fire-size exponent $\tau_s = 1.181$ estimated by direct linear fitting[25]. The dynamics of the forest-fire model will be detailed in the next chapter, when the generalized forest-fire model will be presented.

$$\begin{cases} \hat{\mathcal{P}}_s(S;\Theta) = a_s\, S^{-\tau_s}\, \mathcal{G}_s(\, S \,/\, S_c(\Theta)\,) & \text{with} \quad S_c = b_s\, \Theta^{\lambda_s} \\ \hat{\mathcal{P}}_t(T;\Theta) = a_t\, T^{-\tau_t}\, \mathcal{G}_t(\, T \,/\, T_c(\Theta)\,) & \text{with} \quad T_c = b_t\, \Theta^{\lambda_t} \end{cases} \tag{3.56}$$

$$\begin{cases} \mathcal{P}_s(S) = \displaystyle\int_0^S \hat{\mathcal{P}}_s(S';\Theta)\, dS' \\ \mathcal{P}_t(T) = \displaystyle\int_0^T \hat{\mathcal{P}}_t(T';\Theta)\, dT' \,. \end{cases} \tag{3.57}$$

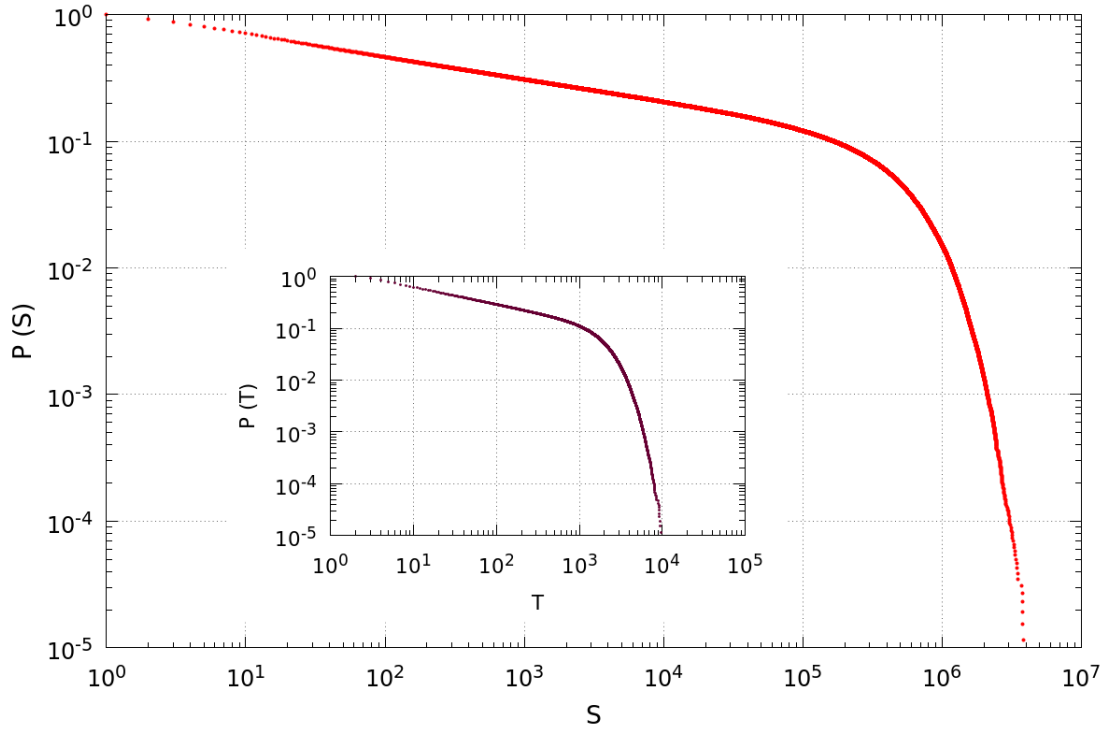

Figure 3.3.3 – Cumulative fire-size distribution $\mathcal{P}_s$ and cumulative duration distribution $\mathcal{P}_t$, in the detail. Linear lattice size $L = 10^4$ and parameter $\Theta = 10^5$. There were analysed near 10^5 fires in the stationary state.

Chapter 4

Generalized forest-fire model

"These imaginary biological systems should be of some help in interpreting real biological forms."
Alan Turing[†]

The Drossel-Schawbl forest-fire model (subsection 3.3.2) has become a paradigmatic model to study self-organized criticality and supplied the literature with several results related to excitable media models. Unfortunately, DSFFM lacks some components of real-life forest fires, since reproduce the behavior of wildfires was not among its goals during its inception.

In 1993, Drossel *et al.* published a forest-fire model with immune trees (FFMIT)[33] based on the same template of DSFFM, but including immune trees and removing the possibility of having sequential lighting strikes – actually, the lattice is struck only once in order to initialize the dynamics. In this model, each tree has a probability $(1 - g)$ of being ignited if it has at least one neighbor on fire, where probability g plays the role of the immunity parameter. In other words, a tree might not catch fire with probability g, even having several burning neighbors. In FFMIT dynamics, the fire spreading and the tree sprouting occur at the same time scale, implying that the system is not led to a long-term stationary behavior.

Meanwhile, Landini *et al.* developed a CA model for studying the morphology of corneal ulcers due to Herpes virus (HSV) infection[57]. In their model, each healthy epithelial cell could present a variable level of susceptibility to viral infection. A permissive cell turns into an infected cell if it has at least one infected neighbor. On the other hand, a resistant cell will get infected depending on the number R of infected neighbors. *In vivo*, corneal ulcers are morphologically classified as dendritic or amoeboid, according to its shape. Under certain parameters, the CA model has yielded fractal ulcers (dendritic phase) and it was also observed that their fractal dimension decayed as their size increased,

[†] Adapted from "The Chemical Basis of Morphogenesis"[109].

shifting from dendritic phase to an amoeboid phase; therefore agreeing qualitatively with the morphological classification.

Following this framework, Camelo-Neto and Coutinho studied a virus spread model using simulations and mean-field theory approach[24]. Late on, they assembled a forest-fire model with resistant trees (FFMRT)[25], in which were considered two distinct populations: susceptible (permissive) trees and resistant trees. Recently, these authors studied a forest-fire model with tree ageing[75], in which the resistance parameter is time-dependent, i.e. $R \equiv R(t_n)$. The time parameter t_n regulates the characteristic life-time of a tree: it sprouts as susceptible tree, reaches a maximum resistance at its mean life-time and then has its resistance decreased – as vitality starts to fade. The parameter t_n also controls the emergence of two distinct long-term behaviors, resembling a dense woodland or a savanna (with *widely spaced, scattered trees*[14]).

The present work aims to generalize some aspects of forest-fire model with resistant trees (static resistance), which may lead to a better comprehension of the role played by wildfires over a forested region. As a model of anomalous diffusion and excitable media, its results can be applied to related subjects immediately, e.g., epidemic spread. As a cellular automata model, the first novelty will be expanding the cell's neighborhood (subsection 4.2.1), which gives the model another pinch of realism. Afterwards, it will be included the possibility of having static forbidden sites (subsection 4.2.2) – that will neither interact with fire, nor trees will be able to sprout on it. Hence, the heterogeneity will not be only due to the resistant trees, but also due to the forbidden site, making the model even more related to percolation theory.

4.1 Forest-fire model with resistant trees

The FFMRT generalizes the DSFFM by introducing a fraction of trees that are resistant to fire, i.e., some trees only will burn if they have at least a certain number of burning neighbors, R. Thus, there are two populations with different flammability, resistant and susceptible, the last needs at least one burning neighbor to be ignited. These distinct fractions of trees (which can also be acres of wildland or bushes) are set with the parameter q, which stands for the probability of sprouting a susceptible tree, whereas a tree has probability $(1 - q)$ of sprouting as resistant. The presence of resistant trees will constrain the reach of the flames, therefore lowering the size of the fires.

The simulation runs in a two-dimensional lattice with linear size L, periodic (toroidal) boundary conditions as in DSFFM and the interaction is allowed within a Moore neighborhood, instead of the von Neumann neighborhood. The possible CA states are: empty, susceptible tree, resistant tree and burning tree. Starting from a random configuration of resistant trees, susceptible trees and empty sites (with probability $p\times(1-q)$,

$p \times q$ and $(1-p)$, respectively), the site to be ignited is chosen at random and afterwards the CA rules below are applied:

▷ If the chosen site has a tree (susceptible or resistant), it becomes a burning tree.

▷ If the chosen site is empty, a set of Θ sites are chosen at random and a tree sprouts at each empty site within this set – with probability q of being susceptible or $(1-q)$ of being resistant.

▷ The fire spreads according to the rules:

- A burning tree dies, becoming an empty site in the next step.
- A susceptible tree with at least one burning neighbor becomes a burning tree in the next step.
- A resistant tree with at least R burning neighbors becomes a burning tree in the next step.

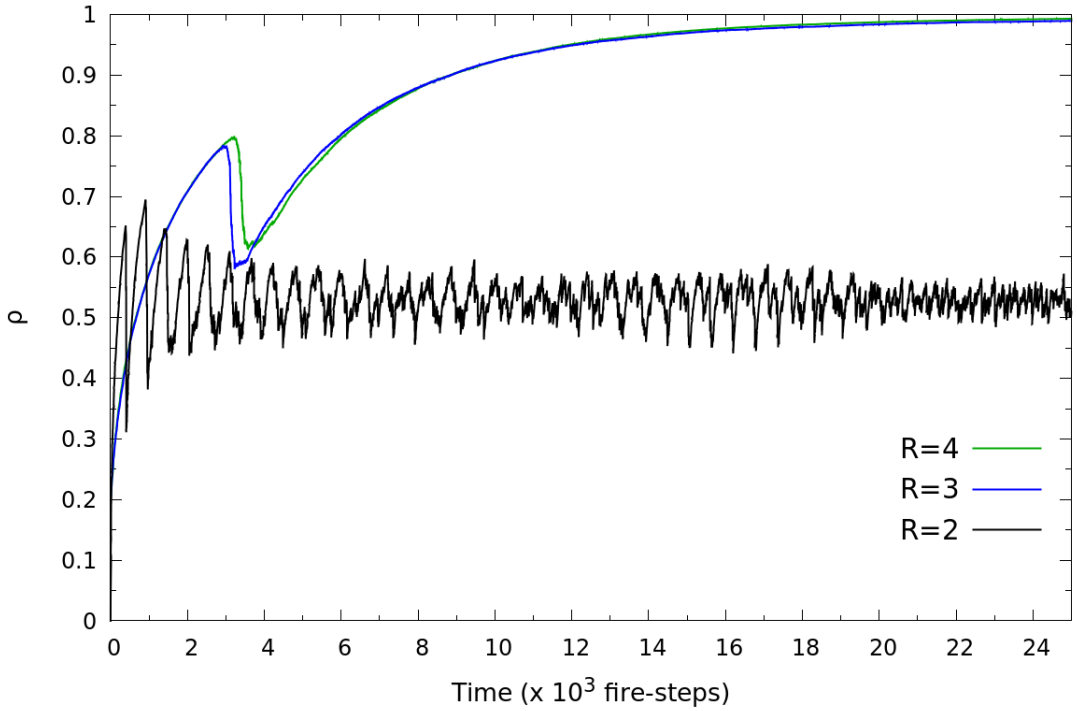

Figure 4.1.1 – Time-series of the total population density $\rho \equiv \rho(t_f)$ – the number of trees is measured at the end of each fire (subsection 3.3.2). Linear lattice size $L = 10^4$ for $R = 2$ and $L = 2 \times 10^4$, for $R = \{3, 4\}$. Parameters $\Theta = 10^5$ and $q = 0.5$, for all cases.

As a site in the Moore neighborhood has 8 neighbors, the values for the resistance parameter R are integers ranging from 1 to 8, $R = \{R \in \mathbb{Z} : 1 \leq R \leq 8\}$. As defined in subsection 3.3.2, the parameter Θ is the 'time-scale separation' parameter, $\Theta \equiv p/f$. In the homogeneous case ($R = 1$), the dynamics of DSFFM is restored, while for $R = 2$ the system is less reactive, as expected. In both regimes ($R \leq 2$), the system exhibits large fluctuations around the mean stationary density, which suggests the occurrence of fires with magnitude greater than the parameter Θ. In fact, for $R = 2$ the standard deviation

of the density in the stationary state is, in average, 2% of the lattice size L^2. Then, using as example the parameters from Figure 4.1.1, for a lattice of size $L^2 = 10^8$, the standard deviation is $\sigma \approx 2 \times 10^6$, being one order of magnitude greater than the parameter $\Theta = 10^5$.

For cases with $R \geq 3$, the total density barely oscillates and the system is rapidly pushed to a high density phase (Figure 4.1.1). In the stationary state, the fluctuation around the mean density practically vanishes, indicating that fires with size greater than Θ are very unlikely. Actually, in these regimes ($R \geq 3$), the system becomes so dense that only few empty sites still available for sprouting trees (subsection 4.4.2). The system response for distinct values of the parameter q, which controls the amount of susceptible trees sprouting at the end of each fire, was analysed by Camelo-Neto and Coutinho[25]. Using the stationary densities for $R = \{3, 4\}$, they reported a critical value $q_c \approx 0.82$ for $R = 3$, above which the dense forest structure that restrains the spread of large fires is broken and displays fluctuations similar to $R = 1, 2$. For $R \geq 4$, this transition only happens for values very close to $q = 1$, which restores the homogeneous behavior (DSFFM).

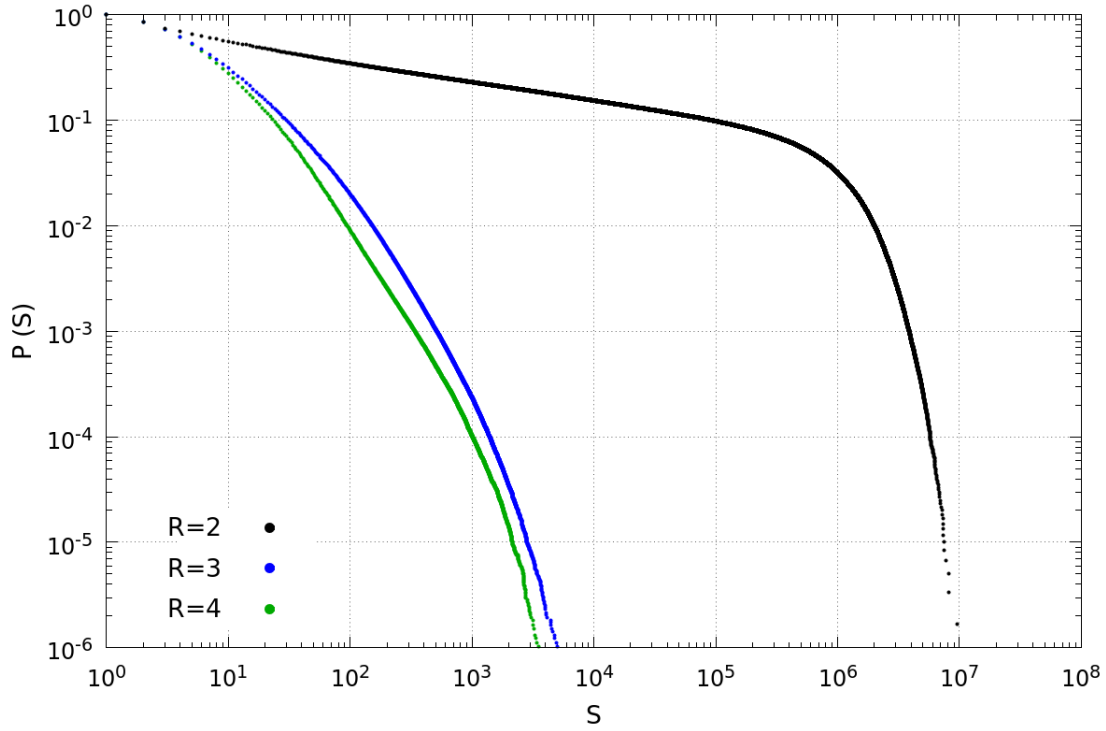

Figure 4.1.2 – Cumulative fire-size distributions. Linear lattice size $L = 10^4$ for $R = 2$ and $L = 2 \times 10^4$, for $R = \{3, 4\}$. Parameters $\Theta = 10^5$ and $q = 0.5$, for all cases. There were analysed nearly 10^6 fires in the stationary state for each R value.

Because their low flammability, resistant trees survive in the lattice longer periods of time than susceptible trees. As result, it is observed the emergence of clumps of resistant trees (large clusters), leading to a robust stationary state that confines the fire propagation

to smaller areas. This can be immediately noticed in the fire-size statistics (Figure 4.1.2). The fire-size distribution for $R = 2$ shows a region of power-law behavior similar to those distributions found in DSFFM, indicating that any scale invariance due to SOC dynamics is not compromised by the fraction of trees with relatively low resistance. On the other hand, a drastic decrease can be observed in the fire-size distributions for $R \geq 3$, showing that the typical SOC signature does not emerge for relatively high resistances.

4.2 Generalized model

The generalized forest-fire model aims to simulate an even more heterogeneous environment by making use of a CA model defined on a square lattice of linear size L, with periodic (toroidal) boundaries, r-Moore neighborhood, where r ($\in \mathbb{Z} : r > 0$) stands for the range of the neighborhood (section 2.3), and 6-state cells. The set of states is comprised by empty, susceptible tree, resistant tree, fire, ash and forbidden site, i.e., $\mathcal{S} = \{\, empty, treeS, treeR, fire, ash, block \,\}$ – the ash state is a temporary state used to account the fire size. The lattice is initialized with trees being placed randomly over the lattice. Each site has probability s of being occupied by a forbidden site, i.e. *block* state. On the remaining fraction of 'available' sites, it has a probability p of being occupied by a tree, otherwise it is an empty site with probability $(1 - p)$. Each occupied site can be either a susceptible tree, with probability q, or a resistant tree, with probability $(1 - q)$. Thus, in the initial configuration, the probability of a lightning strikes an empty site is $(1 - s) \times (1 - p)$, the probability of striking a susceptible tree is $(1 - s) \times p \times q$ or striking a resistant tree, $(1 - s) \times p \times (1 - q)$.

The CA dynamics is split in three stages, a *lightning stage*, a *burning stage* and the *sprouting stage*. The transition rules are listed below:

▷ Lightning stage:

At time step t, one site is chosen randomly.

- If it is an *empty* or *block* site, the system goes into the *sprouting stage*.
- If it is occupied by a tree, not mattering its sort, it is eligible to be ignited, i.e., start burning. Then, in the next step $t + 1$, the tree state is shifted to $fire$.

When a tree is ignited, the system is warned to enter the *burning stage*.

▷ Burning stage:

At time step t,

- A $fire$ site turns to ash in the next step $t + 1$.
- If a $treeS$ site has at least one $fire$ neighbor, it turns to $fire$ in the next step $t + 1$.
- If a $treeR$ site has $fire$ neighbors, it will turn to $fire$ in the next step $t + 1$ only if the number of its $fire$ neighbors $\mathcal{N}_{fire}$ is at least equal to R, that is, $\mathcal{N}_{fire} \geq R$.

If there are no more burning trees ($fire$ sites have extinguished), the ash sites turn

to *empty* sites and then the system goes to the *sprouting stage*.

▷ Sprouting stage:

At time step t, a number of Θ sites are chosen at random.

- If it is an *empty* site, in the next step $t+1$, a *treeS* or a *treeR* sprouts, with probability q and $1-q$, respectively.
- If the site is occupied by either a *treeS*, a *treeR* or a *block*, it remains unchanged.

At the step $t+2$, the system returns to the *lightning stage*.

These rules are slightly different from the FFMRT (section 4.1), once the *block* state was added. The neighborhood range r is not explicitly included in the rules, although it is considered every time a site assess its neighbors state. In Figure 4.2.1, there is an example of the process of fire spreading accomplished in the *burning stage*. Sites that are being assessed by the CA rules have a numerical label. Trees (*treeS*, *treeR*) are labelled with its total number of burning neighbors $\mathcal{N}_{fire}$, whereas sites with other states (*empty*, *fire*, *ash*, *block*) are labelled with its coordinate, in order to indicate the fire displacement.

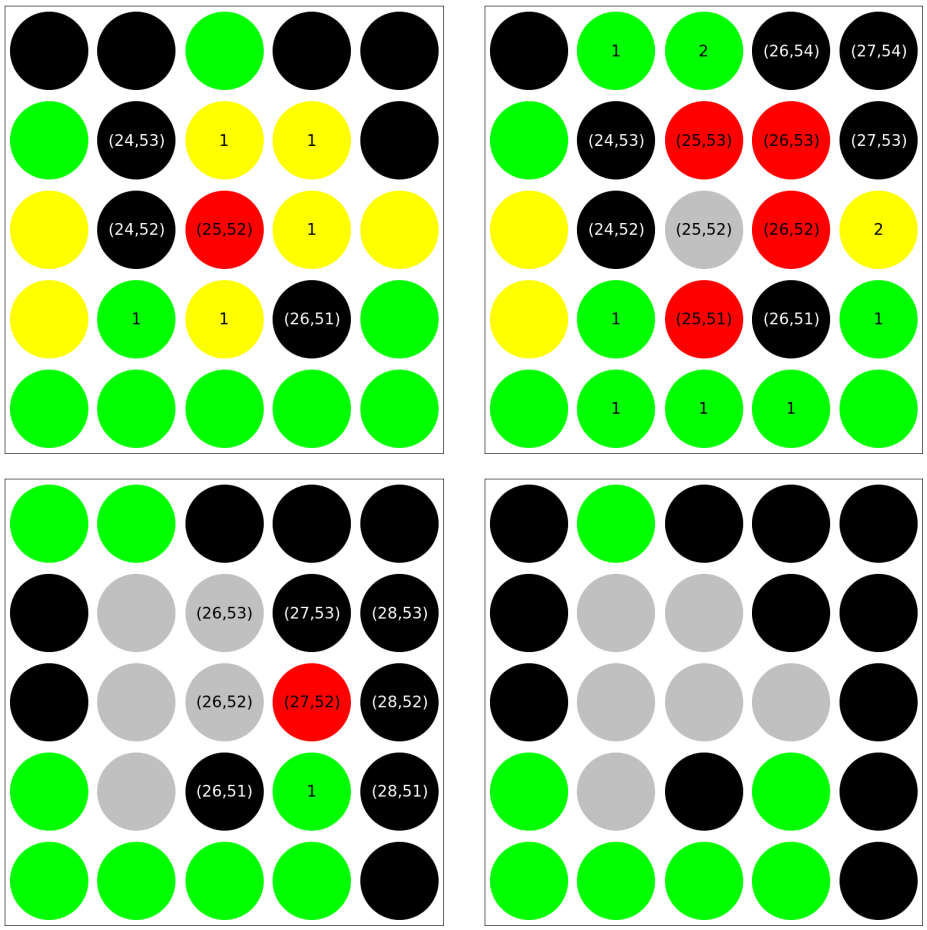

Figure 4.2.1 – Snapshots of the system at the *burning stage*, with Moore neighborhood, resistance $R = 3$ and densities $s = 0$, $p = 0.6$ and $q = 0.5$. Site colors: *empty* (*black*), *treeS* (*yellow*), *treeR* (*green*), *fire* (*red*), *ash* (*grey*).

4.2.1 On enlarged neighborhoods

As a thermodynamic process, the combustion of woods, as it is being dealt here, is an open system, thus there are mass fluxes both in and out of the system as well as energy flows, role that is played by the fire as outcome of a chemical reaction or a gradient of temperature. As a contact model approach, the flame due to a single site is limited to interact only with its nearest neighbors, in this case, the 8 neighbors of the Moore neighborhood. As a sort of conservation law, it is imposed that the fire flames must be confined within a restricted area, although in nature wildfire flames can be extremely intense, creating huge gradients of temperature – and even convection currents – that can permeate further and then starting fires far beyond the flame fronts[103].

Aware of this flaw, the model can be improved in order to simulate the fire spread due to higher temperatures and, therefore, allowing flames to reach further distances by incrementing the parameter r (see Figure 2.3.3), which controls the range of the interaction and hence the number of neighbors. Consider an increment of one unit in the neighborhood range, which leads to the 2-Moore neighborhood that has 24 neighbors, as seen in section 2.3. In the 2-Moore picture, the 8 nearest neighbors comprise the first layer δ_1, whereas the others 16 next-nearest neighbors belong to the second layer, δ_2 (Equation 4.1).

$$\delta_i^{[Mo]}(x_0, y_0) = \begin{cases} \delta_1 = \{(x,y) : 0 < |x - x_0| \leq 1,\ 0 < |y - y_0| \leq 1\} \\ \delta_2 = \{(x,y) : 1 < |x - x_0| \leq 2,\ 1 < |y - y_0| \leq 2\} \\ \delta_3 = \{(x,y) : 2 < |x - x_0| \leq 3,\ 2 < |y - y_0| \leq 3\} \end{cases} \tag{4.1}$$

An example of how the fire spreading dynamics fits on this new framework can be seen in Figure 4.2.4. The first startling impression as one sees this sequence of snapshots is about how bigger the fire has grown or how wider its area has become when compared to the fire spreading in 1-Moore picture, seemingly the capacity of burning further trees has been accomplished. Indeed, once the number of neighbors is raised, the reactivity of the system increases as well, so instead of dealing with 8 neighbors as before, each site needs to assess the state of 16 more neighbors from the second layer, creating a scenario where, at each step, more state transitions are likely to occur. Moreover, the state shifting is also faster, because, for example, a site that only would burn in step $t + 2$ will be catching fire in step $t + 1$. It is important to observe that no asymmetry or hierarchy is assigned between these layers, in other words, each neighbor is equally likely, therefore no gradient of temperature is actually created. Furthermore, the range r is incremented once more, assembling a 3-Moore neighborhood which displays 48 neighbors. This neighborhood displays a third layer δ_3, comprising 24 neighbors (Equation 4.1), which is even more reactive than the previous 1-Moore and 2-Moore.

When working with an homogeneous population (without resistant trees, $q = 1$), the enhancement due to increasing the interaction might sound as a silly choice, because considering a fully dense lattice, the dynamics will only sweep the lattice twice faster for the 2-Moore picture and even faster for 3-Moore, approximately three times faster. As example, a lattice with linear size $L = 500$, fully occupied with susceptible trees (homogeneous population) and with 1-Moore neighborhood, has been completely overrun within 252 time steps, while the 2-Moore did it within 127 steps and 3-Moore completed within 86 steps. Despite that if a percolation approach is considered, the critical density $_c$ decreases approximately by a factor of 2 and a factor of nearly 5, for 2-Moore and 3-Moore pictures, respectively. These factors were estimated from a ratio involving number of neighbors and are straight forward,

$$\begin{aligned} \frac{\mathcal{N}(r=2)-\mathcal{N}(r=1)}{\mathcal{N}(r=1)} &= \frac{24-8}{8} = 2\,, \quad \text{for 2-Moore and} \\ \frac{\mathcal{N}(r=3)-\mathcal{N}(r=1)}{\mathcal{N}(r=1)} &= \frac{48-8}{8} = 5\,, \quad \text{for 3-Moore,} \end{aligned} \tag{4.2}$$

where $\mathcal{N}(r)$ stands for the number of neighbors in a neighborhood of range r. For a quick inspection, it was used the lattice with $L = 500$ and homogeneous population ($q = 1$). The results suggested a $p_c \approx 0.40$ for 1-Moore, which agrees with reported values[70], $p_c \approx 0.17$ for 2-Moore and $p_c \approx 0.09$ for 3-Moore, both within an error of the estimated values (Equation 4.2). As percolation theory is extremely relevant in clarifying the long-term behavior of the system, the enlarged neighborhood required the evaluation of some statistics – see Figure 4.2.2 and Figure 4.2.3.

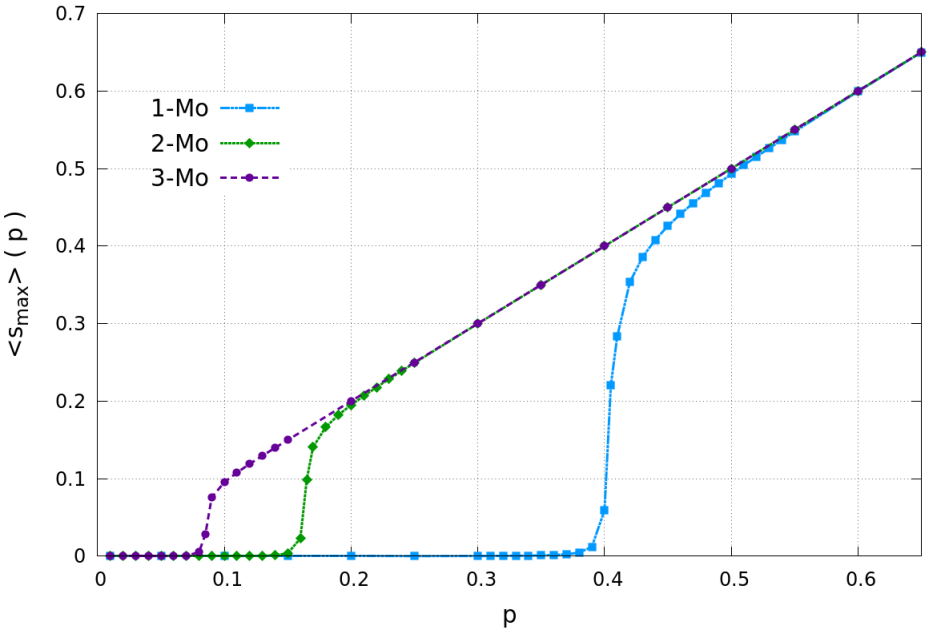

Figure 4.2.2 – Normalized mean of the maximum cluster size $\langle s_{max} \rangle$, for r-Moore neighborhoods ('static' percolation). There were run 100 samples with linear size $L = 1,000$, homogeneous population and periodic boundary conditions.

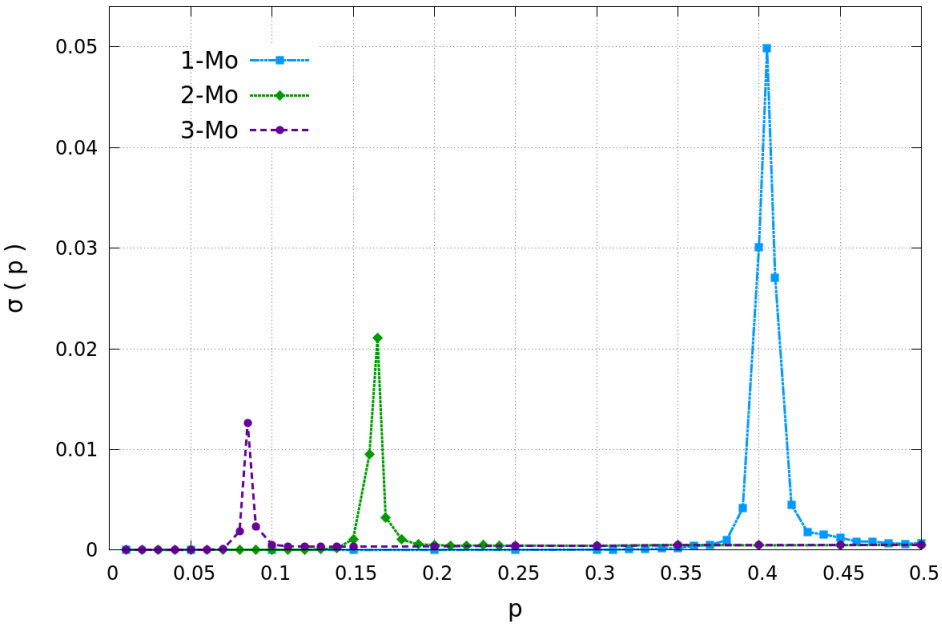

Figure 4.2.3 – Normalized standard deviation of the maximum cluster size σ, for r-Moore neighborhoods ('static' percolation). There were run 100 samples with linear size $L = 1,000$, homogeneous population and periodic boundary conditions.

The statistics indicates that the critical percolation density is $p_c \approx 0.405$ for 1-Moore, $p_c \approx 0.165$ for 2-Moore and $p_c \approx 0.085$ for 3-Moore, at some point corroborating the estimated values. It is also important to remark that as the neighborhood is enlarged, the region of fractal clusters is decreasing – region where the derivative of the curves in Figure 4.2.2 are steeper. In other words, the incrementation of the neighborhood parameter r leads to a regular diffusion process that displays compact clusters.

The expansion of the neighborhood has two important consequences that must be regarded. First, as the reactivity of the system is increased, the ability to burn bigger areas increases likewise. It becomes easier for the fire to reach the boundaries of the lattice which may lead to finite-size effects (beyond a simple upper cut-off) by breaking long-range correlations. In practical terms, the lattice size L^2 used to measure fire sizes in a 1-Moore neighborhood might display a misleading lack of accuracy when analysing r-Moore fire sizes with $r > 1$.

Secondly, the geometry of the burnt trees (ashes) clusters might disagree with regular site percolation. Suppose an idealized example in which a burning site, in a 1-Moore neighborhood, is surrounded by resistant trees, then in the next step the fire will fade because the flame was incapable to spread through the wall of trees. Bringing this example to the 2-Moore picture, the fire will not only pass by the wall of resistant trees placed on the first layer, but its effective intensity will not be diminished by the wall as well. This effect of independent interaction between the main site and each layer δ_i eliminates the

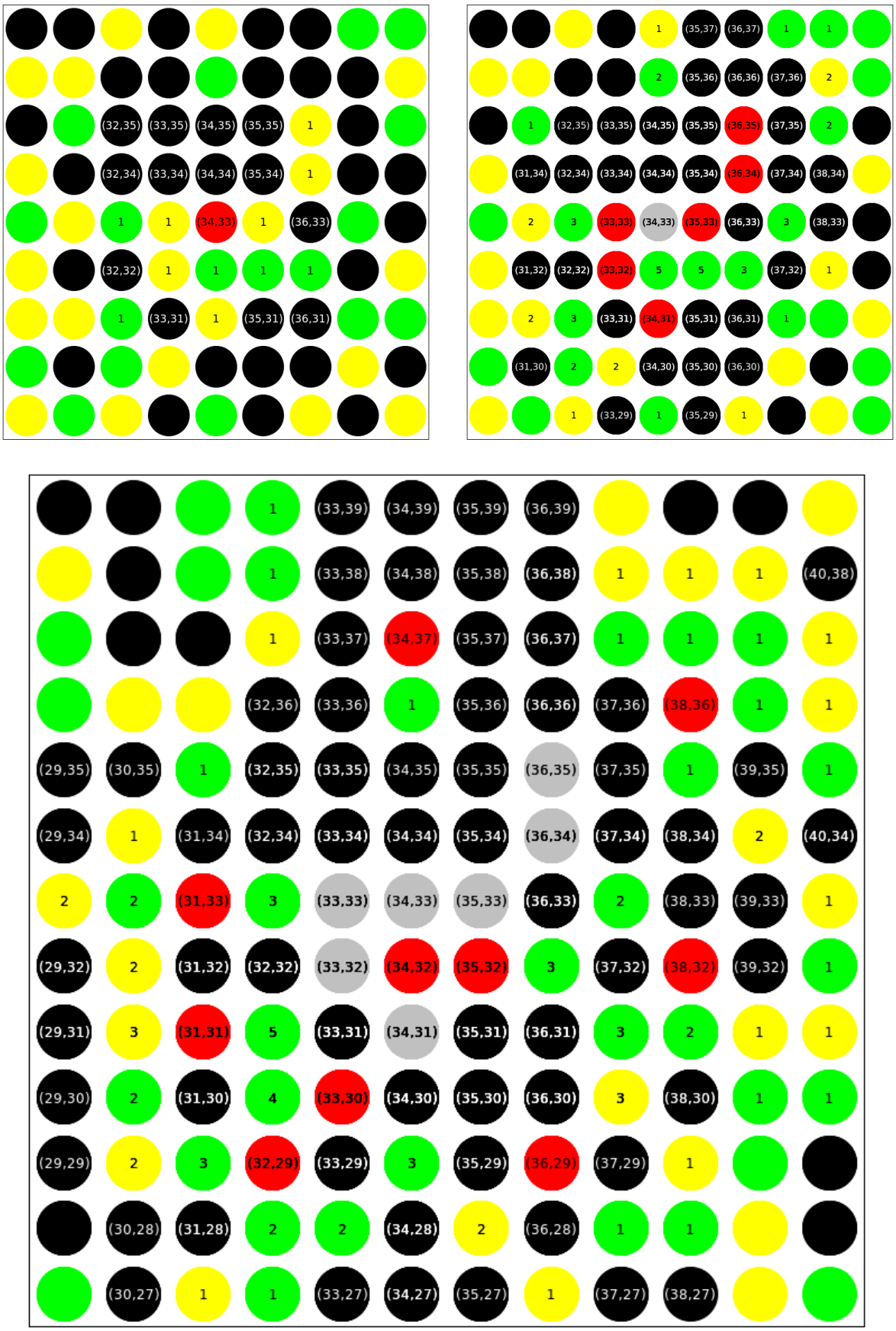

Figure 4.2.4 – Snapshots of the system at the *burning stage*, with 2-Moore neighborhood, resistance $R = 5$ and densities $s = 0$, $p = 0.5$ and $q = 0.5$. Site colors: *empty* (*black*), *treeS* (*yellow*), *treeR* (*green*), *fire* (*red*), *ash* (*grey*).

particle-like aspect of the fire and instead it exhibits the field-like behavior of the flame, mimicking its real role as source of heat. Still about the idealized example, imagine now that the second layer is made of susceptible trees only and that the resistance of the tree in the first layer is $R = 5$. In the time step $t+2$, all the trees in the first layer will be burnt by the burning trees of the second layer. In other words, it means that the fire was able to spread backwards. The snapshots in Figure 4.2.4 show a fire spreading on a 2-Moore neighborhood and resistance parameter $R = 5$. At the first step t, the resistant trees at sites (34,32) and (35,32) are assessed, but having one burning neighbor each, they will not ignite. In the following step $t + 1$, the fire spreads to every susceptible tree in the neighborhood and both (34,32) and (35,32) will have now five burning neighbors each, then at $t + 2$ they finally become burning trees. With a closer look on this arrangement, one can notice that this path was forbidden in the 1-Moore picture, that is, during step $t + 1$ the tree on (34,31) would not be burning, leaving (34,32) with $\mathcal{N}_{fire} = 3$ ($< R = 5$), and tree (35,32) would not reach for burning tree (33,33) and (33,32). Moreover, neither (36,34) would be on fire nor (35,32) could reach that far, then (35,32) would have $\mathcal{N}_{fire} = 1$ ($< R = 5$). At step $t+2$, both (33,32) and (34,32) would remain as $treeR$. Afterwards, the spread would go on through (34,31) $\rightarrow$ (33,30) $\rightarrow$ (32,29), while on the other side branch the fire would have faded out after burning the tree at (36,35).

The observed clusters were already available in the 1-Moore neighborhood, but they have become more evident as the neighborhood was enlarged. Their geometry is built on paths that are forbidden in 'static' site percolation theory. Such clusters are related to the 'fluctuating site percolation', found on the forest-fire model with immune trees, reported by Drossel *et al.*[33]. The r-Moore neighborhoods with $r > 1$ will sweep greater perimeters faster because of its 'further forward' interactions, but it also will create even greater fires/clusters due to their ability of interacting with trees that were left behind the flaming fronts.

4.2.2 On random forbidden sites

The enlargement of the active neighborhood provides higher reactivity on the lattice, but which elements of the model act to suppress the spreading? From the original DSFFM, the states $fire$ and $treeS$ could be regarded as fire propagators, whereas *empty* sites, as well as *ash* sites, act as fire absorbers. The novel $treeR$ state introduced by the FFMRT model can behave as a fire propagator – for relatively low resistance R –, but it mostly acts to constrain the fire spreading – for relatively high R values. The present model introduces a special static CA state named *block*. This state act as a fixed fire absorber, being completely inert to the whole dynamics of the system. A *block* state differs from the *empty* state because the last is eligible for sprouting a tree, while the *block* is a fixed, unchangeable lattice site. The fraction of *block* sites drops the stationary density of

both *treeS* and *treeR*, once less sites are eligible to sprout a tree, and moreover, above a certain threshold, this fraction is capable of toughening tree clusters, i.e., they prevent susceptible trees from sprouting inside a clump of trees. The *block* sites do not change the transition rules, since they do not interact with other sites.

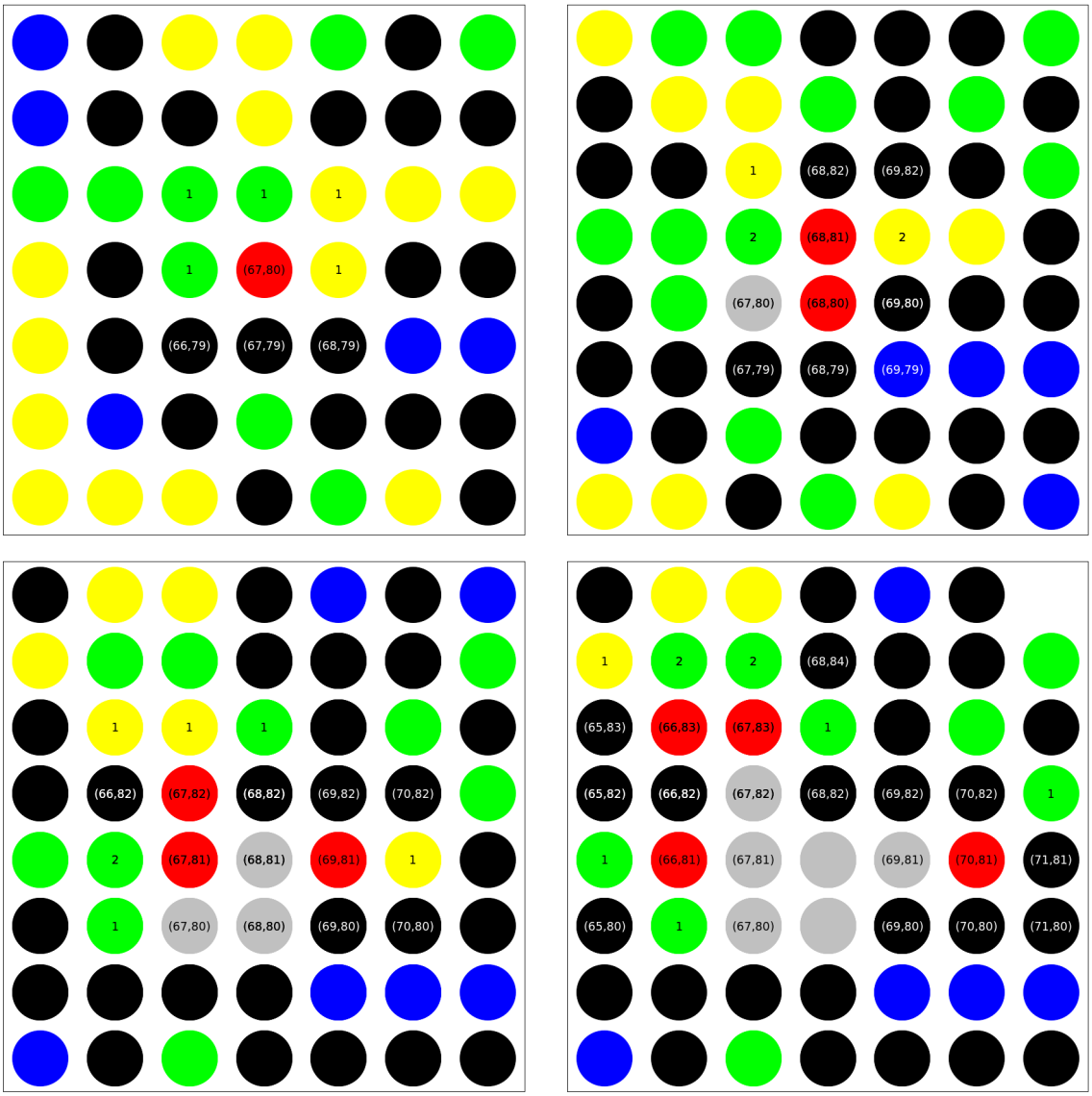

Figure 4.2.5 – Snapshots of the system at the *burning stage*, with 1-Moore neighborhood, resistance $R = 2$ and densities $s = 0.1$, $p = 0.6$ and $q = 0.5$. Site colors: *empty* (*black*), *treeS* (*yellow*), *treeR* (*green*), *fire* (*red*), *ash* (*grey*), *block* (*blue*).

4.3 Computational aspects and algorithms

The process of taking the forest-fire model from the CA rules to a computer simulation is a bit straight forward and an average programmer can do it in a few hours. Once implemented, this program may require some weeks of running time if it uses a lattice

with $L = 5,000$, for example, and unfortunately this lattice size would not yield accurate results (subsection 4.4.1). Even if there was no hurry for the results, static allocation of lattices greater than $L = 10,000$ requires a reasonable amount of memory and at some point the simulation would halt and crash. In order to overcome these issues, part of this work was dedicated to assembling computational algorithms that could optimize the memory allocation required and the simulation running time, by adapting the CA rules though not changing it.

The program was written in the `C++` programming language (`gcc` compiler version 4.8.4 [5]), which is a general-purpose language[3]. The simulation is assembled on an object-oriented syntax, which is one of the advantages of working with `C++`. While the program is running, it can be displayed on the screen by using the API* freeGLUT[4], which is an open-source version of the 'openGL Utility Toolkit', commonly known as GLUT[6]. This graphical version of the simulation runs slower, despite that it is of great use for checking whether some features are working properly, for instance boundary conditions. Other important component was the utility software GNUParallel[99], which was in charge of the optimized distribution of multiple simulations among the processors and hence for running them in parallel, i.e., GNUParallel was responsible for running several simulations at once, each with different parameters. For some numerical and statistical analyses, like linear regression or evaluating the moments of the distribution, it is used the GSL library – GNU Scientific Library[7, 40]. As the largest lattices considered in this work have nearly 10^9 sites and in order to avoid pseudo-random number effects, it is used the 'four-tap' random number generator proposed by R. Ziff[127], which was suggested by Grassberger[46] and also used by Camelo-Neto and Coutinho when working in FFMRT[25].

The first step on building the model in the computer is about bringing the lattice from an abstract form to its computational counterpart. So, the lattice is dynamically allocated in a state matrix $\mathcal{S}_{i,j}$, with set of states $\mathcal{S} = \{empty, treeS, treeR, fire, ash, block\}$. The straight forward method of implementation updates the whole matrix $\mathcal{S}_{ij}$ at each step and the transition rules will return a new state for each site. This procedure will be avoided by analysing only those sites that are directly taking part on the dynamics, that will be called active sites. The stack of active sites will comprise all the $fire$ state sites, its neighbors and its neighbors' neighbors. An object class called `tree` is created to temporally save active sites. The class is made of 3 elements and has 6 functions defined, the first two elements retain the site coordinates (i, j), while the third element retains the site state $\mathcal{S}_{ij}$. The class functions are designed to control the reading and writing process on the state matrix (see Figure 4.3.1).

The state matrix is initialized randomly. The initial set of states does not include neither $fire$ nor ash states. The initial mean fraction of $block$, $treeS$ and $treeR$ are

* Application Programming Interface

```
///set of states
enum state {empty,treeS,treeR,fire,ash,block};

//class def
class tree{
                int x,y; //position
                state s; //state
        public:
                tree() {x=y=0; s=empty;}        //constructor
                ~tree(){}                       //destructor
                void set_x(int i){x=i;}         int get_x(){return x;}
                void set_y(int j){y=j;}         int get_y(){return y;}
                void set_s(state k){s=k;}       state get_s(){return s;}
                //f() writing                   //f() reading
};
///
```

Figure 4.3.1 – Declaration of the states and the object-class `tree`. The set of states is defined using the `C++` default function `enum`. The object-class `tree` has three functions for writing, `set_()`, and other three for reading, `get_()`.

given before the program is executed in terms of the probabilities s, $(1-s)\,p\,q$ and $(1-s)\,p\,(1-q)$, respectively. From the point that the program starts running, no external inputs are accepted and the simulation only responds to the transition rules of each stage, as seen in section 4.2.

Once a *treeS* or *treeR* is ignited by a lightning strike, its state is shifted to $fire$ and it is saved in a `vector` of `tree` objects (`vector<tree>`). `C++` has some default libraries for special types of arrays that are already implemented with dynamic allocation, one of these is the `<vector>` library. These objects act as seeds for the spreading, that is, in the following step they will feed the function `spread()`, in which their neighbors are assessed. Then, the function `count_neighbors()` accounts and returns the number of $fire$ sites in the main site neighbor's neighborhood, meaning that happens a sort of shift in the reference frame, that is, each neighbor of a burning tree temporarily becomes a main site. After that, the `spread()` function assesses which of the *treeR* sites are eligible for ignition, copy them as `tree` objects and move to the `tree vector`, where they are placed along side the *treeS* sites found in that same neighborhood and the $fire$ site that acted as seed. The function `unite()` (Figure 4.3.2) was designed for bonding together the `vectors` resulting of each active site, it also identifies and gets rid off duplicated `tree` objects and for doing so it makes use of modified versions of the functions `Comp()` and `Equal()`, both from the default library `<algorithm>`. After all neighbors of $fire$ sites have been swept and their object version been allocated in the `vector` of flammable trees, they are properly updated: $fire$ sites turn to *ash*, whereas *treeS* and *treeR* sites turn to $fire$. At last, the new states are updated in the state matrix. The main point of applying the described functions is that at each step there is no algorithm sweeping the whole matrix looking for burning trees, but instead the $fire$ sites are tracked down from the very moment of the first ignition (lightning strike).

```
///// f() for <vector> of trees - (L/R)HS = (left/right) hand side
bool Comp(tree lhs, tree rhs ){ //Compare LHS and RHS
        if((lhs.get_x())==(rhs.get_x())) return (lhs.get_y())<(rhs.get_y());
        else return (lhs.get_x())<(rhs.get_x());
        //If X equal, ordering using y.
        //else, ordering using x
        }
bool Equal(tree lhs, tree rhs){ //LHS=RHS, if both coordinates are equal.
        return (lhs.get_x())==(rhs.get_x())&&(lhs.get_y())==(rhs.get_y());
        }
/////

vector<tree> unite(vector<tree> X,vector<tree> Y){
//unites two vectors but erases duplicated elements

        int ns=X.size(); int nr=Y.size();
        vector<tree> V(ns+nr);
        merge (X.begin(),X.end(),Y.begin(),Y.end(), V.begin(), Comp);
        sort (V.begin(),V.end(), Comp);
        V.erase( unique( V.begin(), V.end(), Equal ), V.end() );

        return V;
        }
//end func unite
```

Figure 4.3.2 – Declaration of functions `Comp()`, `Equal()` and `unite()`. The first two are modified versions of default functions from the `<algorithm>` library.

As an open system, throughout the dynamics particles are always coming in and out of the system. The particle interactions through the different stages of the simulation requires a balance, i.e. a conservation law. The total number of sites must be conserved, that is, at the end of each fire the number of trees, *treeS* and *treeR* states, plus the number of *empty* and *block* must remain equal to number of cells, $\mathcal{N}_{treeS}+\mathcal{N}_{treeR}+\mathcal{N}_{empty}+\mathcal{N}_{block} = L^2$. This might sound as an obvious comment, but if this relation is not well defined it can, for example, mislead the procedure of finding the system's stationary state, since it depends on the total density of trees, $\rho = (\mathcal{N}_{treeS} + \mathcal{N}_{treeR})/L^2$.

4.4 Stationary state

A stochastic process is said to be *stationary*, if the probability distribution of a certain observable is explicitly time independent[48]. It means that the moments of the distribution must not depend on the time variable t, that is

$$\frac{d}{dt}\langle X_i\rangle = 0\,, \tag{4.3}$$

where $\langle X_i\rangle$ is the ith moment of the distribution. This definition of stationary state is very restrictive and in natural phenomena is quite unusual to find a system with such peculiarity. Therefore, a system is said to be *weakly stationary* if its first and second moments (mean and variance) are not explicitly dependent of time. So, it must satisfy the conditions

$$\frac{d}{dt}\langle X_1\rangle = 0\,, \quad \frac{d}{dt}\langle X_2\rangle = 0\,. \tag{4.4}$$

In the present work, the world *stationary* always refers to a weakly stationary process. By the way, it is appropriate to recall that *stationary state* and *absorbing state* are not interchangeable terminologies. The last refers to a process that got stuck in a particular configuration of the system, that is, it was absorbed by a state at which the probability of transition to another state is null[105].

The density of trees in the forest-fire models has much to say about the underlying dynamics. As seen in Figure 4.1.1, depending on the parameter R, the system can perform either great fires – displaying a highly fluctuating density– or smaller fires – mostly with density increasing monotonically. In Figure 4.4.2, it can be observed how densities reach the stationary state.

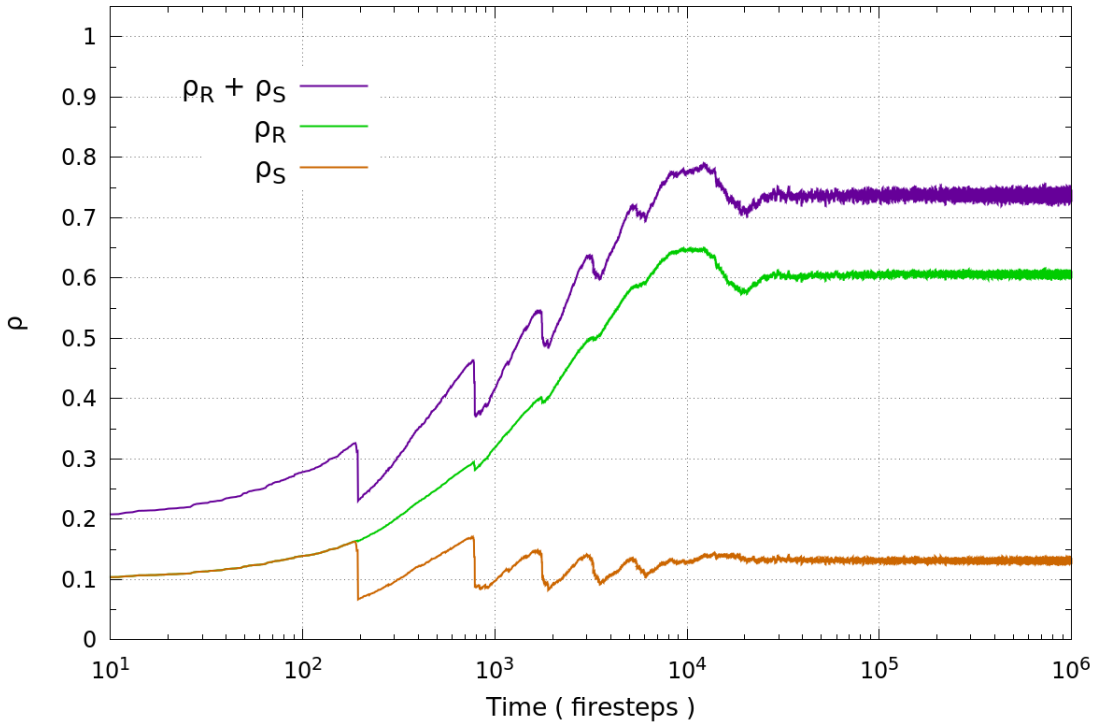

Figure 4.4.1 – Density mono-log plot. Total density ρ (*purple*), *treeS* density ρ_S (*orange*), *treeR* density ρ_R (*green*). Parameters: 2-Moore, $R = 5$, $L = 3 \times 10^4$, $\Theta = 2.25 \times 10^5$, $s = 0$, $p = 0.2$ and $q = 0.5$.

The process of detecting the stationary state is divided in three steps. First, it is made a copy of the raw data, in which is registered the quantity of *treeS* and *treeR* after each fire. Then, these quantities are summed and normalized by the lattice size L^2, $\rho \equiv (\mathcal{N}_{treeS} + \mathcal{N}_{treeR})/L^2$. Secondly, the mean value $\langle\rho\rangle$ and the standard deviation $\sigma(\rho)$ are evaluated at each set of 10^4 elements, i.e. 10^4 density values ($\rho(t_f)$). At last, it is done a linear regression (using χ^2 method) for every set of 10 values of both the mean and the standard deviation, which returns two fitting lines,

$$Y_i = \alpha_i T + \beta_i \,. \tag{4.5}$$

The system is said to be stationary if both slopes of fitting lines α_1 and α_2 are lower than a certain threshold α_{thresh}, that is $\alpha_1 < \alpha_{thresh}$ and $\alpha_2 < \alpha_{thresh}$. In order to have the same threshold for systems with different parameter R, it was settled a threshold value $\alpha_{thresh} \equiv 2 \times 10^{-8}$. As the statistics is calculated in an interval $\Delta t = 10^5$ and $\rho_{max} = 1$, the secant in this region is $\rho_{max}/\Delta t = 10^{-5}$. Hence, the threshold parameter is 0.02% of the slope of the secant that crosses the region used in the statistics.

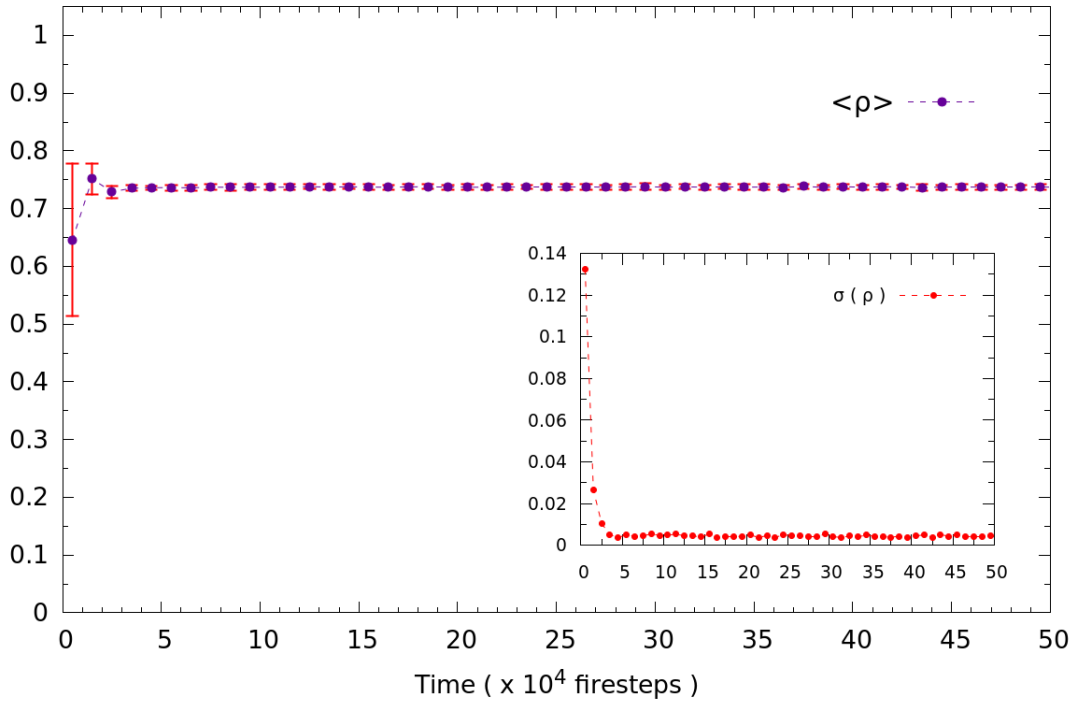

Figure 4.4.2 – Mean $\langle\rho\rangle$ and standard deviation σ of the total density of trees. Parameters: 2-Moore, $R = 5$, $L = 3 \times 10^4$, $\Theta = 2.25 \times 10^5$, $s = 0$, $p = 0.2$ and $q = 0.5$.

4.4.1 On the lattice size

Issues related to the finite size of the sample are present in most complex systems; at criticality, the long-range correlation lengths become bound by the system size (subsection 3.2.3,Equation 3.52). Whenever the system is restrained by a relatively small lattice, the long-range correlations may not emerge its full output, which yields some misleading results. The first fire-size measures on the enlarged neighborhood were a bit deceiving because of finite-size effects[77, 78]. The plots of the total density varying with the lattice size suggest that the system with $R = 6$ (Figure 4.4.4) has a robust absorbing state, while for $R = 5$ (Figure 4.4.3) the absorbing state does not linger as the lattice size is increased. The parameter Θ is set proportional to the lattice size, i.e. $\Theta = (2.5 \times 10^{-4}) \times (L^2)$. The quantitative results for lattices $L = 20,000$ and $L = 30,000$ ensures that both are reliable enough to be used in the simulations with 2-Moore and 3-Moore neighborhoods.

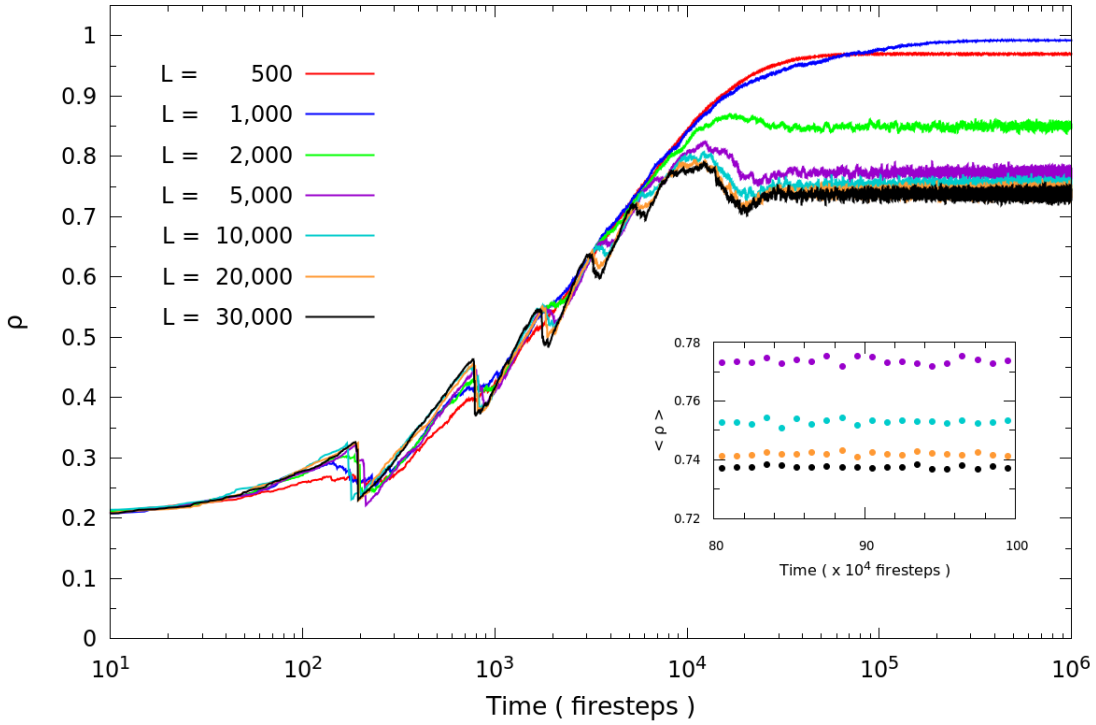

Figure 4.4.3 – Total density $\rho(t_f)$ mono-log plot for each linear lattice size L. Parameters: 2-Moore, $R = 5$, $\Theta = (2.5 \times 10^{-4}) \times (L^2)$, $s = 0$, $p = 0.2$, $q = 0.5$.

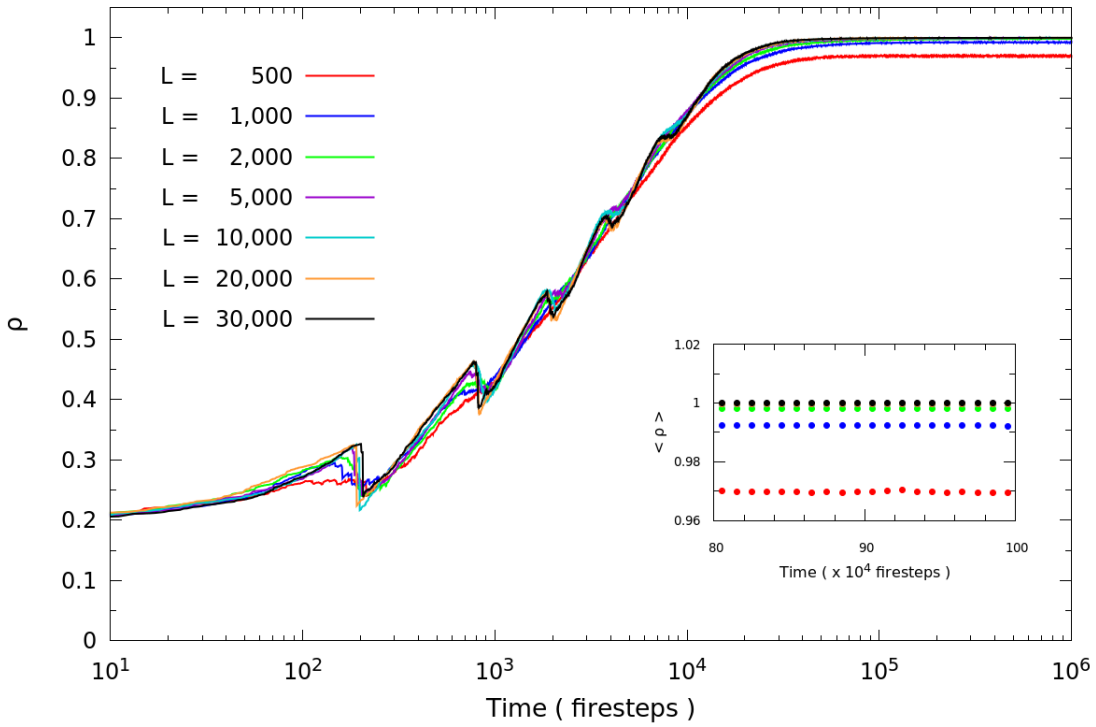

Figure 4.4.4 – Total density $\rho(t_f)$ mono-log plot for each linear lattice size L. Parameters: 2-Moore, $R = 6$, $\Theta = (2.5 \times 10^{-4}) \times (L^2)$, $s = 0$, $p = 0.2$, $q = 0.5$.

4.4.2 Mean sprouting rate

The addition of trees with relatively high resistance has changed the dynamic role of the Θ parameter. As the lattice becomes asymptomatically full, having most of its sites filled with *treeR*, the mean fire size is drastically decreased. Therefore, it is left even less empty sites that would be eligible for receiving a tree during the *sprouting stage*. This can be pictured by evaluating the mean influx of tree, that is, the mean sprouting rate, $\langle \Phi_{in} \rangle$. The sprouting rate Φ_{in}, at firestep t_f, is given by the Equation 4.6 below,

$$[\Phi_{in} - \Phi_{out}]_{t_f} = [\mathcal{N}_{treeR} + \mathcal{N}_{treeS}]_{t_f} - [\mathcal{N}_{treeR} + \mathcal{N}_{treeS}]_{t_f - 1}\,, \tag{4.6}$$

where the r.h.s. term is the total number of trees at firestep t_f minus the total number of trees at the previous firestep $(t_f - 1)$. The rate of trees that leave the system Φ_{out}, at firestep t_f, is simply the fire size at this same firestep. In the original model (DS-FFM), this effect is not of concern, because the low stationary density does not imply such correlation. As the parameter R increases, the correlation becomes stronger. See Figure 4.4.5.

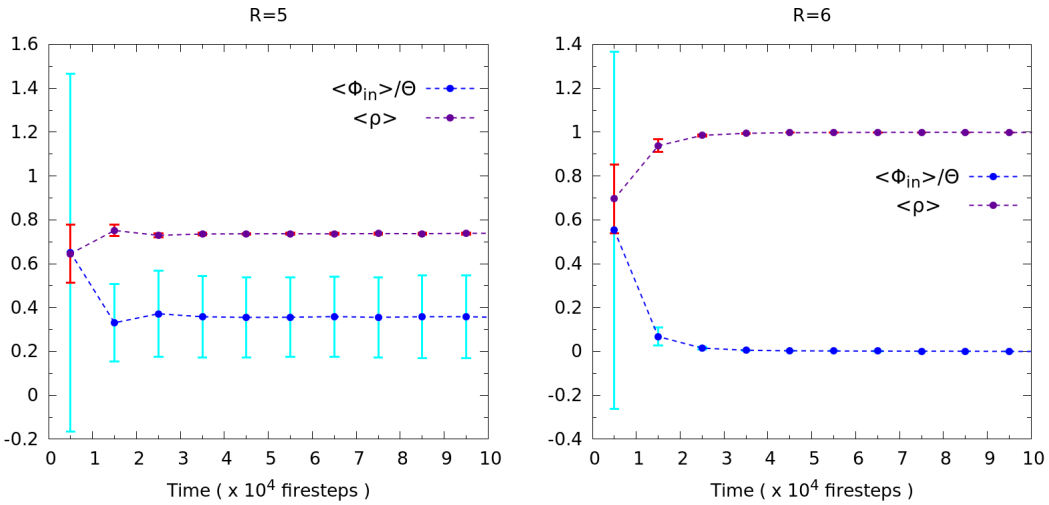

Figure 4.4.5 – Plot of the mean density $\langle \rho \rangle$ and the mean sprouting rate normalized by the parameter Θ, $\langle \Phi_{in} \rangle / \Theta$. Parameters: 2-Moore, $L = 3 \times 10^4$, $\Theta = 2.25 \times 10^4$, $s = 0$, $p = 0.2$, $q = 0.5$.

This chapter was concerned with introducing the generalized forest-fire model and explains most of its details. Some relevant results, such as fire-size distributions, will be presented in the next chapter.

Chapter 5

Results

"Data-driven predictions can succeed – and they can fail.
It is when we deny our role in the process that the odds of failure rise."
Nate Silver[†]

The proposed generalized model (section 4.2) has many parameters that, at some point of view, can be considered as control parameters. Indeed, the combination of r, s, R and q implies in several possible configurations. In the results presented throughout this chapter, it was regarded that each tree has equal probability of sprouting either as a resistant tree ($treeR$) or as a susceptible tree ($treeS$), i.e. $q = 0.5$ – the q parameter has been extensively explored by Camelo-Neto and Coutinho[25]. Firstly, it will be analysed the role of the enlarged 2-Moore neighborhood (section 5.1). Thereafter in section 5.2, it will be presented the avalanche size distributions due to the 3-Moore neighborhood. In section 5.3, a particular configuration (2-Moore neighborhood with $R = 5$) will be considered for testing the effect of the forbidden sites (*block* state sites). The chapter ends with a brief discussion about the results and perspectives for upcoming research (**??**).

5.1 On enlarged neighborhoods: 2-Moore

The fires-size distributions for the first enlarged neighborhood (i.e. 2-Moore neighborhood) presents higher values of R displaying a power-law behavior, which was expected since the number interactions for each site has risen from 8 to 24 neighbors. All values of $R \leq 5$ are characterized by scale invariance in the avalanche size distribution, which seems a bit awkward because $R = 5$ shows a dense stationary state with $\langle\rho\rangle \approx 0.737 \pm 0.004$ (Figure 5.1.1). For values of $R \geq 7$, the system is fully dense of resistant trees and the fire sizes are much smaller than the lattice size, i.e. $S \ll L^2$, and are characterized by a heavy-tailed distribution (Figure 5.1.2).

[†] From "The Signal and the Noise: Why So Many Predictions Fail – But Some Don't"[92].

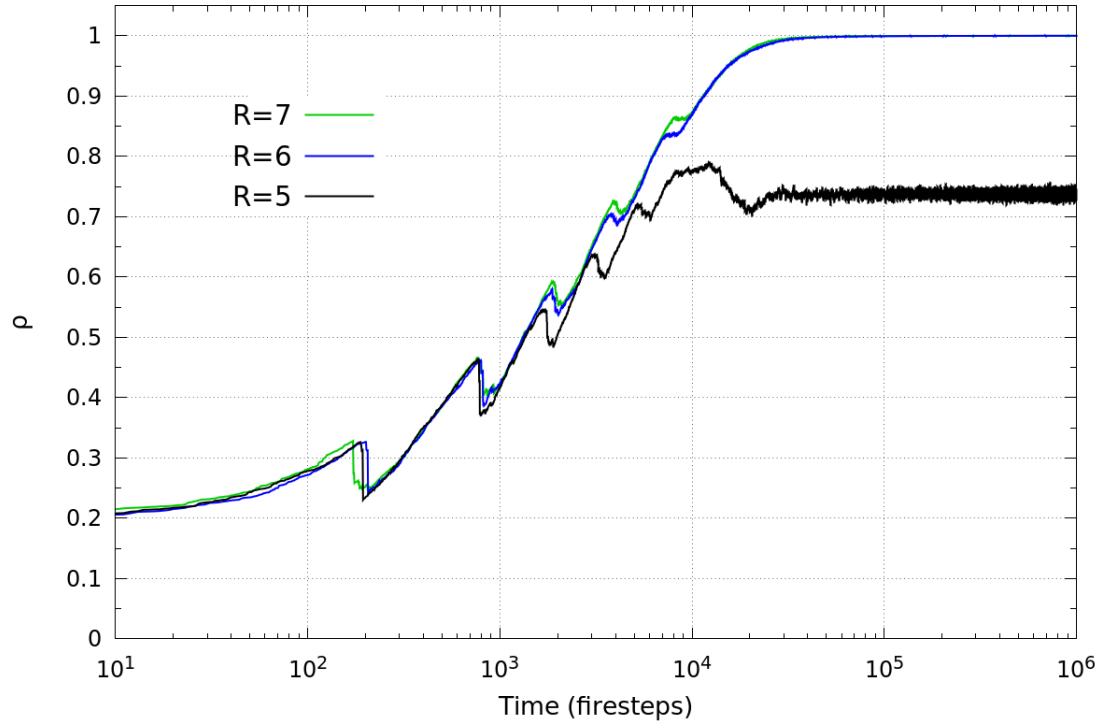

Figure 5.1.1 – Total density $\rho(t_f)$ mono-log plot. Parameters: 2-Moore, $L = 3 \times 10^4$, $\Theta = 2.25 \times 10^5$, $s = 0$, $p = 0.2$ and $q = 0.5$.

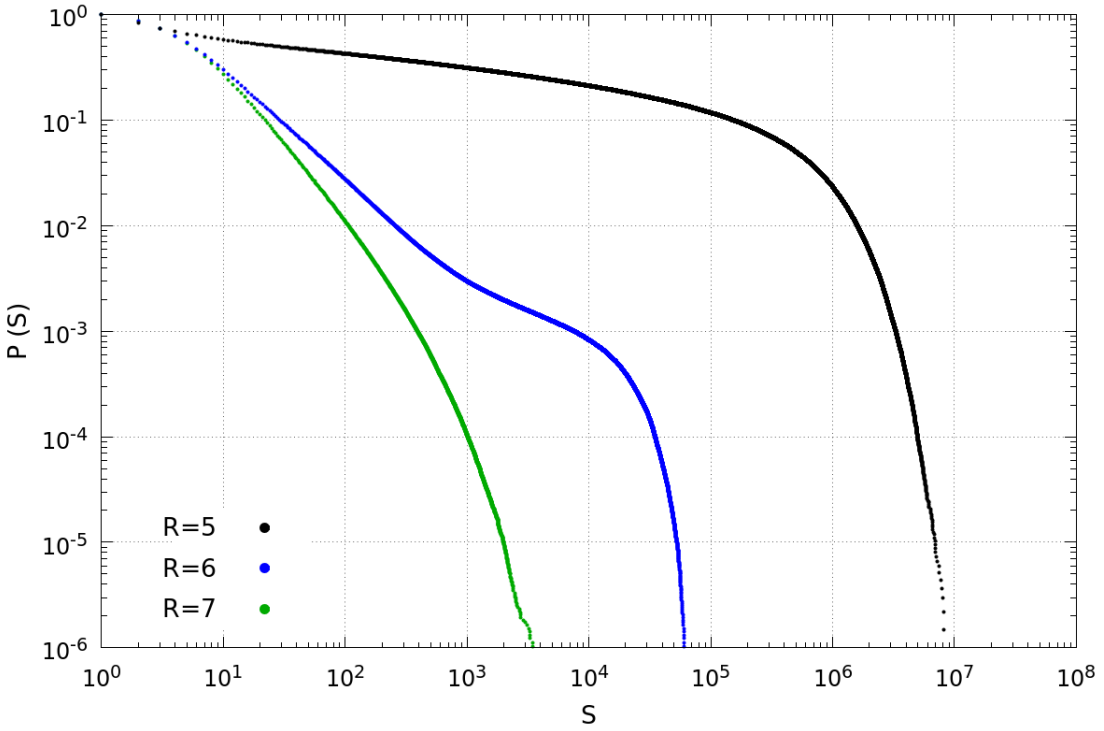

Figure 5.1.2 – Cumulative fire-size distributions. Parameters: 2-Moore, $L = 3 \times 10^4$, $\Theta = 2.25 \times 10^5$, $s = 0$ and $q = 0.5$. There were analysed nearly 10^6 fires in the stationary state for each value of R.

At $R = 6$, the system is also fully dense of resistant trees, but the fire-size distribution shows a crossover between a steep slope region and a plateau, before decaying as a finite-size cut-off. This crossover bevahior in the fire-size distribution has not been observed previous models (DSFFM, FFMRT). Although the system with $R = 6$ constrains long-range fire spread, it allows 'fire-clusters' 10 times larger than other fully dense (resistant) configurations ($R \geq 7$).

5.1.1 2-Moore neighborhood: $R = 5$

As shown by the density time series of the system with 2-Moore neighborhood and parameter $R = 5$ (Figure 4.4.2), at the stationary state it is densely occupied by trees: nearly 60% of the lattice is occupied by resistant trees, whereas approximately 13% is occupied by susceptible trees. In the snapshots of Figure 5.1.3 and Figure 5.1.4, the largest 'fire-clusters' – in a time interval of $\Delta t_f = 10^4$ fires – at the stationary state were captured. It should be observed that due to the lattice high density, the 'fire-clusters' have some compact regions connected by narrow clusters, which in percolation theory are called *blobs* and *linkers*[36], respectively. The combination of these geometrically distinct clusters ensures a greater level of permeation of the fire, despite the high density of resistant trees ($treeR$) in this configuration.

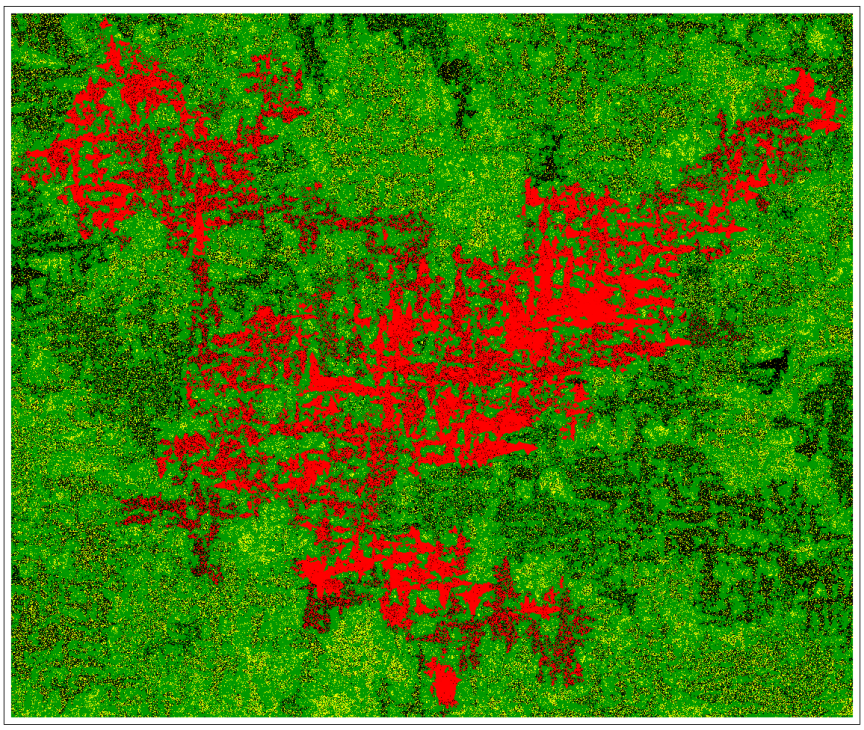

Figure 5.1.3 – The largest 'fire-cluster' in a time interval of $\Delta t_f = 10^4$ firesteps, at the stationary state. Window area: 2165×1876. Parameters: 2-Moore, $R = 5$, $L = 10^4$, $\Theta = 2.5 \times 10^4$, $s = 0$ and $q = 0.5$. State colors: *empty* sites (*black*), $treeS$ (*yellow*), $treeR$ (*green*), $fire$ (*red*).

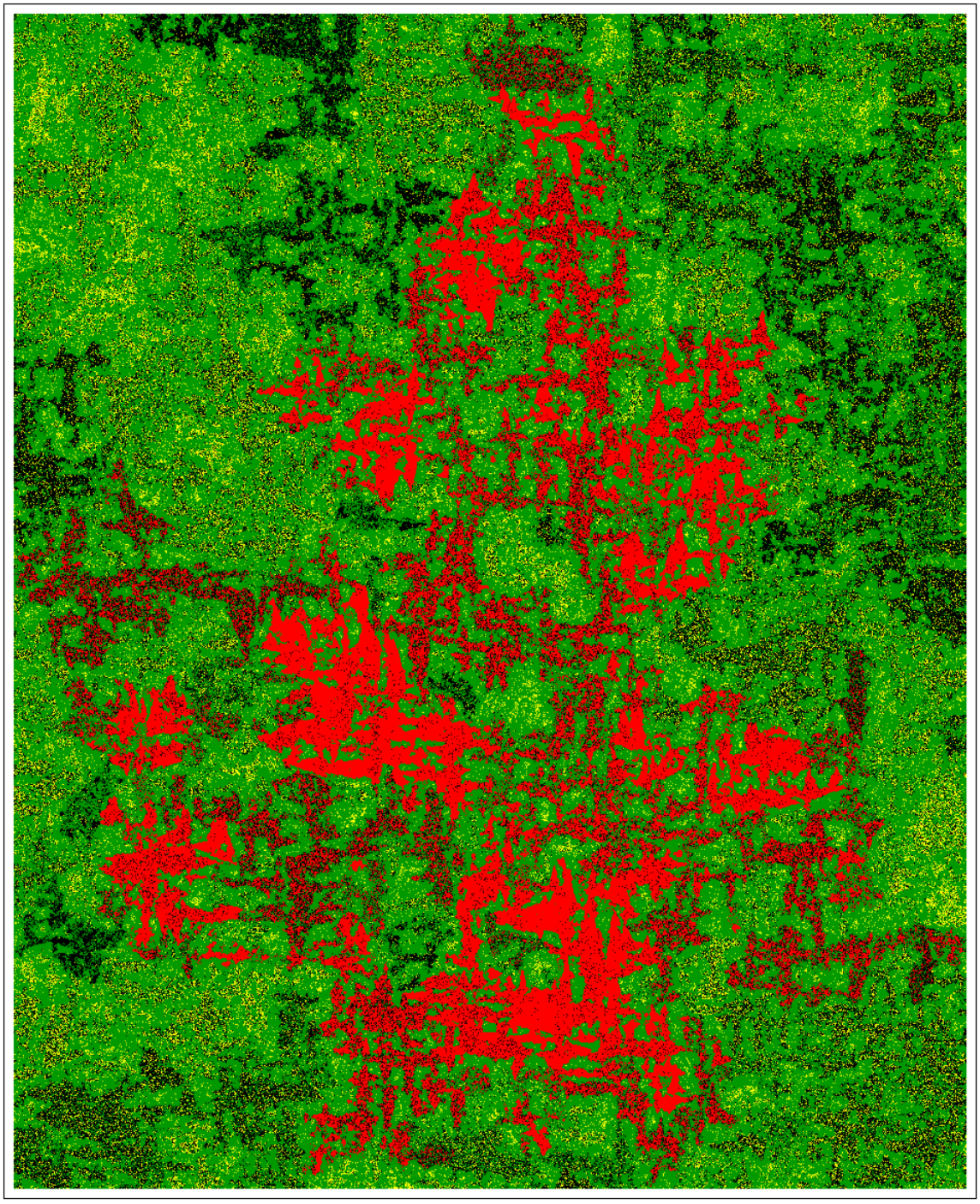

Figure 5.1.4 – The largest 'fire-cluster' in a time interval of $\Delta t_f = 10^4$ firesteps, at the stationary state. Window area: 1833×2238. Parameters: 2-Moore, $R = 5$, $L = 10^4$, $\Theta = 2.5 \times 10^4$, $s = 0$ and $q = 0.5$. State colors: *empty* sites (*black*), $treeS$ (*yellow*), $treeR$ (*green*), $fire$ (*red*).

For the 2-Moore neighborhood case with $R = 5$, the fitted avalanche size exponent is $\tau_s \simeq 1.155$, which is slightly lower than the exponents previously found: $\tau_s \simeq 1.184$ and $\tau_s \simeq 1.181$, considering 1-Moore neighborhood with $R = 2$ and $R = 1$, respectively[25]. The relation $\tau_s = 2 - (1/\lambda_s)$ (Equation 3.55), originally derived from the moment analysis method, was applied in order to estimate the cut-off exponent, $\lambda_s \simeq 1.183$.

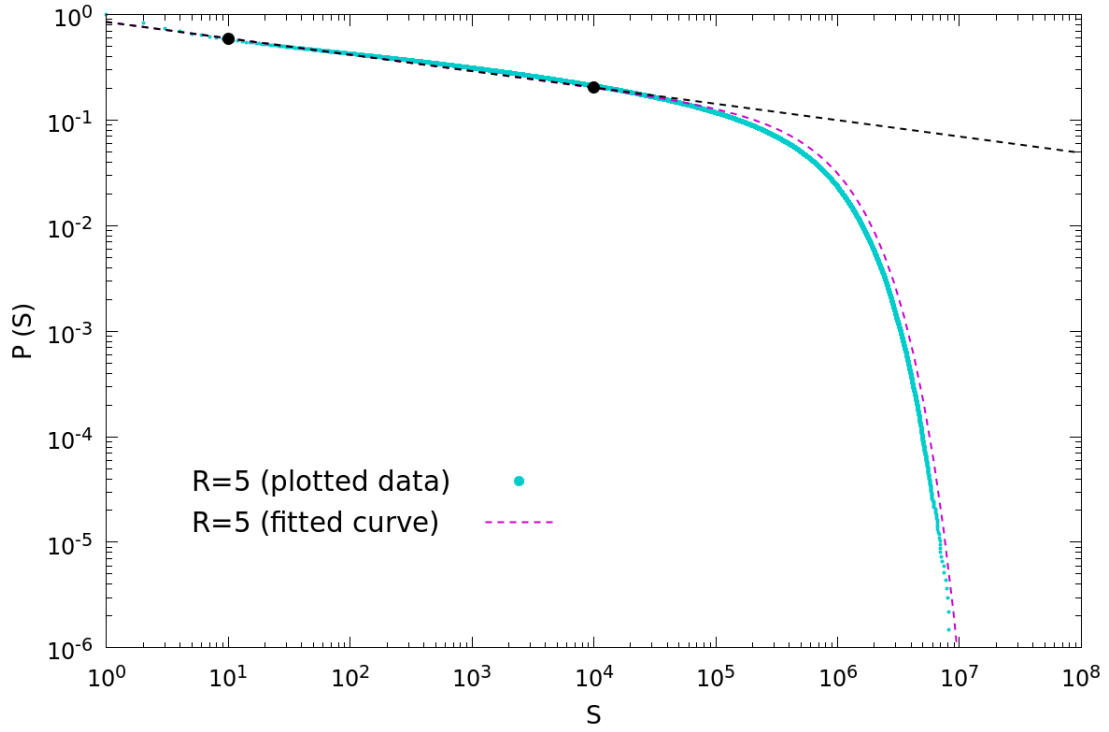

Figure 5.1.5 – Fitted fire-size distribution $\mathcal{P}_s(S;\Theta) = a_s\, S^{1-\tau_s} \exp(\, S \,/\, b_s \Theta^{\lambda_s})$, with $a_s = 0.85$, $b_s = 0.4$, $\tau_s \simeq 1.155$, $\lambda_s \simeq 1.183$. The points $S_1 = 10$ and $S_2 = 10^4$ (*black dots*) determine the region of the power-law fitting (*black dashed line*). Parameters: 2-Moore, $R = 5$, $L = 3 \times 10^4$, $\Theta = 2.25 \times 10^5$, $s = 0$ and $q = 0.5$. There were analysed nearly 10^6 fires in the stationary state.

5.1.2 2-Moore neighborhood: $R = 6$

The effect of the variation of the Θ parameter on a fixed size lattice ($L = const$) has already been studied independently by Grassberger[46] and by Jensen and Pruessner[82], in the context of the DSFFM, and by Camelo-Neto and Coutinho[25], in the context of the FFMRT. Hence, the effect of the Θ parameter solely will be considered only for the crossover distribution due to the 2-Moore, $R = 6$ configuration. For forest-fire simulations exhibiting distributions with power-law regions, as the parameter Θ is increased the distribution cut-off tail is shifted towards higher fire-size values, which is expected since the scaling function depends on Θ – i.e. $\mathcal{G}_s(S;\Theta) = \exp(\, S \,/\, b_s \Theta^{\lambda_s})$. Otherwise, for relatively high resistances of trees in the FFMRT, the fire-size distribution is not bounded neither by the system size L^2 nor by the Θ parameter, therefore the distribution $\mathcal{P}_s(S;\Theta)$ stays unchanged as the Θ parameter is increased.

For the configuration with 2-Moore neighborhood and parameter $R = 6$, the Θ parameter not only pushes the distribution cut-off tail to higher 'fire-cluster' sizes S, but also pulls the distribution curve to more frequent large fires, lowering the avalanche size exponent τ_s and breaking the crossover curve. In Figure 5.1.6, the crossover behavior is more evident in the the *black* curve (Figure 5.1.6) – which has the same ratio $L^2/\Theta = 4\times10^3$ as the $R = 6$ curve in Figure 5.1.2. Despite the power-law region found in the *green* curve ($\Theta = 100,000$), its cut-off region is far from the expected finite-size cut-off effect. For example, consider a system with 2-Moore neighborhood, $R = 5$, $L = 10^4$, $\Theta = 25,000$, the maximum fire size S_{max} is $S_{max}(R = 5) \approx 8 \times 10^6$, which would be even higher in case $\Theta = 100,000$. Considering the same parameters but $R = 6$ instead (*black* curve in Figure 5.1.6), the maximum fire size does not even reach 10^4 (i.e. $S_{max}(R = 6) < 10^4$), suggesting that the finite-size cut-off for the 2-Moore, $R = 6$ case is due to clumps of resistant trees that became static, impermeable clusters, thus decreasing the effective lattice size.

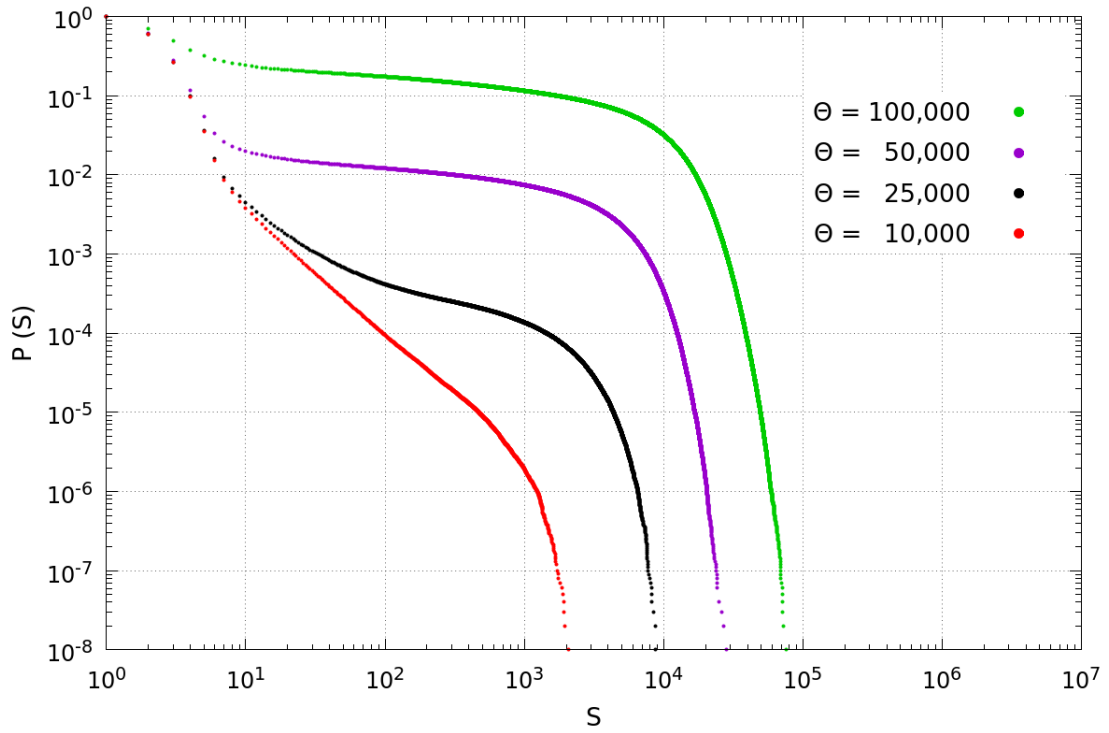

Figure 5.1.6 – Cumulative fire-size distributions. Parameters: 2-Moore, $R = 6$, $L = 10^4$, $s = 0$ and $q = 0.5$, for all cases. There were analysed nearly 10^8 fires in the stationary state for each value of the Θ parameter.

As observed previously in 2-Moore neighborhood with $R = 5$, the 'fire-clusters' in $R = 6$ are composed by blobs and linkers that can be easily identified due to much smaller firesizes. In Figure 5.1.7, it can also be noticed that clumps of resistant trees have assembled *inside* the burnt clusters.

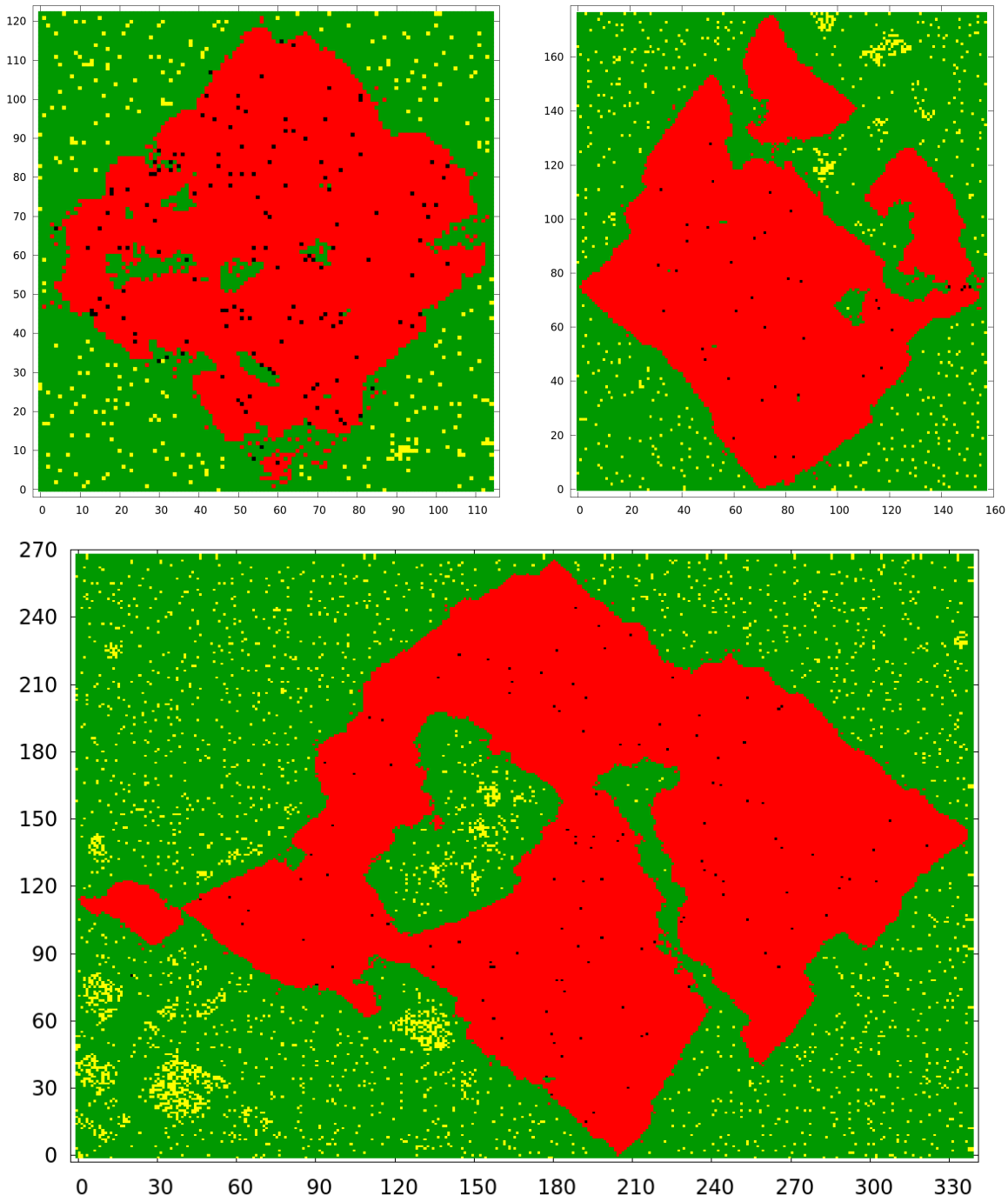

Figure 5.1.7 – The largest 'fire-cluster' on the same time interval of $\Delta t_f = 10^4$ at the stationary state, but with different values of the Θ parameter: $\Theta = 2.5 \times 10^4$ (*top left*), $\Theta = 5 \times 10^4$ (*top right*) and $\Theta = 10^5$ (*bottom*). Parameters: 2-Moore, $R = 6$, $L = 10^4$, $s = 0$ and $q = 0.5$, for all cases. State colors: *empty* sites (*black*), $treeS$ (*yellow*), $treeR$ (*green*), $fire$ (*red*).

5.2 On enlarged neighborhoods: 3-Moore

The simulations with the 3-Moore neighborhood display a power-law behavior distribution for $R \leq 9$, whereas heavy-tailed distributions are found for $R \geq 11$ (Figure 5.2.1). The configuration due to $R = 10$ has a crossover behavior similar to that exhibited by the 2-Moore, $R = 5$ case. Though the similarities, the plateau region in 3-Moore, $R = 10$ is wider, that is, it is much stretched. If the slope τ_s of these curves are indeed related to its clusters' fractal dimension, the wider plateau region suggests more compact 'fire-clusters' than in the 2-Moore, $R = 5$ case – this assumption agrees with the percolation threshold of both neighborhoods (Figure 4.2.2 and Figure 4.2.3).

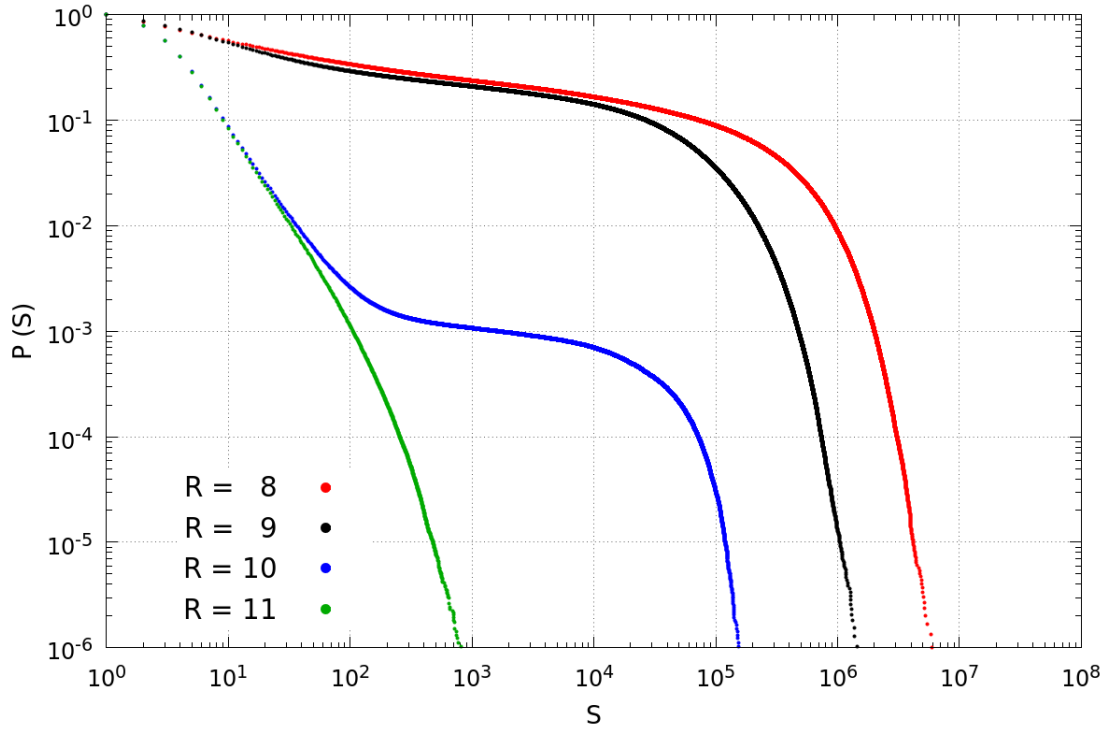

Figure 5.2.1 – Cumulative fire-size distributions. Parameters: 3-Moore, $L = 2 \times 10^4$, $\Theta = 10^5$, $s = 0$ and $q = 0.5$. There were analysed nearly 10^6 fires in the stationary state for each value of R.

5.3 On forbidden sites

In order to test the effect of forbidden sites over the avalanche size distribution, it has been chosen the 2-Moore, $R = 5$ configuration, because it was the fastest running simulation among those displaying a power-law behavior. Throughout this section, the results refer to systems with 2-Moore neighborhood and parameter $R = 5$. The total density of trees in the $s = 0.2$ case (Figure 5.3.3) behaves similar to the 2-Moore, R=6 density curve (Figure 5.1.1). In both cases, the system becomes fully dense around $t_f = 10^5$. The density curve for $s = 0.1$ follows a much different trend from the time series that have

been presented so far. In this case, the density increases until almost reaching a complete occupation $\rho \approx 0.86$ ($< \rho_{max} = 0.9$). Thereafter, it decays towards a stationary state that fluctuates around $\rho = 0.75$ – theses fluctuations are smaller that the case without *block* sites. The snapshots in Figure 5.3.1 show smaller clusters of *empty* sites in $s = 0.1$ than in the $s = 0$ case. There are almost no *empty* sites at the $s = 0.2$ case. In a detailed snapshot (Figure 5.3.2), it is not possible to identify any difference between $s = 0$ and $s = 0.1$ cases.

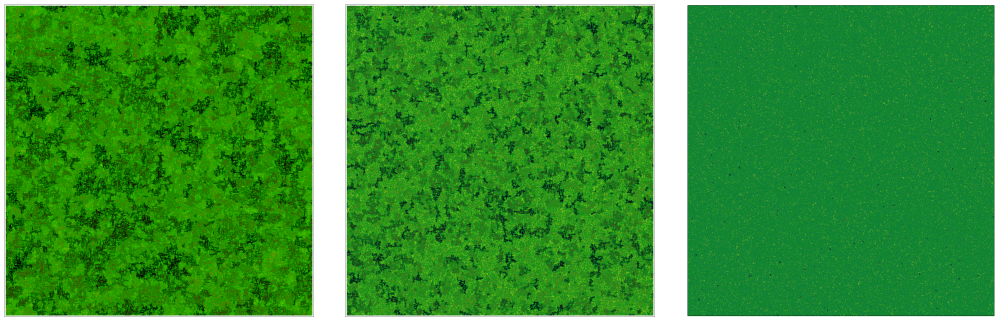

(a) $s = 0$ (b) $s = 0.1$ (c) $s = 0.2$

Figure 5.3.1 – Snapshots of a forest-fire lattice at the stationary state. Parameters: 2-Moore, $R = 5$, $L = 10^4$, $\Theta = 2.5 \times 10^4$, $p = 0.2$ and $q = 0$. State colors: *empty* sites (*black*), *treeS* (*yellow*), *treeR* (*green*), *block* (*blue*).

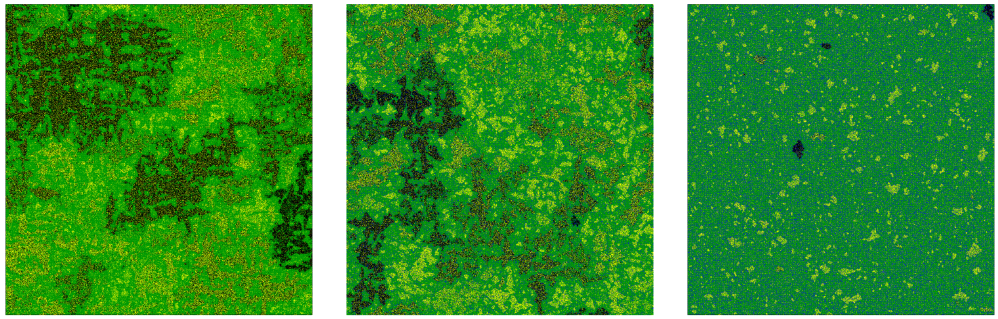

(a) $s = 0$ (b) $s = 0.1$ (c) $s = 0.2$

Figure 5.3.2 – Fragments of a forest-fire lattice at the stationary state. Window: $L_x = [1; 1,000]$ and $L_y = [1; 1,000]$, for each respective lattice (Figure 5.3.1). Parameters: 2-Moore, $R = 5$, $L = 10^4$, $\Theta = 2.5 \times 10^4$, $p = 0.2$ and $q = 0$. State colors: *empty* sites (*black*), *treeS* (*yellow*), *treeR* (*green*), *block* (*blue*).

The avalanche size distributions are plotted in Figure 5.3.4. The fire-size distribution for $s = 0.1$ presents more frequent 'fire-clusters' between $S = 10$ and $S = 4 \times 10^4$, than the case with no *block* sites ($s = 0$), suggesting a lower avalanche size exponent τ_s. It can also be noticed that the cut-off exponent λ_s is reduced as the effective lattice size decreases, but it still not restraining large 'fire-clusters'. The restraining effect of the forbidden sites turns evident for $s = 0.2$.

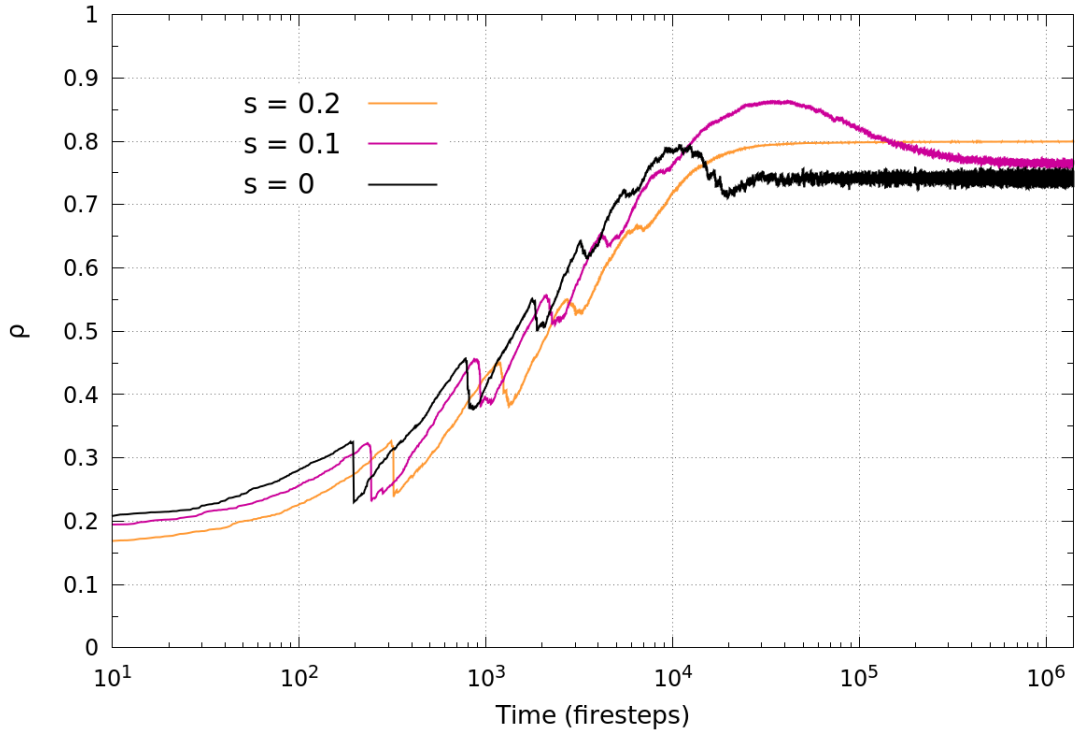

Figure 5.3.3 – Total density $\rho\,(t_f)$ mono-log plot. Parameters: 2-Moore, $R = 5$, $L = 2 \times 10^4$, $\Theta = 10^5$, $p = 0.2$ and $q = 0.5$.

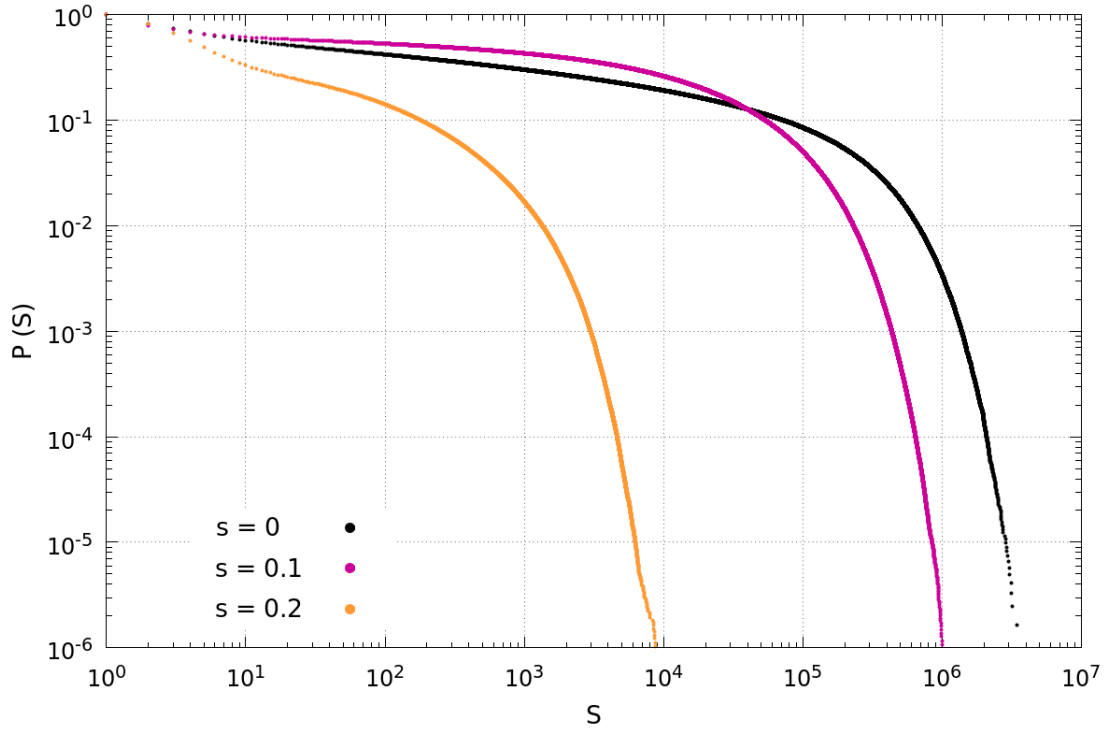

Figure 5.3.4 – Cumulative fire-size distributions. Parameters: 2-Moore, $R = 5$, $L = 2 \times 10^4$, $\Theta = 10^5$ and $q = 0.5$. There were analysed nearly 10^6 fires in the stationary state for each value of s.

These results do not clarify whether the narrower 'fire-clusters' are due to a perimeter constrain or simply because of the absence of trees at the *block* sites, which would be accounted to the fire size. Henceforth, it must be considered a dichotomy between avalanche size and avalanche area, that is, fire size and fire area shall be regarded as distinct measures in this new framework with forbidden sites (*block* sites).

Before any further assumptions about the role of forbidden sites, it is required an investigation about the static percolation of the lattice with 2-Moore, $R = 5$. A brief research showed that, in this framework, the 'percolation' curves are distinct from those due to 'homogeneous' static percolation (Figure 5.3.5). Moreover, for studying static percolation in the resistant, highly correlated lattice yielded by the forest-fire model it will be required a control parameter rather than the static percolation density parameter p.

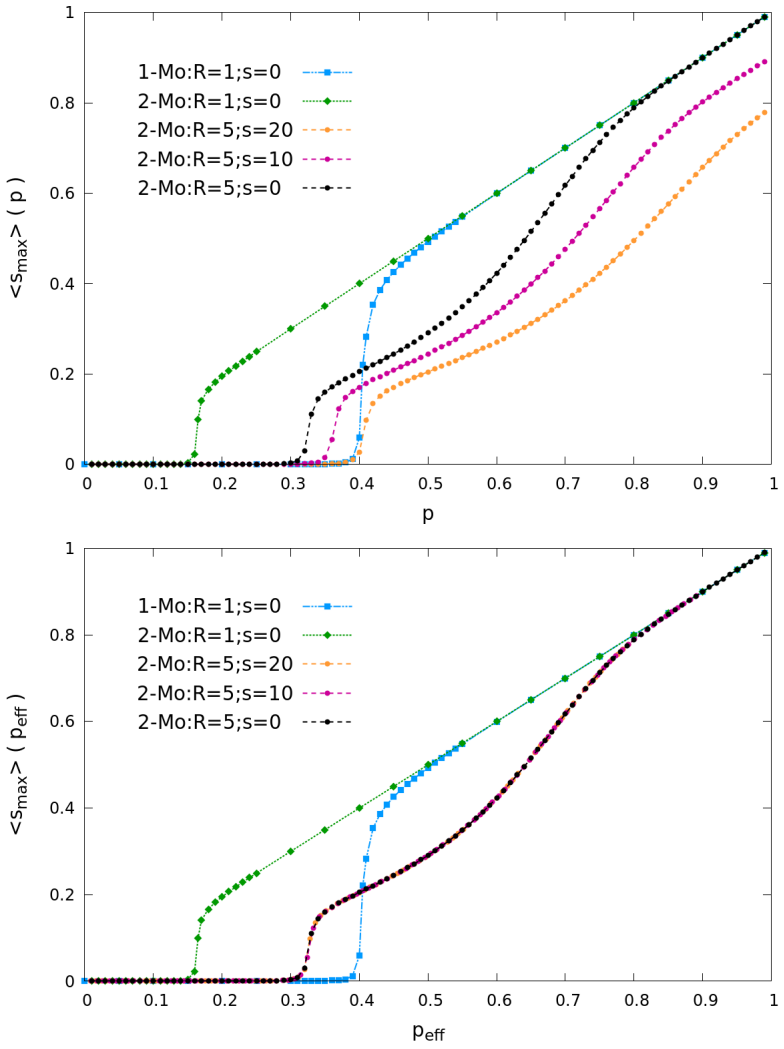

Figure 5.3.5 – Normalized mean of the maximum cluster size for r-Moore neighborhoods. The effective density is given by $p_{\text{eff}} \equiv (1 - s) \times p$. There were run 100 samples with linear size $L = 1,000$ and periodic boundary conditions.

5.4 Conclusion and perspectives

The forest-fire model with resistant trees (section 4.2) yields two distinct phases depending on the resistance parameter R: an active phase with fire-size distributions displaying power-law behavior ($R < 3$), and another phase that leads the system to an absorbing state where the largest fire size is far below the system size, i.e. $S_{max} \ll L^2$, showing 'heavy-tailed' distributions ($R \geq 3$). In this work, it was reported that the generalized model with enlarged neighborhoods (2-Moore and 3-Moore) and no forbidden sites ($s = 0$) also displays these two distinct phases.

The absorbing states are related to relatively high resistance parameter, for instance $R \geq 7$ in 2-Moore template and $R \geq 11$ in 3-Moore template. As the resistance R increases, resistant trees are more likely to be stable since it sprouts and, hence, only susceptible trees are removed by the fire spread. As the lattice becomes full of resistant trees, the normalized sprouting rate tends to zero, i.e. $(\Phi_{in}/\Theta) \to 0$ (subsection 4.4.2), due to lacking of empty sites. The dense forest is also a result of the absence of natural death, the model supposes that trees will die from no other reason but consumed by a wildfire. Therefore, it seems reasonable to think about whether the system will remain in this absorbing state when natural death is considered.

The Θ parameter sustains the active phase, which is characterized by a fluctuating density and fire-size distributions with power-law signatures, retrieving some results to be compared with DSFFM and other SOC models (Figure 5.1.5). As the parameter R is increased, from $R = 1$ to $R = 5$ and from $R = 1$ to $R = 9$, with 2-Moore and 3-Moore neighborhoods, respectively, the fluctuations decrease and, moreover, the stationary densities rise, yielding nearly dense forests.

Some isolated behavior had been reported for FFMRT with Moore neighborhood and parameter $R = 3$[25]. Similarly, it was found an unique cross-over behavior on the fire-size distribution for 2-Moore, $R = 6$ and 3-Moore, $R = 10$ frameworks, suggesting bimodal distributions. At these configurations, the system is fully dense ($\rho \to 1$), but were observed larger fires than those occurred in absorbing states (subsection 5.1.2).

As the forbidden sites (*block* sites) were introduced in the model, it came to surface a need for measuring the total fire area. The size of the 'fire-clusters' decrease as the fraction of *block* sites is raised, as expected. Nonetheless, it is not clear whether the decrease is due to *block* sites restraining the fire or due to missing accountable trees. A fire-area measure compared to the fire sizes would indicate either or both as causes. Another fundamental question is related to the static percolation with heterogeneous populations. As seen in Figure 5.3.5, the system with resistant trees does not follow the typical profile of the incipient cluster curves. Heterogeneous static percolation and its properties must be studied in detail, as well as percolation on forests yielded by the model.

In spite of the results presented throughout this work, the generalized forest fire model still lacking some important features such as wind-driven fires, fire intensity regimes and tree natural death, which may be considered in future investigations. However, before including new features, it seems essential to research on 'forest-fire' static percolation and implement other measures rather than avalanche size and duration, such as fire area and fractions of resistant and susceptible trees accounted within each 'fire-cluster'.

Bibliography

1 Binary tree. http://mathworld.wolfram.com/BinaryTree.html. 2 citations in pages 9 and 52.

2 Coffee percolator. http://en.wikipedia.org/wiki/Coffee_percolator. 2 citations in pages 9 and 45.

3 Cplusplus.com – the C++ resources network. http://www.cplusplus.com/. Cited on page 73.

4 Freeglut – the open-source openGL utility toolkit. http://freeglut.sourceforge.net/. Cited on page 73.

5 GCC – the GNU compiler collection. http://gcc.gnu.org/. Cited on page 73.

6 GLUT – the openGL utility toolkit. http://www.opengl.org/resources/libraries/glut/. Cited on page 73.

7 GSL – GNU scientific library. http://www.gnu.org/software/gsl/. Cited on page 73.

8 Heavy-tailed distribution. http://en.wikipedia.org/wiki/Heavy-tailed_distribution. Cited on page 16.

9 Landsat8. http://landsat.gsfc.nasa.gov/landsat-8/. Cited on page 16.

10 Nasa's earth observatory: Wildfire scars california towns. http://earthobservatory.nasa.gov/NaturalHazards/view.php?id=86663. 3 citations in pages 8, 16, and 18.

11 Nasa's earth observatory: Wildfires in the west. http://earthobservatory.nasa.gov/IOTD/view.php?id=86366. 2 citations in pages 8 and 18.

12 Operational land imager. http://landsat.gsfc.nasa.gov/operational-land-imager-oli/. Cited on page 16.

13 Percolation. http://en.wikipedia.org/wiki/Percolation. Cited on page 44.

14 Savanna. http://en.wikipedia.org/wiki/Savanna. Cited on page 62.

15 The Nobel Prize in Physiology or Medicine 1962. Nobelprize.org. 2014. http://www.nobelprize.org/nobel_prizes/medicine/laureates/1962/index.html. Cited on page 22.

16 W. F. Ames. *Numerical methods for partial differential equations*. Computer science and applied mathematics. Academic Press, 1977. Cited on page 25.

17 P. Bak. *How nature works: the science of self-organized criticality*. Copernicus Series. Copernicus, 1996. 2 citations in pages 16 and 56.

18 Per Bak, Kan Chen, and Chao Tang. A forest-fire model and some thoughts on turbulence. *Physics letters A*, 147(5):297–300, 1990. Cited on page 57.

19 Per Bak, Chao Tang, and Kurt Wiesenfeld. Self-organized criticality: An explanation of the 1/f noise. *Physical review letters*, 59(4):381, 1987. Cited on page 56.

20 Hans A. Bethe. Statistical theory of superlattices. *Proceedings of the Royal Society of London. Series A, Mathematical and Physical Sciences*, 150(871):552–575, 1935. Cited on page 50.

21 C. Borgnakke and R. E. Sonntag. *Fundamentals Of Thermodynamics, 7th edition*. Wiley India Pvt. Limited, 2009. Cited on page 41.

22 C. L. R. Braga. *Notas de Física Matemática*. Editora Livraria da Física, 2006. Cited on page 53.

23 Simon R. Broadbent and John M. Hammersley. Percolation processes. In *Mathematical Proceedings of the Cambridge Philosophical Society*, volume 53, pages 629–641. Cambridge Univ Press, 1957. Cited on page 45.

24 G. Camelo-Neto and S. Coutinho. Dynamical model for virus spread. *Fractals*, 04(02):113–122, June 1996. Cited on page 62.

25 G. Camelo-Neto and S. Coutinho. Forest-fire model with resistant trees. *Journal of Statistical Mechanics: Theory and Experiment*, 2011(06):P06018, June 2011. 9 citations in pages 17, 59, 60, 62, 64, 73, 80, 84, and 91.

26 Manoel Cardoso, Carlos Nobre, Gilvan Sampaio, Marina Hirota, Dalton Valeriano, and Gilberto Câmara. Long-term potential for tropical-forest degradation due to deforestation and fires in the brazilian amazon. *Biologia*, 64(3):433–437, 2009. Cited on page 16.

27 John L. Cardy and Peter Grassberger. Epidemic models and percolation. *Journal of Physics A: Mathematical and General*, 18(6):L267, 1985. Cited on page 45.

28 K. Christensen and N. R. Moloney. *Complexity and Criticality*. Advanced physics texts. Imperial College Press, 2005. 7 citations in pages 39, 47, 50, 51, 52, 54, and 56.

29 Edward F. Codd. *Cellular automata*. ACM monograph series. Academic Press, 1968. Cited on page 20.

30 Antonio Coniglio, H. Eugene Stanley, and W. Klein. Site-bond correlated-percolation problem: A statistical mechanical model of polymer gelation. *Phys. Rev. Lett.*, 42:518–522, February 1979. Cited on page 45.

31 M. Crichton. *Jurassic Park: A Novel*. A Borzoi book. Knopf, 1990. Cited on page 39.

32 M. De Menech, A. L. Stella, and C. Tebaldi. Rare events and breakdown of simple scaling in the abelian sandpile model. *Physical Review E*, 58(3):R2677, 1998. Cited on page 57.

33 B. Drossel and F. Schwabl. Forest-fire model with immune trees. *Physica A: Statistical Mechanics and its Applications*, 199(2):183–197, 1993. 2 citations in pages 61 and 71.

34 Barbara Drossel and Franz Schwabl. Self-organized critical forest-fire model. *Physical review letters*, 69(11):1629, 1992. 2 citations in pages 17 and 57.

35 R. Eckhardt. Stan Ulam, John von Neumann, and the Monte Carlo Method. *Los Alamos Science Special Issue, Stanislaw Ulam 1909-1984*, 15, 1987. Cited on page 20.

36 J. Feder. *Fractals*. Physics of Solids and Liquids. Springer, 1988. Cited on page 82.

37 R. P. Feynman and R. Leighton. *"Surely You're Joking, Mr. Feynman!": Adventures of a Curious Character*. W. W. Norton, 2010. Cited on page 19.

38 Michael E. Fisher and John W. Essam. Some cluster size and percolation problems. *Journal of Mathematical Physics*, 2(4):609–619, 1961. Cited on page 51.

39 U. Frisch, B. Hasslacher, and Y. Pomeau. Lattice-gas automata for the navier-stokes equation. *Phys. Rev. Lett.*, 56:1505–1508, Apr 1986. Cited on page 36.

40 M. Galassi and B. Gough. *GNU Scientific Library: Reference Manual*. GNU manual. Network Theory, 2009. Cited on page 73.

41 M. Gardner. Mathematical games: the fantastic combinations of John Conway's new solitaire game 'Life'. *Scientific American*, 223(4):120–123, October 1970. The original description of Conway's Game of Life. 2 citations in pages 21 and 31.

42 Murray Gell-Mann. What is complexity? In *Complexity and industrial clusters*, pages 13–24. Springer, 2002. Cited on page 39.

43 Pablo M. Gleiser, Luce Prignano, Conrad J. Pérez-Vicente, and Albert Díaz-Guilera. Pacemakers in a cayley tree of kuramoto oscillators. *International Journal of Bifurcation and Chaos*, 22(07):1250161, 2012. 2 citations in pages 9 and 51.

44 M. A. F. Gomes, J. B. C. Garcia, T. I. Jyh, T. I. Ren, and T. R. M. Sales. Nonlinear dynamics of the cellular-automaton "game of life". *Physical Review E*, 48(5):3345, 1993. Cited on page 32.

45 E. S. R. Gopal. Critical opalescence. *Resonance*, 5(4):37–45, 2000. Cited on page 44.

46 Peter Grassberger. Critical behaviour of the drossel-schwabl forest fire model. *New Journal of Physics*, 4(1):17, 2002. 3 citations in pages 57, 73, and 84.

47 G. Grimmett. *Percolation*. Die Grundlehren der mathematischen Wissenschaften in Einzeldarstellungen. Springer, 1999. 3 citations in pages 25, 47, and 54.

48 J. D. Hamilton. *Time Series Analysis*. Princeton University Press, 1994. Cited on page 75.

49 A. Honecker and I. Peschel. Length scales and power laws in the two-dimensional forest-fire model. *Physica A: Statistical Mechanics and its Applications*, 239(4):509–530, 1997. Cited on page 59.

50 Peter Howard. *Flammable Planet*. 2014. http://costofcarbon.org/files/Flammable_Planet___Wildfires_and_Social_Cost_of_Carbon.pdf. Cited on page 16.

51 A. Illy and R. Viani. *Espresso Coffee: The Science of Quality*. Elsevier Academic, 2005. Cited on page 44.

52 Michael B. Isichenko. Percolation, statistical topography, and transport in random media. *Reviews of modern physics*, 64(4):961, 1992. Cited on page 45.

53 H. J. Jensen. *Self-Organized Criticality: Emergent Complex Behavior in Physical and Biological Systems*. Cambridge Lecture Notes in Physics. Cambridge University Press, 1998. Cited on page 56.

54 Yueyang Jiang and Qianlai Zhuang. Extreme value analysis of wildfires in canadian boreal forest ecosystems. *Canadian journal of forest research*, 41(9):1836–1851, 2011. Cited on page 16.

55 P. R. King, S. V. Buldyrev, Nikolay V. Dokholyan, S. Havlin, Y. Lee, G. Paul, and H. E. Stanley. Applications of statistical physics to the oil industry: predicting oil recovery using percolation theory. *Physica A: Statistical Mechanics and its Applications*, 274(1):60–66, 1999. Cited on page 45.

56 D. Kondepudi and I. Prigogine. *Modern Thermodynamics: From Heat Engines to Dissipative Structures*. CourseSmart. Wiley, 2014. 3 citations in pages 40, 41, and 44.

57 G. Landini, G. Misson, and P. I. Murray. Fractal characterisation and computer modelling of herpes simplex virus spread in the human corneal epithelium. In M. M. Novak, editor, *Fractals in the Natural and Applied Sciences*, pages 241–253. North-Holland, Amsterdam, 1994. Cited on page 61.

58 Chris G. Langton. Computation at the edge of chaos: Phase transitions and emergent computation. *Physica D: Nonlinear Phenomena*, 42(1-3):12–37, June 1990. 3 citations in pages 22, 24, and 35.

59 Christopher G. Langton. Self-reproduction in cellular automata. *Physica D: Nonlinear Phenomena*, 10(1-2):135–144, January 1984. 2 citations in pages 19 and 20.

60 Christopher G. Langton. Studying artificial life with cellular automata. *Physica D: Nonlinear Phenomena*, 22(1):120–149, 1986. Cited on page 34.

61 Rosa Lasaponara, Adriano Santulli, and Luciano Telesca. Time-clustering analysis of forest-fire sequences in southern italy. *Chaos, Solitons & Fractals*, 24(1):139–149, 2005. Cited on page 16.

62 A. Lesne and M. Laguës. *Scale Invariance: From Phase Transitions to Turbulence*. Springer Berlin Heidelberg, 2011. 2 citations in pages 44 and 56.

63 Wentian Li, Norman H. Packard, and Chris G. Langton. Transition phenomena in cellular automata rule space. *Physica D: Nonlinear Phenomena*, 45(1):77–94, 1990. 2 citations in pages 22 and 35.

64 Jianyi Lin and Sergio Rinaldi. A derivation of the statistical characteristics of forest fires. *Ecological Modelling*, 220(7):898–903, 2009. Cited on page 16.

65 António M. Lopes and J. A. Tenreiro Machado. Dynamic analysis and pattern visualization of forest fires. *PloS one*, 9(8):e105465, 2014. Cited on page 16.

66 Gary MacKay and Naeem Jan. Forest fires as critical phenomena. *Journal of Physics A: Mathematical and General*, 17(14):L757, 1984. Cited on page 47.

67 Bruce D. Malamud. Tails of natural hazards. *Physics World*, 17(8):25, 2004. Cited on page 16.

68 Bruce D. Malamud, James D. A. Millington, and George L. W. Perry. Characterizing wildfire regimes in the united states. *Proceedings of the National Academy of Sciences of the United States of America*, 102(13):4694–4699, 2005. Cited on page 16.

69 Bruce D. Malamud, Gleb Morein, and Donald L. Turcotte. Forest fires: an example of self-organized critical behavior. *Science*, 281(5384):1840–1842, 1998. Cited on page 16.

70 Krzysztof Malarz and Serge Galam. Square-lattice site percolation at increasing ranges of neighbor bonds. *Phys. Rev. E*, 71:016125, January 2005. 3 citations in pages 25, 53, and 68.

71 John Mayer. Daughters. *Heavier Things* album, September 2003. Cited on page 33.

72 L. H. A. Monteiro. *Sistemas dinâmicos*. Editora Livraria da Física, 2006. Cited on page 36.

73 Edward F. Moore. Machine models of self-reproduction. In *Mathematical problems in the biological sciences: Proc. Symp. Appl. Math*, volume 14, pages 17–33, 1962. 2 citations in pages 21 and 25.

74 M. E. J. Newman and R. M. Ziff. Efficient monte carlo algorithm and high-precision results for percolation. *Physical Review Letters*, 85(19):4104, 2000. Cited on page 53.

75 Rebeca C. Novaes. Efeitos de incêndios florestais sobre distribuição etária em florestas heterogêneas. Master's thesis, Physics Department, Federal University of Pernambuco, July 2015. Supervisors: Gustavo Camelo-Neto and Sérgio G. Coutinho. Cited on page 62.

76 Dennis C. Odion, Chad T. Hanson, Andre Arsenault, William L. Baker, Dominick A. DellaSala, Richard L. Hutto, Walt Klenner, Max A. Moritz, Rosemary L. Sherriff, Thomas T. Veblen, et al. Examining historical and current mixed-severity fire regimes in ponderosa pine and mixed-conifer forests of western north america. *PloS one*, 9(2):e87852, 2014. Cited on page 16.

77 F. G. Oliveira, S. G. Coutinho, and Gustavo Camelo-Neto. Incêndios florestais em ambientes heterogêneos com vizinhaça ampliada. In *XXX Encontro de físicos do Norte e Nordeste*, 2012. Cited on page 77.

78 F. G. Oliveira, S. G. Coutinho, and Gustavo Camelo-Neto. Forest fires in heterogeneous environment with extended moore neighborhood. In *XXXVI Brazilian meeting on condensed matter physics*, 2013. Cited on page 77.

79 Romualdo Pastor-Satorras and Alessandro Vespignani. Corrections to scaling in the forest-fire model. *Physical Review E*, 61(5):4854, 2000. Cited on page 57.

80 G. Pruessner. *Self-Organised Criticality: Theory, Models and Characterisation*. Self-organised Criticality: Theory, Models, and Characterisation. Cambridge University Press, 2012. 2 citations in pages 56 and 57.

81 Gunnar Pruessner and Henrik Jeldtoft Jensen. Broken scaling in the forest-fire model. *Physical Review E*, 65(5):056707, 2002. Cited on page 57.

82 Gunnar Pruessner and Henrik Jeldtoft Jensen. Efficient algorithm for the forest fire model. *Physical Review E*, 70(6):066707, 2004. 2 citations in pages 57 and 84.

83 William J. Reed and Kevin S. McKelvey. Power-law behaviour and parametric models for the size-distribution of forest fires. *Ecological Modelling*, 150(3):239–254, 2002. Cited on page 16.

84 Carlo Ricotta, Margarita Arianoutsou, Ricardo Dıaz-Delgado, Beatriz Duguy, Francisco Lloret, Eleni Maroudi, Stefano Mazzoleni, José Manuel Moreno, Serge Rambal, Ramon Vallejo, et al. Self-organized criticality of wildfires ecologically revisited. *Ecological Modelling*, 141(1):307–311, 2001. Cited on page 16.

85 S. Roberts. A Life in Games. (Profile: John Conway). *Quanta Magazine*, August 2015. http://www.quantamagazine.org/20150828-john-conway-a-life-in-games. Cited on page 21.

86 S. Roberts. *Genius At Play: The Curious Mind of John Horton Conway*. Bloomsbury Publishing, 2015. Cited on page 21.

87 H. E. Roman, A. Bunde, and W. Dieterich. Conductivity of dispersed ionic conductors: A percolation model with two critical points. *Physical Review B*, 34(5):3439, 1986. Cited on page 45.

88 Muhammad Sahimi. Long-range correlated percolation and flow and transport in heterogeneous porous media. *Journal de Physique I*, 4(9):1263–1268, 1994. Cited on page 45.

89 B. Sapoval, A. Baldassarri, and A. Gabrielli. Self-stabilized fractality of seacoasts through damped erosion. *Phys. Rev. Lett.*, 93:098501, August 2004. Cited on page 36.

90 Hansjörg Seybold, José S. Andrade, and Hans J. Herrmann. Modeling river delta formation. *Proceedings of the National Academy of Sciences*, 104(43):16804–16809, 2007. Cited on page 36.

91 C. E. Shannon and J. McCarthy (editors). *Automata Studies: Annals of Mathematics Studies. Number 34*. Annals of mathematics studies. Princeton University Press, 1972. Cited on page 21.

92 N. Silver. *The Signal and the Noise: Why So Many Predictions Fail – but Some Don't*. Penguin Publishing Group, 2012. Cited on page 80.

93 Marcelo F. Simon, Rosaura Grether, Luciano P. de Queiroz, Cynthia Skema, R. Toby Pennington, and Colin E. Hughes. Recent assembly of the cerrado, a neotropical plant diversity hotspot, by in situ evolution of adaptations to fire. *Proceedings of the National Academy of Sciences*, 106(48):20359–20364, 2009. Cited on page 16.

94 M. Sipser. *Introduction to the Theory of Computation*. Cengage Learning, 2012. 2 citations in pages 8 and 23.

95 R. V. Solé. *Phase Transitions*. Primers in Complex Systems. Princeton University Press, 2011. Cited on page 39.

96 Weiguo Song, Jian Wang, Kohyu Satoh, and Weicheng Fan. Three types of power-law distribution of forest fires in japan. *Ecological Modelling*, 196(3):527–532, 2006. Cited on page 16.

97 Weiguo Song, Fan Weicheng, Wang Binghong, and Zhou Jianjun. Self-organized criticality of forest fire in china. *Ecological Modelling*, 145(1):61–68, 2001. Cited on page 16.

98 S. H. Strogatz. *Nonlinear Dynamics and Chaos: With Applications to Physics, Biology, Chemistry, and Engineering*. Studies in nonlinearity. Westview Press, 2008. 2 citations in pages 34 and 36.

99 O. Tange. Gnu parallel - the command-line power tool. *;login: The USENIX Magazine*, 36(1):42–47, February 2011. http://www.gnu.org/s/parallel. Cited on page 73.

100 G. A. Taubes. Physics whiz goes into biz. *Fortune*, 17:90–93, April 1988. Cited on page 21.

101 Claudio Tebaldi, Mario De Menech, and Attilio L. Stella. Multifractal scaling in the bak-tang-wiesenfeld sandpile and edge events. *Physical Review Letters*, 83(19):3952, 1999. Cited on page 57.

102 Luciano Telesca, Giuseppe Amatulli, Rosa Lasaponara, Michele Lovallo, and Adriano Santulli. Time-scaling properties in forest-fire sequences observed in gargano area (southern italy). *Ecological Modelling*, 185(2):531–544, 2005. Cited on page 16.

103 P. A. Thomas and R. S. McAlpine. *Fire in the Forest*. Cambridge University Press, 2010. 2 citations in pages 17 and 67.

104 T. Toffoli. Cellular automata as an alternative to (rather than an approximation of) differential equations in modeling physics. *Physica D: Nonlinear Phenomena*, 10(1):117–127, 1984. Cited on page 36.

105 T. Tomé and M. J. Oliveira. *Stochastic Dynamics and Irreversibility*. Graduate Texts in Physics. Springer International Publishing, 2014. Cited on page 76.

106 Mark E. Tuckerman. *Statistical Mechanics: Theory and Molecular Simulation*. Oxford Graduate Texts. OUP Oxford, 2010. Cited on page 26.

107 Donald L. Turcotte, Bruce D. Malamud, Fausto Guzzetti, and Paola Reichenbach. Self-organization, the cascade model, and natural hazards. *Proceedings of the National Academy of Sciences*, 99(suppl 1):2530–2537, 2002. Cited on page 16.

108 Alan M. Turing. On computable numbers, with an application to the entscheidungsproblem. In *Proceedings of the London Mathematical Society 2*, volume 42, pages 230–265, 1936. Cited on page 20.

109 Alan M. Turing. The chemical basis of morphogenesis. *Philosophical Transactions of the Royal Society of London B: Biological Sciences*, 237(641):37–72, 1952. Cited on page 61.

110 Alasdair Turner. A simple model of the belousov-zhabotinsky reaction from first principles. 2009. Cited on page 36.

111 Pedro Verruma. Conway's game of life. http://pmav.eu/stuff/javascript-game-of-life-v3.1.1/. Cited on page 28.

112 J. Von Neumann and Arthur W. Burks. *Theory of Self-reproducing Automata*. University of Illinois Press, 1966. 2 citations in pages 19 and 25.

113 M. M. Waldrop. *Complexity: The Emerging Science at the Edge of Order and Chaos*. Simon & Schuster, 1993. 2 citations in pages 22 and 39.

114 J. D. Watson and F. H. C. Crick. Genetical Implications of the Structure of Deoxyribonucleic Acid. *Nature*, 171(4361):964–967, May 1953. Cited on page 22.

115 J. D. Watson and F. H. C. Crick. Molecular Structure of Nucleic Acids: A Structure for Deoxyribose Nucleic Acid. *Nature*, 171(4356):737–738, April 1953. Cited on page 22.

116 Eric W. Weisstein. Moore Neighborhood. From MathWorld – a Wolfram web resource. http://mathworld.wolfram.com/MooreNeighborhood.html. Cited on page 25.

117 Eric W. Weisstein. von Neumann Neighborhood. From MathWorld – a Wolfram web resource.
http://mathworld.wolfram.com/vonNeumannNeighborhood.html. Cited on page 25.

118 M. H. F. Wilkins, A. R. Stokes, and H. R. Wilson. Molecular Structure of Nucleic Acids: Molecular Structure of Deoxypentose Nucleic Acids. *Nature*, 171(4356):738–740, April 1953. Cited on page 22.

119 Thomas Williams, Colin Kelley, and many others. Gnuplot 4.4: an interactive plotting program, March 2010. http://gnuplot.sourceforge.net/. Cited on page 17.

120 Arthur T. Winfree. The prehistory of the belousov-zhabotinsky oscillator. *J. Chem. Educ*, 61(8):661, 1984. Cited on page 36.

121 S. Wolfram. Universality and complexity in cellular automata. *Physica D: Nonlinear Phenomena*, 10(1):1–35, 1984. 2 citations in pages 22 and 33.

122 Stephen Wolfram. Statistical mechanics of cellular automata. *Rev. Mod. Phys.*, 55:601–644, July 1983. 3 citations in pages 21, 32, and 33.

123 Stephen Wolfram. Cellular automata as models of complexity. *Nature*, 311:419–424, 1984. 2 citations in pages 22 and 33.

124 William K. Wootters and Chris G. Langton. Is there a sharp phase transition for deterministic cellular automata? *Physica D: Nonlinear Phenomena*, 45(1):95–104, 1990. Cited on page 35.

125 J. M. Yeomans. *Statistical Mechanics of Phase Transitions*. Clarendon Press, 1992. Cited on page 43.

126 Mark R. Yoder, Donald L. Turcotte, and John B. Rundle. Forest-fire model with natural fire resistance. *Physical Review E*, 83(4):046118, 2011. Cited on page 16.

127 Robert M. Ziff. Four-tap shift-register-sequence random-number generators. *Computers in Physics*, 12(4):385–392, 1998. Cited on page 73.

128 Rita Maria Zorzenon dos Santos and Sérgio Coutinho. Dynamics of HIV infection: a cellular automata approach. *Phys. Rev. Lett.*, 87:168102, September 2001. Cited on page 36.

129 L. A. Zubkov and Vadim P. Romanov. Critical opalescence. *Soviet Physics Uspekhi*, 31(4):328, 1988. Cited on page 44.